The Thesis Committee for Reed Smart Roush
Certifies that this is the approved version of the following thesis:

Regional Stratigraphic and Core-based Characterization of the Cline Shale, Midland Basin, Texas

APPROVED BY
SUPERVISING COMMITTEE:

Supervisor:

William Fisher

William Ambrose

Charles Kerans

H. Scott Hamlin

Regional Stratigraphic and Core-based Characterization of the Cline Shale, Midland Basin, Texas

by

Reed Smart Roush, B.S. Geo. Sci.

Thesis

Presented to the Faculty of the Graduate School of

The University of Texas at Austin

in Partial Fulfillment

of the Requirements

for the Degree of

Master of Science in Geological Sciences

The University of Texas at Austin

May, 2015

Dedication

To my family.

Acknowledgements

This study was an integrated work of many individuals. I would first like to thank my committee members for their total support. My tenure at the Jackson School was funded by Project STARR at the Bureau of Economic Geology with Bill Ambrose as the primary investigator. Many researchers shared their awesome ideas and immense knowledge for this project: Robert Baumgardner, Dr. Robert Loucks, Tucker Hentz, Dr. Farzam Javadpour, Dr. Robert Reed, Dr. Stephen Ruppel, David Hull, and Erik Kavle. Dr. Harry Rowe was instrumental in collecting the XRF data and helping interpret it, with Michael Nieto assisting. Devon Energy allowed me access to their proprietary Cline Shale core, and they funded the rock-properties dataset. The XRD was performed by K-T GeoServices, Inc., the thin sections were prepared by Greg Vardilos, and the rock-eval pyrolysis, TOC, bulk density, porosity, and permeability measurements were taken by Weatherford Labs. Heirarchical cluster analysis was performed using Tibco Spotfire © and the regional stratigraphic analysis was performed using IHS Petra ©. The core-based analysis would not be possible without the assistance of the staff in the Core Research Center: James Donnelly, Nate Ivicic, Brandon Williamson, and Joseph Smitherman. Joseph also assisted me, along with Nick Strawn, in XRF acquisition of the Harris core. I would also like to thank my friends and my peers for always supporting me and helping me keep an even keel.

Abstract

Regional Stratigraphic and Core-based Characterization of the Cline Shale, Midland Basin, Texas

Reed Smart Roush, M.S. Geo. Sci.

The University of Texas at Austin, 2015

Supervisor: William Fisher

The Cline Shale is an organic-rich mudrock that was deposited in the Midland Basin during the latest Pennsylvanian. Deposits of the Cline Shale are restricted to basinal facies and contain great lateral and vertical heterogeneity. The basinal deposits are bounded by the Eastern Shelf to the east, the Horseshoe Atoll to the north, the Central Basin Platform to the west, and the Ozona Arch to the south. The boundaries do not only vary in morphology, but also in sediment type.

High-resolution (2 to 3-inch spacing) x-ray fluorescence (XRF) data were obtained from four cores in the basin. The data were interpreted within a chemofacies framework using agglomerative hierarchal clustering analysis, a statistical grouping method, calibrated with mineralogy and organic matter measurements. The high-resolution XRF chemofacies framework was used to core-calibrate a regional dataset of wire-line logs to determine quantitative lithofacies cutoffs from gamma ray logs of carbonates, organic matter-poor siliciclastics, and organic matter-rich siliciclastics. The lithofacies were mapped throughout the Southern Midland Basin. The maps were created

for the Lower Cline, Middle Cline, and Upper Cline, three distinct units within the Cline Shale. An integrated core-based dataset was also used to glean relationships between mineralogy, porosity, permeability, organic content, thermal maturity, and grain density within the Cline Shale on the foot-scale. The results of this study have allowed the synthesis of core-based chemofacies trends analysis and regional composite lithofacies distributions in the Lower Cline, Middle Cline, and Upper Cline.

Table of Contents

List of Tables

List of Figures

Introduction

The Cline Shale is an Upper Pennsylvanian mudrock unit deposited in the Midland Basin, a Paleozoic epicratonic basin. The Cline Shale was first evaluated as a potential unconventional hydrocarbon play in 2006 (Keith Skaar, personal communication). The Cline Shale is a colloquial name for the unit, an emerging mudrock that does not have a formalized stratigraphic name (Skaar, 2012). The Cline Shale is predominantly composed of mudrocks. According to the definition by Folk (1980), a mudrock is a broad definition of fine-grained sedimentary rocks; while a shale implies fissility, an uncommon characteristic of the unit. The Cline Shale was studied utilizing high-resolution (two to three-inch interval) x-ray fluorescence (XRF) geochemistry, foot-scale x-ray diffraction (XRD), Rock-Eval pyrolysis, total organic carbon (TOC), bulk density, porosity, and permeability measurements, and core-calibrated regional wire-line log stratigraphy to present a core-based and regional stratigraphic characterization.

The specific objectives of this study were to (1) provide a geologic and regional stratigraphic background of the Cline Shale, (2) distinguish mineralogy and organic matter (OM) content from elemental geochemistry proxies in Cline Shale cores, (3) characterize the Cline Shale based on integrated XRD, Rock-Eval pyrolysis, TOC, bulk density, porosity, and permeability measurements, and (4) interpret core-based chemofacies trends and core-calibrated regional lithofacies distributions of the Cline Shale.

STUDY AREA

The Cline Shale occurs throughout most of the Midland Basin in west Texas (Figure 1). The study area covers parts of 32 counties. The organic-rich Cline facies are restricted to the basin, but time-equivalent facies occur on the slopes and shelf edges surrounding the Midland Basin (Brown et al., 1990). Cline Shale facies are bounded to the west by the Central Basin Platform, to the north by the Horseshoe Atoll, to the east by the Eastern Shelf, and to the south by the Ozona Arch. Time-equivalent basinal facies occur north of the Horseshoe Atoll. However, XRF analysis shows that these facies are independent of Cline Shale facies to the south of the Horseshoe Atoll, and the deposits to the north lack many of the unique qualities present in the Cline such as elevated redox-sensitive trace elements that co-vary with organic matter content. This analysis and multiple previous studies establish considerable relief of the Horseshoe Atoll from the sea floor during the latest Pennsylvanian (Vest, 1970; Waite, 1994). Using the Horseshoe Atoll as the boundary, the Midland Basin is separated into two sub-basins during the Upper Pennsylvanian: the Northern Midland Basin and the Southern Midland basin. The present study is restricted to the Southern Midland Basin—the area containing the productive Cline Shale facies.

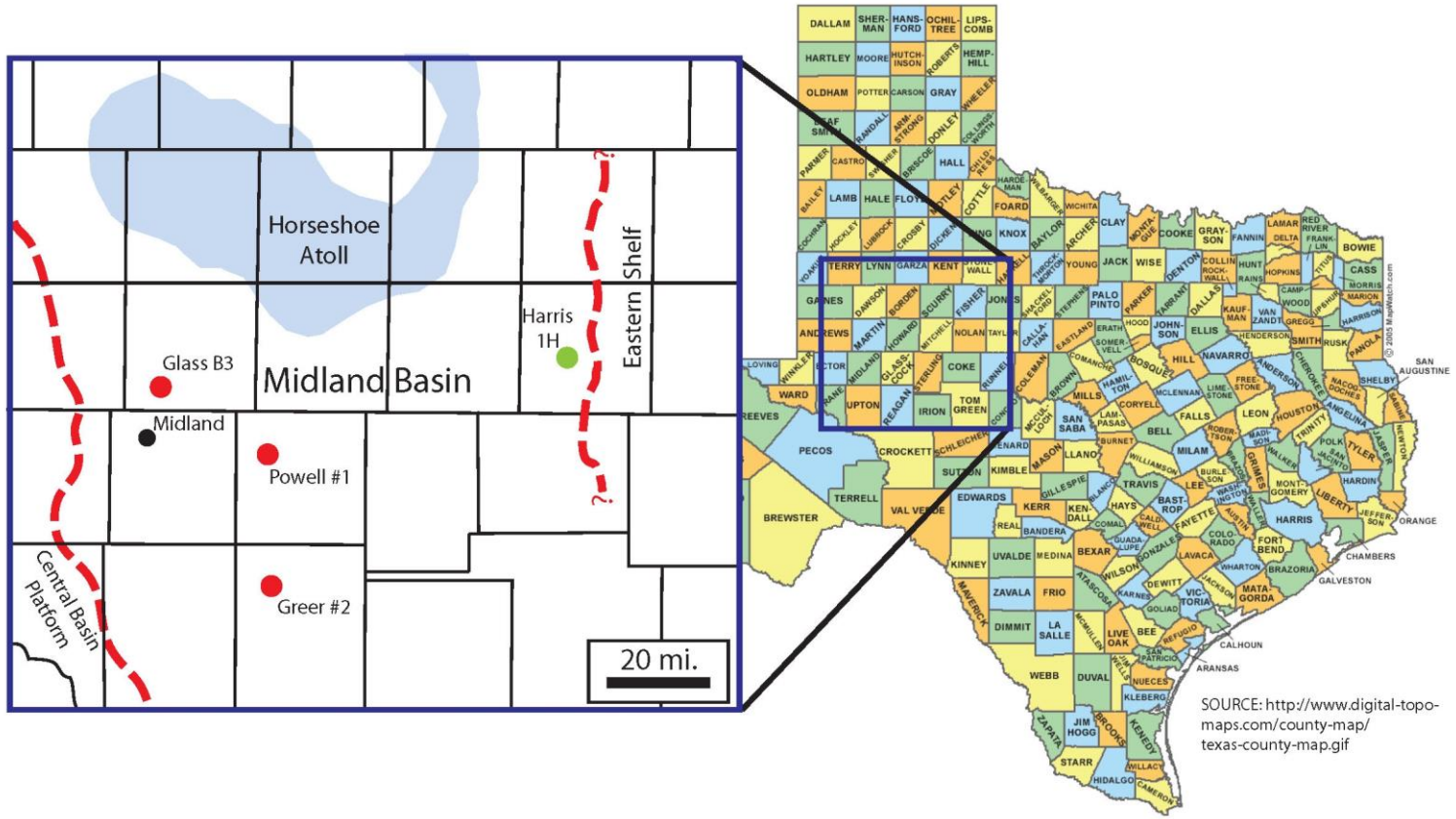

Figure 1: Geographic location of the study area in the Southern Midland Basin. The basin-centered cores are colored red, the Harris core is colored green, and the city of Midland is colored black for reference. The red dashed lines represent shelf edge positions at the end of Cline Shale deposition.

REJUVENATION OF THE PERMIAN BASIN THROUGH UNCONVENTIONAL RESOURCE PLAYS

Exploration and production activity in the Permian Basin has significantly increased since 2009, and an exponential increase in horizontal wells drilled in the Midland Basin began in late 2010 (Sutton, 2015). The increase in activity is attributed to new unconventional resource plays that have been developed throughout the greater Permian Basin; most development has been focused on the basinal deposits of the Delaware Basin and the Midland Basin (Figure 2). Unconventional resource play is not a strictly defined term. In this study, unconventional resource play is used to broadly describe shale gas and shale oil plays that consist primarily of low permeability mudrock formations. The Permian Basin is an exceptional target for unconventional resource play development and horizontal drilling because it contains thousands of feet of potentially productive mudrocks. The immense aggregate thickness of the mudrocks lends itself to multiple potential drilling targets and further to multiple stacked horizontal wells from a single drill-site. Over 50 million barrels of oil were produced in 2011 from the Wolfberry play in the Midland Basin (Hamlin and Baumgardner, 2012). The Cline Shale is a mudrock unit deposited stratigraphically deeper than the Wolfberry play (Figure 3); it is an important part of the Midland Basin total petroleum system (Skaar, 2012).

Exploration and production success has been varied in the Cline Shale. Apache Corporation reported a 30-day initial production average from 341 to 623 barrels of oil equivalent per day (BOEPD) from four wells in Glasscock County, and Laredo

Petroleum, Inc. reported a 30-day initial production average of 831 to 1,331 BOEPD from five wells also in Glasscock County (Jacobs, 2013). Pioneer Natural Resources has experienced positive results in Andrews County. Their fourth Cline well (Pioneer labels this interval as Wolfcamp 'D'), the University 7-43 10H, had a peak initial production of 3,605 BOEPD (Pioneer Natural Resources Company, 2013). The Devon Harris 1H (used in this study) had a 30-day initial production rate of 169 BOEPD (Ben Hermann, personal communication). Though multiple successful wells have been drilled in the Cline Shale, the Wolfcamp, on average, is cheaper to produce and has better rates of return (Jacobs, 2013). For this reason and poorly understood variable production rates, the Cline Shale has been treated as a secondary target in developing the Midland Basin unconventional resource plays.

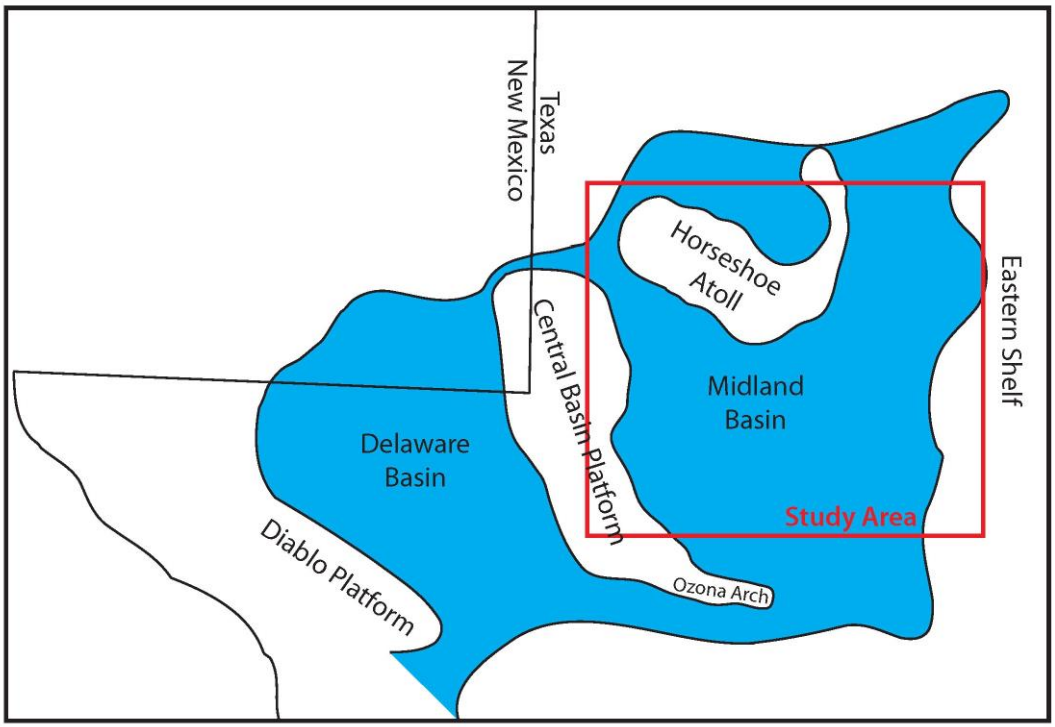

Figure 2: Regional paleogeography of the Midland Basin. The Southern Midland Basin is bounded by the Central Basin Platform, the Horseshoe Atoll, the Eastern Shelf and the Ozona Arch. Modified from Brown et al. (1990), Atchley et al. (1999), and Hamlin and Baumgardner (2012).

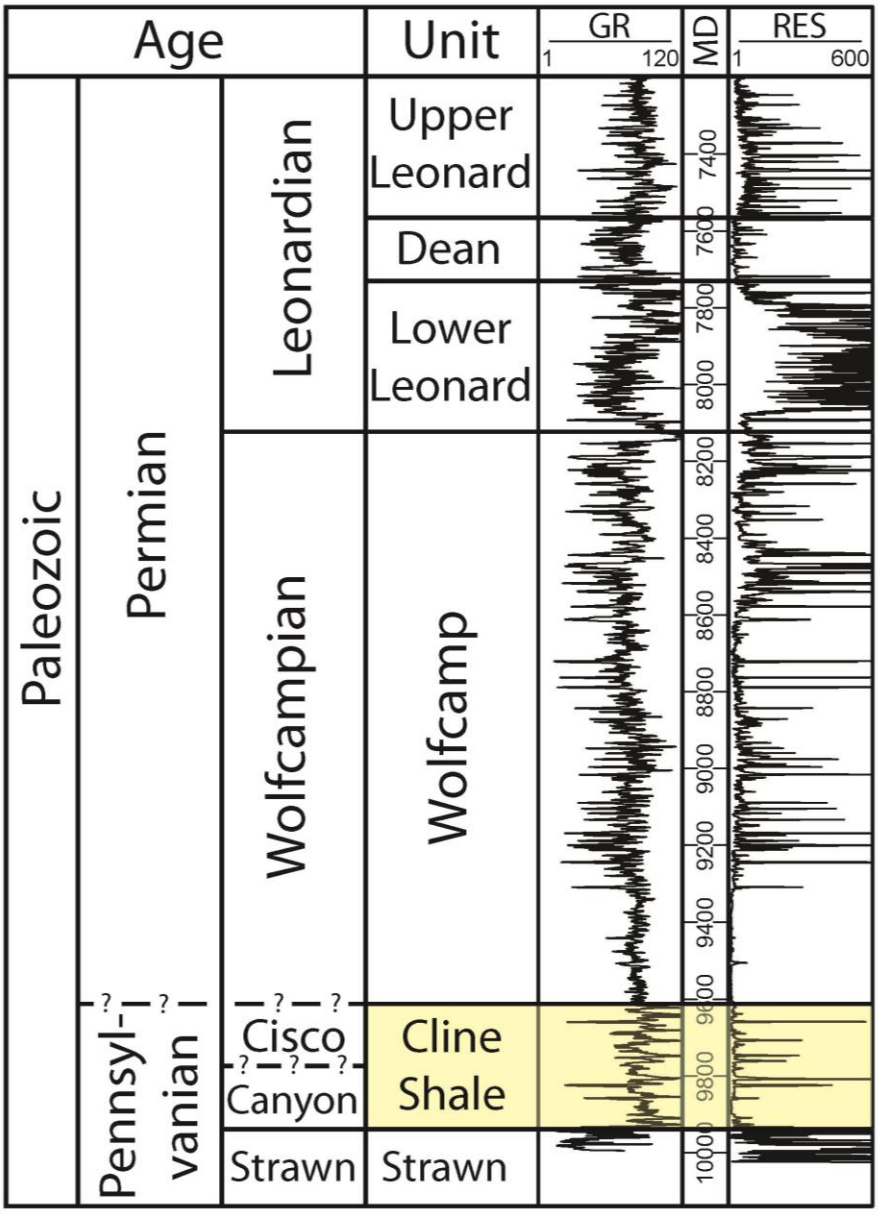

Figure 3: Generalized stratigraphy of the Southern Midland Basin, including the Cline Shale. Stratigraphy based on Hamlin and Baumgardner (2012). (API: 42-383-10575, Reagan County)

PREVIOUS WORK AND NOMENCLATURE HISTORY

The Cline Shale is an understudied formation with a convoluted naming history. Adams (1951) discussed an Upper Pennsylvanian shale within the Midland Basin as part of his starved basin hypothesis—little work was done to further characterize the unit beyond describing it as a black shale. Davis (1953) and Matchus and Jones (1984) delineated the basic Pennsylvanian stratigraphy of the basin. Hamlin and Baumgardner (2012) presented an Upper Pennsylvanian Shale in their regional cross sections; however, the focus of their study was on the overlying Wolfberry unit.

The extent of previous work on Pennsylvanian basinal units of the Midland Basin is limited, but a few detailed studies on Pennsylvanian formations associated with shallow-water deposition are documented (Vest, 1970; Brown et al., 1990; Waite, 1993; Saller, 1994, Kerans and Anonymous, 2001). These shelf and slope studies give an accommodation-based context to the basinal Cline Shale deposits. Brown et al. (1990) performed a detailed study of the northern portion of the eastern shelf, utilizing outcrop and subsurface information to map multiple Pennsylvanian mixed carbonate-siliciclastic cycles. Saller (1994) utilized a cycle stacking analysis of Pennsylvanian shallow water carbonate cycles on the Central Basin Platform. The Horsheshoe Atoll to the north has also been studied extensively (Vest, 1970; Waite, 1993; Kerans and Anonymous, 2001). Waite (1993) distinguished multiple Upper Pennsylvanian third-order sequences in the Horseshoe Atoll section from a 3-dimensional seismic analysis.

The Cline Shale was named by Keith Skaar in December of 2006 after the Baytech Ray Cline #1, a vertical well that produced from the uppermost 50 feet of the Cline (Keith Skaar, personal communication). Other names associated with the same stratigraphic interval are the Black Shale, Three Forks, and the Wolfcamp 'D' (Skaar, 2012). The Cline Shale has become a name associated more with the eastern part of the basin. This is mostly due to industry's nomenclature and calling the unit the Wolfcamp 'D' in the western portion of the basin—a misnomer because it is not Wolfcampian in age (Wahlman et al., in preparation). For this study, the Cline Shale is defined as the Upper Pennsylvanian basinal mudrocks deposited above the Strawn Formation and below the Wolfcamp interval in the Southern Midland Basin (Figure 3).

DATASET

Two core-based datasets, and a regional dataset of wire-line logs are used in this study. The core-based datasets were differentiated due to the scale of investigation, where one dataset was used to investigate the core on an inch scale, and the other method was used to investigate the core on a foot scale. All three datasets were evaluated individually and used in conjunction with each other throughout the study.

Four cores are used in this study (Table 1). Three of the cores were recovered from the inferred basin-center during deposition of the Cline Shale; they are the Gulf Oil Corp. Glass B3, the Pan American Powell 1, and the Clinton Oil Company O.L. Greer 2 (Figure 1). In this study, these wells are designated as the basin-centered wells. These cores are stored at the Bureau of Economic Geology Core Research Center in Austin, TX,

and only a portion of the Cline is cored in all three of the cores (Figure 4). The fourth core is the Devon Energy Harris 1H. It was recovered from the eastern margin of the basin in central Nolan County (Figure 1). The core represents an almost continuous section of the Cline Shale, with only the uppermost portion of the Cline omitted, where the facies change to time-equivalent slope facies (Figure 4). The core is a proprietary Devon Energy core, and it is stored at the Oklahoma Petroleum Information Center in Norman, OK.

API	42173102040000	42317001300000	42353333430000	42383105750000
Well Number	1	3	1H	2
Well Name	POWELL EL	GW GLASS B	HARRIS	GREER OL
Operator	PAN AMERICAN	GULF OIL CORP	DEVON ENERGY PROD	CLINTON OIL CO
County	GLASSCOCK	MARTIN	NOLAN	REAGAN
Surf Latitude	31.9420072	32.1652975	32.2446864	31.511047
Surf Longitude	-101.6601901	-102.0929409	-100.4839845	-101.5700495

Table 1: Table of cored wells, located in Figure 1.

A high-resolution XRF dataset is the first core-based dataset (Table 2). XRF measurements were taken at over 2,500 points from all four cores. A 2-inch sampling interval was used for the basin-centered cores, and a 3-inch interval was used for the Harris core, owing to timing constraints. Calibrated XRF measurements yield elemental compositions. Based on preliminary XRF interpretations, XRF sample-matched powders were drilled at 86 locations. The samples were evaluated for TOC and mineralogy, using XRD. From these 86 points, empirical relationships between the XRF and TOC and XRF

and mineralogy were determined. The XRF, XRD, and TOC measurements were all generated in-house at the Bureau of Economic Geology. The integrated geochemical dataset is referred to as the high-resolution XRF dataset (Appendix A).

The second core-based dataset, termed the rock properties dataset (Table 2), consists of 65 integrated analyses of XRD, bulk density, porosity, permeability, TOC, Rock-Eval Pyrolysis, and thin-sections. The rock properties dataset is exclusive to the basin-centered cores (Appendix B).

The wire-line well log dataset consists of over 350 raster logs (Table 2). The top and base of the Cline, as well as two intra-Cline surfaces were picked based on Hamlin and Baumgardner (2012), Brown et al. (1990), and core-calibrated log relationships. Of the rasters, more than 150 gamma ray logs were digitized and core-calibrated in the Cline interval to produce quantitative lithofacies cutoffs. The digitized wells used in this dataset are located in appendix C.

Dataset	**High-Resolution XRF Dataset**	**Rock Properties Dataset**	**Regional Stratigraphic Dataset**
Data Source	All cores	Basin-centered cores	Wire-line logs
Contents	XRF calibrated with XRD and TOC	XRD, bulk density, porosity, permeability, TOC, rock-eval pyrolysis, and thin-sections	Raster logs and core-calibrated digitized logs of the Cline interval
Resolution	Inch Scale	Foot Scale	Foot Scale to Mile Scale

Table 2: Table of datasets.

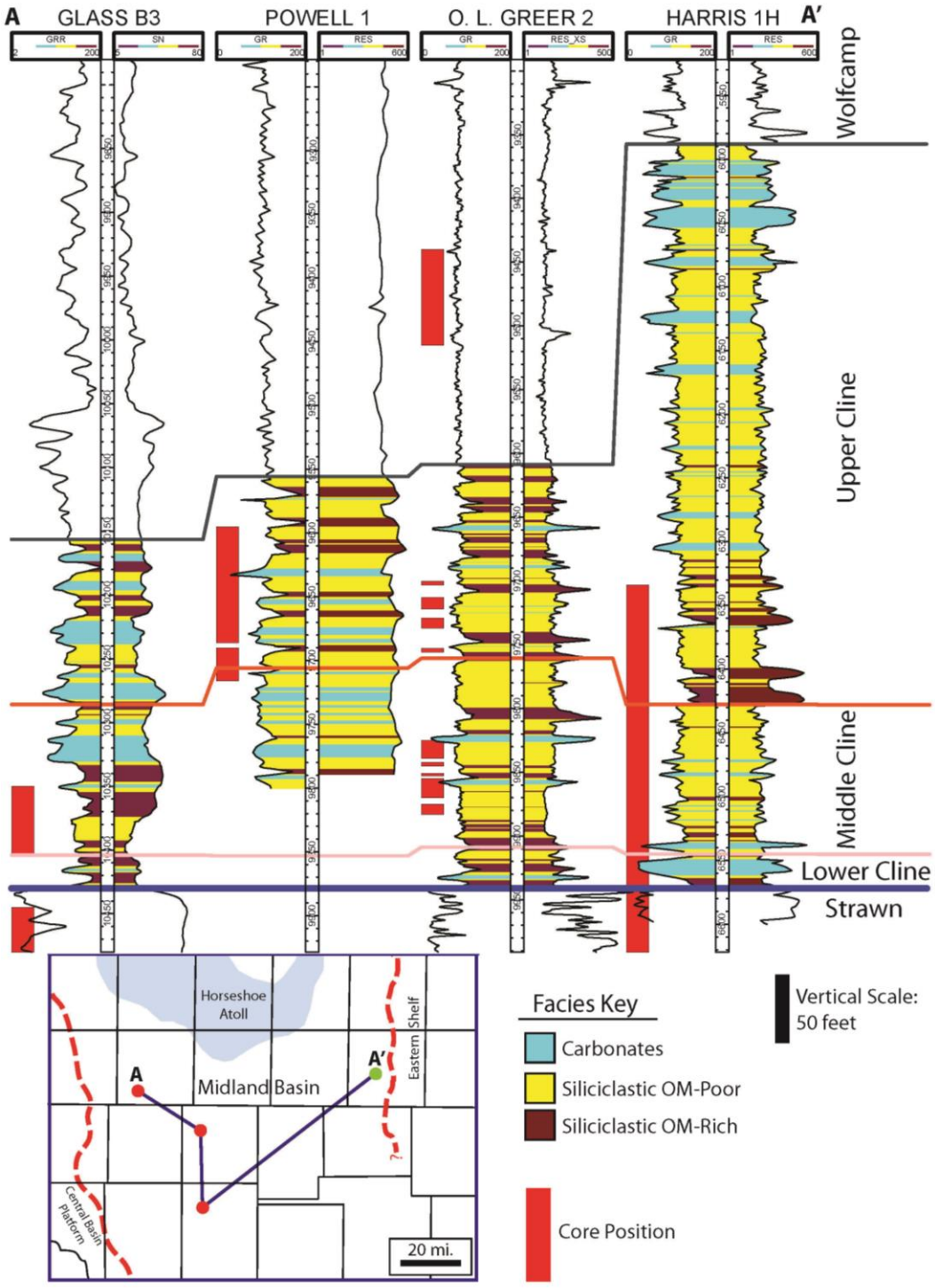

Figure 4: West to east cross section displaying core positions and stratigraphic units. The delineated lithofacies are based on core-calibrating the gamma ray log.

Geologic Setting

The Cline Shale is an organic-rich mudrock deposited during the Missourian and Virgilian Series of the Upper Pennsylvanian (Wahlman et al., in preparation). The Missourian and Virgilian correspond to the local Canyon and Cisco Series of the Permian Basin respectively (Cheney et al., 1945). The Cline Shale was deposited in the Midland Basin, an epicratonic foreland basin of the Marathon-Ouachita orogenic belt and the eastern sub-basin of the greater Permian Basin (Figure 2) (Yang and Dorobek, 1995). Cline Shale deposition was constrained geographically by the Central Basin Platform to the west, the Horseshoe Atoll to the north, the Eastern Shelf to the east, and the Ozona Arch and Southern Shelf to the south. Productive Cline Shale facies are restricted to basinal mudrocks, although there was considerable siliciclastic and carbonate deposition on the slopes and shelves contemporaneous with Cline deposition (Brown et al., 1990).

Age of Deposition and Regional Stratigraphy

Previous studies and this study both point to latest Pennsylvanian as the time of deposition of the Cline Shale. Until recently, there were no biostratigraphic ages associated with the Cline Shale in the Midland Basin. Shelf to basin correlation was the only age dating tool. Adams (1951) surmised there must be an uppermost Pennsylvanian Shale in the Midland Basin because a considerable thickness of Canyon and Cisco units were deposited on the shelf surrounding the basin, and no structure exists that may have prevented deposition from the shelf to the basin. Mazzullo and Reid (1988, 1989)

documented the occurrence of an Upper Pennsylvanian shale in the Midland Basin to the north of the Horseshoe Atoll. Brown et al. (1990) used outcrop studies and wire-line logs to correlate Upper Pennsylvanian and Lower Permian aged deposits from the Eastern Shelf to the Midland Basin, wherein considerable mudrock thicknesses were documented in the basinal units. Yang and Dorobek (1995) showed annotated seismic lines with Canyon and Cisco strata in the Midland Basin. Hamlin and Baumgardner (2012) display an Upper Pennsylvanian Shale in their regional cross sections equivalent to what is called the Cline Shale in this study. A recent study of fusulinids and conodonts by Wahlman et al. (in preparation) has added biostratigraphic controls to Cline Shale deposition. The fusulinid data from within the study area show the Cline Shale contains Missourian (Canyon) and probably Virgilian (Cisco) aged deposits. Conodont based dates in a core north of the Horseshoe Atoll corroborate that the stratigraphic base of the Cline Shale equivalent is Missourian (Canyon).

The timing of the upper contact of the Cline Shale is less certain. A basinwide lithostratigraphic top of the Cline Shale has been delineated in this study (Figure 3). Distinct log signature differences, the most notable of which is a change in the gamma ray log from closely spaced maximum and minimum values in the Cline Shale to a stable gamma ray signature in the Wolfcamp interval, define this lithostratigraphic boundary. However, assigning an age to the Cline-Wolfcamp boundary is problematic. Jones (1980) explained that it is possible that the Pennsylvanian-Permian boundary crosses lithologic boundaries—making log correlations of the boundary quite difficult; although

regional continuous lithostratigraphic boundaries have been correlated in basinal facies throughout the younger Wolfberry interval (Hamlin and Baumgardner, 2012). The Pennsylvanian-Permian boundary has also shifted up in the stratigraphic section significantly since the majority of studies discussed previously in this section (Davydov et al., 1998; Wahlman, 2013). A lack of biostratigraphic controls on the Cline-Wolfcamp contact and a poorly understood Pennsylvanian-Permian boundary contribute to the uncertainty of the timing of the top of the Cline Shale contact.

TECTONISM AND INFLUENCE ON BASIN MORPHOLOGY

The Permian Basin is a foreland basin produced during the Marathon-Ouachita orogeny (Ross, 1986). The Midland Basin is the Eastern sub-basin of the Permian Basin (Figure 2). It is separated from the Delaware Basin to the west by the Central Basin Platform (Galley, 1958). Rapid subsidence of the Permian Basin, including the Midland Basin, began during middle Pennsylvanian time and continued throughout the remainder of the Pennsylvanian (Yang and Dorobek, 1995).

The Cline Shale marks the beginning of the transition from the ramp carbonates deposited in the Strawn to rimmed platforms ubiquitous on the Eastern Shelf during the Wolfcampian (Mazzullo and Reid, 1988). The paleobathymetric relief from the Eastern Shelf to the Midland Basin increased from 600ft to at least 2000ft during Cline and Wolfcamp deposition (Brown et al., 1990). Basin deepening is attributed to an acceleration of subsidence that allowed for sufficient physiographic relief and the development of slope environments (Brown et al., 1973).

GEOLOGIC BOUNDARIES OF THE MIDLAND BASIN

The Cline Shale is restricted to the Southern Midland Basin. Geologic features can be used to distinguish the boundaries of the basin during the deposition of the formation. The western and southern boundaries, the Central Basin Platform and Ozona Arch respectively, are tectonically uplifted basement blocks (Yang and Dorobek, 1995; Hamlin and Baumgardner, 2012). The northern boundary, the Horseshoe Atoll, is a large carbonate buildup (Vest, 1970; Waite, 1993). The eastern boundary is the slope to shelf profile of the Eastern Shelf. These three distinct boundary types all produce positive relief relative to the Midland Basin, controlling facies changes in the time-equivalent depositional package.

The boundaries controlling the deposition of the Cline Shale range from narrow to gradational. The Central Basin Platform and the Ozona Arch form abrupt boundaries that are tectonically influenced, and a narrow range of faults and folds associated the uplifts create a very steep and complex margin (Yang and Dorobek, 1995). The Horseshoe Atoll is also an abrupt margin. The deposition of the Horseshoe Atoll encompasses Strawn, Canyon, Cisco, and locally Wolfcampian age units (Cys and Gibson, 1988). The Horseshoe Atoll is a product of shallow-water carbonate deposition at the same time as Cline Shale deposition, and had an influence on proximal Cline deposition (Vest, 1970). Considerable synoptic relief between the atoll and the basinal deposits of the Cline Shale occurred during the Upper Pennsylvanian (Waite, 1993). The Eastern Shelf is a shallow-water mixed carbonate and clastic shelf (Cys and Gibson, 1988; Brown et al., 1990). The

Eastern Shelf is retrogradational, aggradational, and progradational during the Canyon and Cisco; the eastern boundary of the Cline is not a static feature (Brown et al., 1990). The shelf edge of the Eastern Shelf can be difficult to assess due to its gradational nature (Hoak et al., 1991).

These boundaries not only define the lateral extent of Cline Shale deposition, but also influence water mass flow from the open ocean (Figure 5). The Cline Shale was deposited in a basin with preconditioned water mass. Sediment enrichment of elements emanating from the water mass, such as molybdenum, has been documented in the Leonardian Delaware Basin (Nance and Rowe, 2014; Calvert and Pedersen, 2007). Leonardian foreland basin arrangement was similar to the Upper Pennsylvanian arrangement (Nance and Rowe, 2014); it is interpreted that similar changes of the water mass in basins separating the Midland Basin from the open ocean, such as the Delaware Basin, were associated with deposition of the Cline Shale. The distance from the open ocean to the Midland Basin increases the likelihood of geochemical evolution of the water mass; the most important of which is the loss of redox-sensitive trace elements that aid in interpreting the paleoredox conditions of the formation.

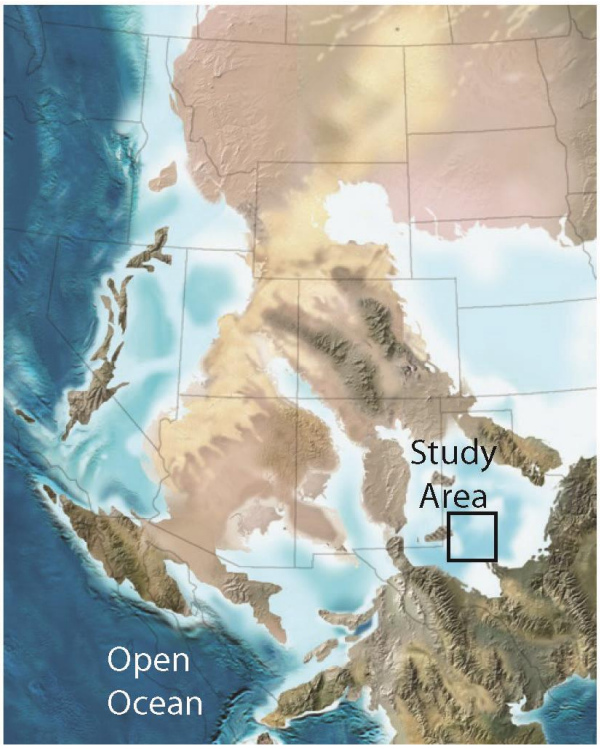

Figure 5: Paleogeographic map of the southwestern United States during the uppermost Pennsylvanian, 300 Ma. The study area is located a great distance from the open ocean; water that circulates into the study area will have undergone many chemical changes. Modified from Blakey (2013).

SEQUENCE STRATIGRAPHY

The Cline was deposited under complex sequence-stratigraphic conditions. A trajectory analysis, using the accommodation method from Neal and Abreu (2009), of the Eastern Shelf from cross section A to A' in Brown et al. (1990) located in southern Nolan and Taylor Counties revealed an aggrading to prograding sequence set from the late Canyon through Cisco. Trajectory analysis of early Canyon deposits from the A to A' cross-section was problematic because it was dominated by a limestone bank, and no

shelf edge was apparent. The aggrading to prograding sequence set is interpreted as a normal regression event. Near the end of the Canyon, there was a rejuvenation of the Ouachita fold belt that delivered more sediment to the Eastern Shelf (Brown et al., 1990). This was probably an influence on the beginning of the lower-order regression that occurred from during the Upper Canyon through the Wolfcampian on the Eastern Shelf. Cycle stacking analysis on the Central Basin Platform has shown the Lower Canyon as a transgressive unit and the upper Canyon and Cisco as regressive units (Saller, 1994). The Central Basin Platform could not have received sediment from the Ouachitas because it is an isolated platform, which points to a eustatic driver of relative sea level as the dominant sequence-stratigraphic control on the Central Basin Platform during the Upper Pennsylvanian. Waite (1993) utilized seismic sequence stratigraphic analysis of the Horseshoe atoll to interpret a retrogradational isolated carbonate platform that formed as a product of long term relative sea-level rise in the Midland Basin. Cycle thickness analysis from Formation Microimager (FMI) logs in Midland and Upton Counties was interpreted to display maximum basinal accommodation in the Midland Basin as uppermost Canyon in age (Figure 6; Prochnow and Hinterlong, 2014). Local differences in sequence-stratigraphy in and around the Midland Basin have an effect on the sequence-stratigraphy of the Cline Shale, possibly creating diachronous sequence-stratigraphic surfaces in the basin.

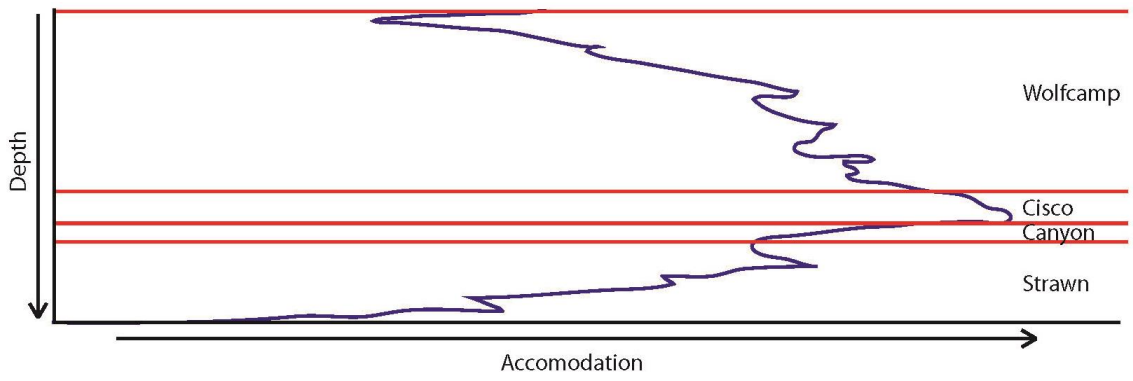

Figure 6: Idealized plot of accommodation versus depth of Upper Pennsylvanian and Lower Permian formations of the Midland Basin. Modified from Prochnow and Hinterlong, (2014).

CYCLICITY

The Late Pennsylvanian was a time of icehouse conditions, although it has recently been interpreted that major contractions in global ice sheets did occur during this time, possibly contribution to a long-term sea level rise (Montañez and Poulsen, 2013; Eros et al., 2012). A single depositional cycle on the Easter Shelf has been documented to be associated with between 230 feet and 558 feet of relative sea level rise and fall (Aldis, 1988). The duration of these cycles is comparable to Pleistocene glaciation and Milankovitch orbital cycles (Hayes et al., 1976; Heckel, 1986; Veevers and Powell, 1987). These large, relative sea level fluctuations are interpreted to promote increased heterogeneity in the Cline Shale facies both vertically and laterally by constantly flooding the surrounding shelves and reorganizing the basin. Yancey and McLerran (1988)

championed eustatic changes in sea level as the dominant driver of Eastern Shelf cyclicity. Brown et al. (1990) also favored eustacy as the predominant driver of sea level change in the Upper Pennsylvanian, but recognized the importance of tectonics and autocyclic processes as drivers of relative sea level change on higher orders.

Understanding shelf cyclicity may lead to clues of the drivers of cyclicity in the basin during Cline Shale deposition. Brown et al. (1990) has shown the dominant carbonates of the Pennsylvanian Eastern Shelf occur during transgression, and clastics are delivered to the shelf during regression. This principle can be applied to basinal deposits as well using the reciprocal sedimentation model; shelf flooding promotes increased basinal deposition of carbonates, while shelf regression corresponds to increased siliclastics in the basin (Van Siclen, 1958).

Methods

HIGH-RESOLUTION XRF ANALYSIS

XRF Acquisition

High-resolution energy dispersive XRF data were generated using a Bruker Tracer III (T3S2270) and a Bruker Tracer IV (T4S2594), specifically calibrated for mudrock matricies (Rowe et al., 2012). The XRF spectrometers were connected to, and controlled by, a laptop computer. The XRF spectrometers stood on a stand where the scanning window faced up (Figure 7). A flat surface (slabbed core), was required to obtain an accurate XRF reading. Before scanning, the cores were washed thoroughly with tap water to eliminate surface impurities. Multipurpose labels (Avery #5412) were used to record the exact position of every scan. Each data point was scanned twice; once for major elements, and once for trace elements. Major elements were scanned with the XRF gun under vacuum—for this a Bruker Vacuum was attached to the instrument. The analysis for major element concentrations was undertaken for a 60-second count time, and trace element concentrations were analyzed for a 90-second count time. The scanning times were determined as the minimum time required for quantitative results. Before scanning for trace elements, a 0.006" Cu, 0.001" Ti, and 0.012" Al filter was inserted into the instrument to attenuate major element characteristic x-rays. Raw data for each scan recorded the duration of the scan and the count of photons *versus* energy

signatures (kV). The T3S2270 was used to scan all of the samples except the traces of the Harris well, where the T4S2594 was used.

The XRF calibration was developed by Rowe et al. (2012) using samples from various mudrock formations as a calibration tool. Samples from different mudrocks were evaluated by mass spectrometry and by the XRF technique, the results of which provide quantitative elemental concentrations for mudrock matrices. A quality assurance shale pellet was scanned three times daily before scanning samples, serving as an internal quality assurance and quality control (QA/QC) method to prevent instrument drift. From this calibration, the composition of 29 different elements can be reported from each data point; Na, Mg, Al, Si, P, S, K, Ca, Ti, Mn, Fe, Ba, V, Cr, Co, Ni, Cu, Zn, Ga, As, Pb, Th, Rb, U, Sr, Y, Zr, Nb, and Mo.

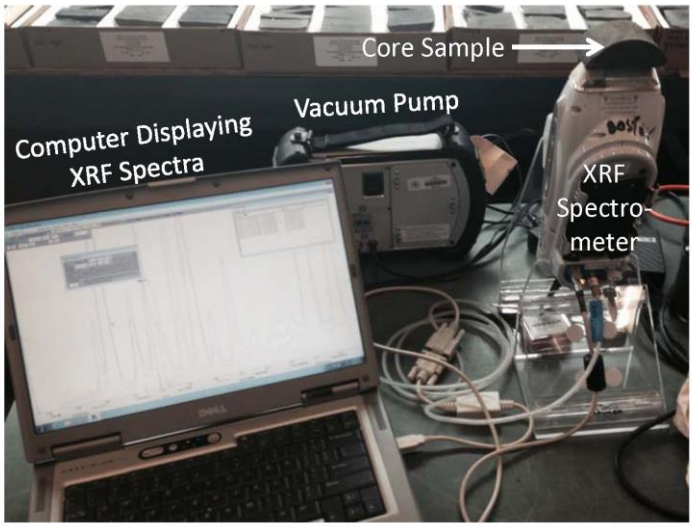

Figure 7: Annotated photograph of the XRF acquisition setup. The XRF spectrometer is located on a stand with the analyzing window facing up. A slabbed core sample is placed on the window to be measured. The computer controls the XRF spectrometer, and displays the XRF spectra in real time for quality assurance and quality control. The vacuum pump is connected to the instrument during major element acquisition to mitigate air interference of the x-rays emitted and photons produced during the measurement process.

XRD and TOC Acquisition

The elemental composition data were empirically calibrated as proxies of mineralogy and organic matter content, using XRD and TOC data, respectively. To produce these data, powder was drilled out of the back of each core at a total of 86 intervals. Each drill location corresponded to an XRF location. The drill samples were selected by first examining the XRF data and attempting to incorporate all potential mineralogies and organic matter concentrations across the dataset. When drilling the samples, the drill bit was first cleaned with a cloth and powder generated from the first

few mm of the drilled sample was discarded to eliminate contaminants; between 0.5 and 1 mL of powdered sample was taken and stored in economy microtubes with snap caps. Each sample was evaluated for both mineralogy and TOC.

An XRD analysis was used for the mineralogy. A small sample of the drill powder was measured using an Inxitu BTX308. Samples were measured from 2-55 degrees two theta. The XRD spectra were interpreted with XPowder, utilizing the ICDD PDF 2 database. The clays were not glycolated, and a Reitveld refinement was not utilized—resulting in an underestimation of total clays in the system (Harry Rowe, personal communication).

The TOC was analyzed using a portion of the same drill powder as the XRD. A small amount of drill powder was weighed into silver capsules. The silver capsules were exposed to fuming HCl for a period of one week, and drops of sulfurous acid were added to dissolve all inorganic carbon in the samples. The samples dried in an oven at 80 degrees Celsius before analysis. The capsules were combusted in a Costech 4010 elemental analyzer. Their byproducts passed through a Thermo Finnigan ConFlo IV, and were measured with a Thermo Finnigan Delta-V Isotopic Ratio Mass Spectrometer (IRMS) (Rowe et al., 2002).

XRF Interpretation with Hierarchical Cluster Analysis

High-resolution XRF datasets are powerful because they contain 29 elements per data point. Agglomerative hierarchical cluster analysis can be used to group the XRF data into groups based on all these elements simultaneously. From the groups, or

clusters, a robust chemofacies scheme can be produced for the XRF data by interpreting the statistically derived clusters based on mineralogy and organic matter content. Applying the hierarchical clustering method to XRF data was derived by Nestor Phillips and Dr. Harry Rowe (Nestor Phillips, personal communication).

Hierarchical Cluster Analysis Theory

Hierarchical cluster analysis is a multivariable statistical grouping method. Hierarchical cluster analysis is used to segment collections of data into groups that are known as clusters based on their similarity; the method produces groups of data that are more similar to each other than the remainder of the data in the dataset (Hastie et al., 2008). Hierarchical cluster analysis is an exploratory method for use with large datasets with many variables (such as the elements in an XRF dataset). The benefit of hierarchical cluster analysis is that the clustering algorithm is based on all data available, not just a select handful of variables, or elements. Though the method is rare, it has been used previously for geologic applications. Phillips (1991) applied this technique to benthic faunal assemblages to discern paleobathymetry, and Templ et al. (2008) used cluster analysis to group geographic locations based on their geochemistry. In this study, the method was applied to XRF data in mudrocks, and a chemofacies scheme was determined based on geological interpretation of the clusters.

There are two divisions of hierarchical cluster analysis; agglomerative (bottom-up) and divisive (top-down) (Hastie et al., 2008). Agglomerative hierarchical cluster analysis begins with each data point in its own cluster and the clusters are grouped until

the population is all grouped into in one cluster (Figure 8). Divisive hierarchical cluster analysis is just the opposite; the population of data points begins as one large group, and is divided into smaller, more similar clusters until each data point is represented by its own cluster. This study utilizes the agglomerative method for statistical analyses.

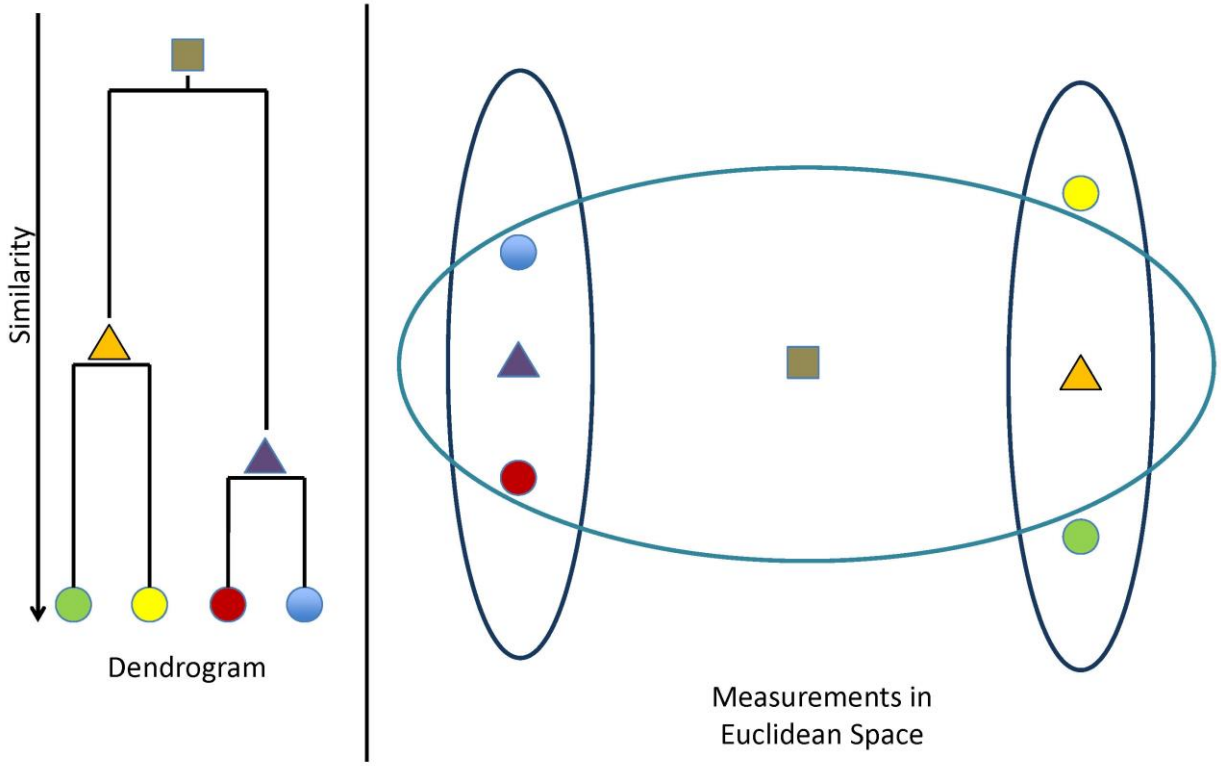

Figure 8: Theoretical example of agglomerative hierarchical cluster analysis. Agglomerative cluster analysis begins with individual measurements (green, yellow, red, and light blue circles). The measurements are grouped or clustered, in this case, based on proximity to each other in two dimensional Euclidean space, also known as similarity. The two most similar (closest) measurements are the red and light blue measurements; their cluster average is represented by the purple triangle. A hierarchy is built in this way until all points can be represented by one cluster (the brown square in this case). The height of each node in the dendrogram is a measure of how similar each original measurement in the group or cluster is to each other.

There are multiple agglomerative hierarchical cluster analysis algorithms—each has unique benefits that must be considered when deciding on the clustering algorithm. The single linkage clustering method looks at the two closest data points in adjacent clusters and clusters based on the closest pairs. The complete linkage clustering method examines the two data points furthest away in each adjacent cluster and combines clusters that have the closest of the furthest data points (the exact opposite of single linkage clustering) (Romesburg, 1989). The average linkage clustering method merges clusters based on the similarity of all members of each cluster (Seifoddini, 1989). Unweighted Pair Grouping Method with Arithmetic-mean (UPGMA) and Weighted Pairing Grouping Method with Arithmetic-mean (WPGMA) focus on pairing clusters with minimal dissimilarity at each hierarchical step (Legendre and Legendre, 1998). Ward's method finds the cluster combinations that will produce the smallest amount of internal variance, or the sum-of-squares index, when combined (Romesburg, 1989). Ward's method combines the two most similar clusters relative to the entire grouping. Temple et al. (2008) showed the best results using Ward's method with their data, and after multiple trials, Ward's method has been used in this study as the agglomerative hierarchical clustering algorithm as well.

Data preparation is an important step in the cluster analysis process. Templ et al. (2008) highlight normalization as an important process, especially for performing cluster analysis on major and trace elements as one dataset. Major elements are presented in percentages, while trace elements are presented in parts per million (ppm). The

clustering algorithm does not take units into account, and the relative importance of each element cannot be based on its concentration. The relative concentration of each element sampled is not reflective of that element's importance, and therefore the data must be normalized to eliminate this variable in the analysis. This is completed by normalizing each element to values between 0 and 1. Normalization is necessary when clustering major and trace elements; however, this process creates a dataset where no one single element is any more important than another. The importance of each element is not proportional to their concentration, and normalization eliminates that variable.

The hierarchical cluster analysis was performed using Tibco Spotfire © software. The cluster analysis produces a dendrogram and heat map (Figure 9). The required number of clusters is adjusted using the red pruning line; moving the pruning line to the right will result in more clusters with higher similarity, and vice versa when moving the pruning line to the left. After multiple iterations of the cluster analysis it was evident that the Harris well and the basin-centered wells have very different elemental systems, especially in their redox-sensitive trace elements. They were run through the clustering algorithm separately to avoid clusters that only contain samples from one of the well groups. After multiple iterations, it was determined the basin-centered wells required 21 clusters and the Harris well required 18 clusters. The count, average value, and standard deviation of the elemental assemblages of each cluster are presented in appendix A.

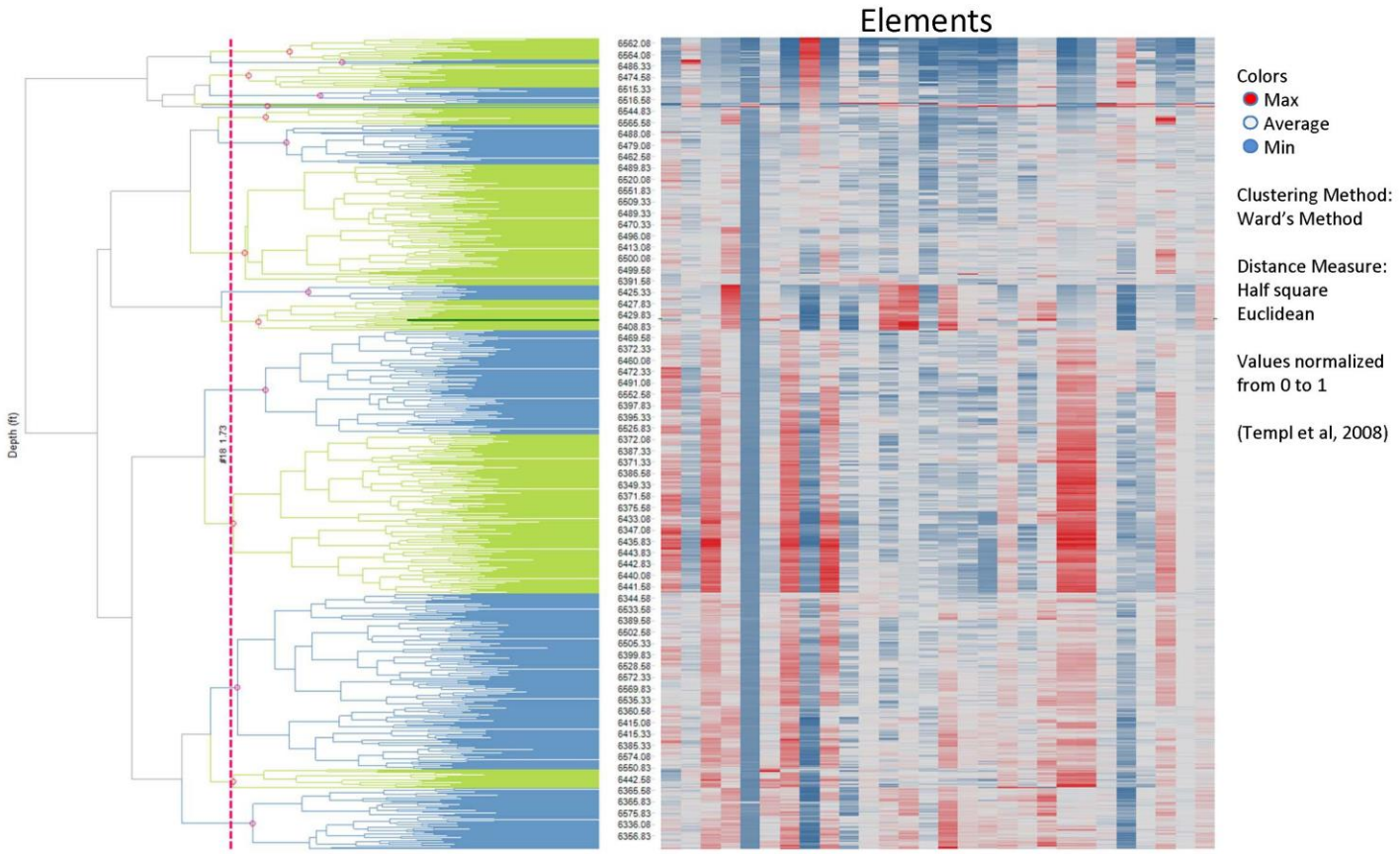

Figure 9: Dendrogram and heat map of the Harris well. The heat map on the right is displaying the relative values of each element used in the agglomerative hierarchical cluster analysis. Each row in the heat map is an individual point. The row position is determined by the dendrogram (on the left side of the figure). The dendrogram has been pruned with the red dotted line to produce eighteen clusters from the cluster analysis.

Geologic Interpretation of Hierarchical Cluster Analysis

Agglomerative hierarchical cluster analysis is an iterative process. The data have to be processed through the cluster analysis algorithm multiple times to produce a sufficient number of clusters to capture the variability that is available at such a high resolution while not producing so many clusters that interpretation becomes convoluted. This process is based on expert knowledge of the formation. Once the appropriate number of clusters has been distinguished, geologic interpretation may begin. Up to this point in the process, the clusters are products of a statistical grouping algorithm; no geological interpretation has been introduced to the groups of elemental data. The next step is to analyze each cluster based on geologic parameters. A chemofacies scheme was distinguished based on mineralogy and organic matter content—two qualities that can be gleaned using the XRF data calibrated to XRD for mineralogy and TOC for organic matter content.

The Cline Shale is a ternary system with regards to mineralogy—quartz, clays, and carbonates are the dominant minerals. These three groups of minerals can be used to describe the mineralogy of the majority of the samples. Multiple linear relationships can be drawn between the XRF and XRD data; Si and quartz, Al and kaolinite and illite, and Ca and calcite and dolomite are three important examples (Figures 10-11). These linear relationships can be used to extrapolate the mineralogy of the rocks to the XRF data. The exception to this rule exists with regards to nodules; most are predominantly phosphatic,

but they are readily distinguished in the dataset due to obvious enrichment in uncommon elements.

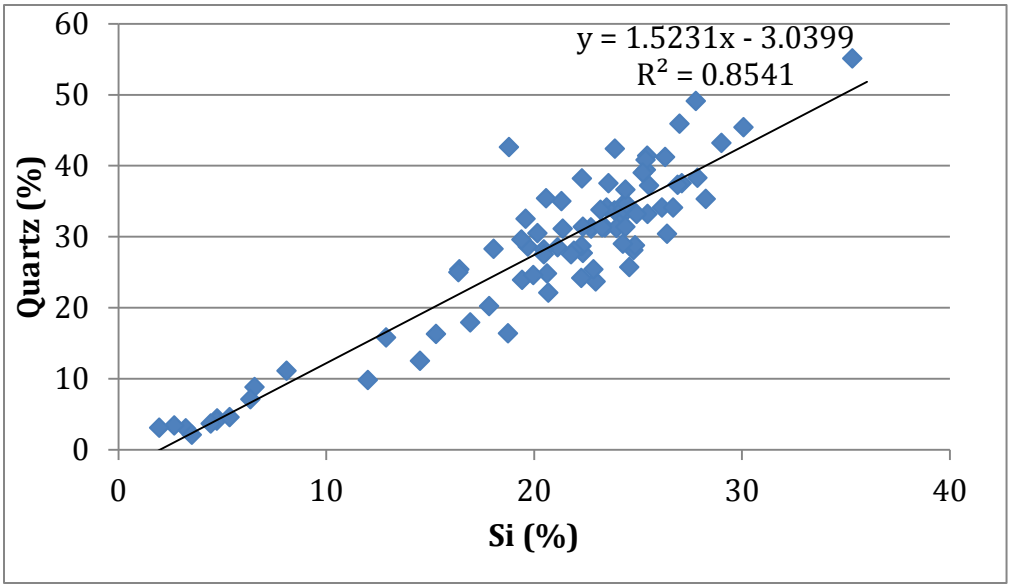

Figure 10: Plot of quartz (%) from XRD measurements vs. Silica (%) from XRF measurements. It can be inferred from the plot that percent Si can be used as a proxy for percent quartz.

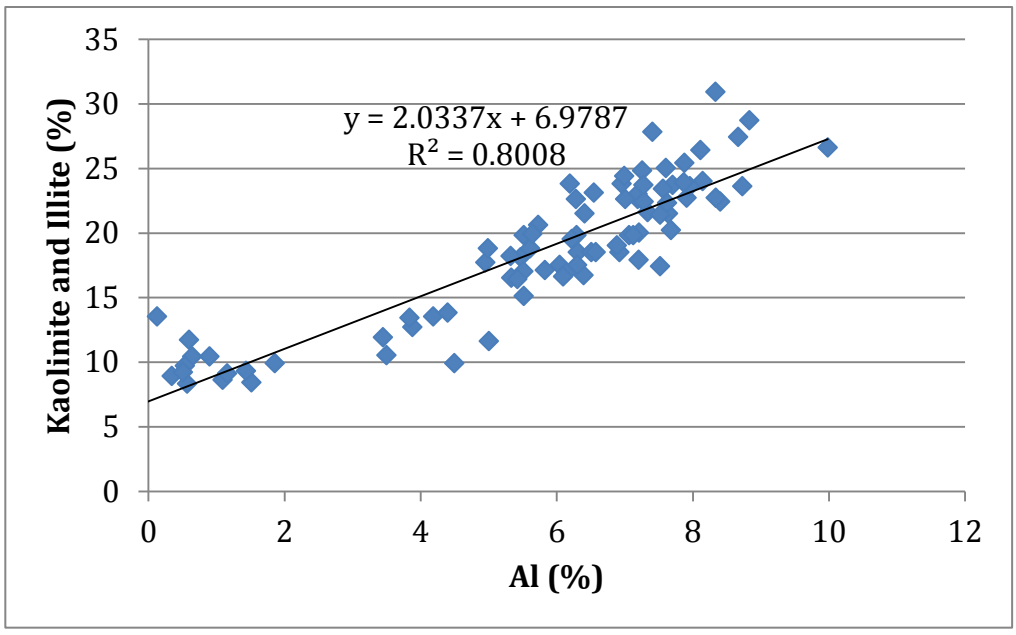

Figure 11: Plot of kaolinite and illite (%) from XRD measurements vs. Aluminum (%) from XRF measurements. It can be inferred from the plot that percent Al can be used as a proxy for percent kaolinite and illite.

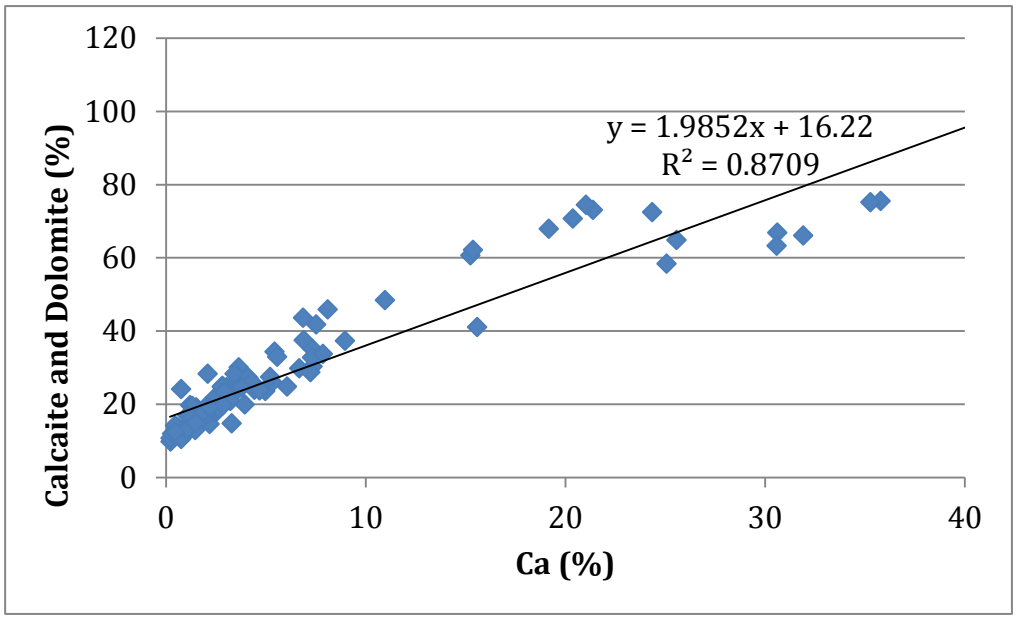

Figure 12: Plot of calcite and dolomite (%) from XRD measurements vs. Calcium (%) from XRF measurements. It can be inferred that percent Ca can be used as a proxy for percent calcite and dolomite.

Plotting the cluster averages on a ternary diagram is the simplest way to assess the variations of mineralogy across the dataset (Figure 13 and Figure 14). Plotting organic-rich mudrocks data on a ternary diagram with end members of $5XAl_20_3$, 2XCaO, and SiO_2 was developed by Brumsack (1989), these plots enhance the visual ternary spread of the data. The Cline Shale system can be regarded as a continuum of siliciclastic mudrocks that are diluted by carbonates. This dilution is evident when plotting Ca vs. TOC; this plot exhibits an inverse relationship of TOC and calcium (Figure 15). This inverse relationship shows the dilution of organic matter by input of carbonates. This being the case, we can plot a line from any point on the Al_2O_3-SiO_2 continuum that

extends to 2XCaO as a calcium dilution line (Figures 13 and 14). These lines are important as empirical cutoffs that can be used to distinguish the different mineralogical facies present in the siliciclastic continuum.

In this system, there are three calcium dilution lines that separate the siliciclastic facies into four groups (Figure 13 and Figure 14). The groups and cutoffs are based on empirical evidence and previous work that evidence these groups as different facies with distinct properties. Thousands of XRD measurements were taken from mudrocks spanning the globe; from these measurements, Wedepohl (1971) produced an average grey shale value (red square on figures 13 and 14). The Cline Shale is enriched in aluminum, and therefore the intermediate facies must be shifted toward aluminum as well. The most aluminum-rich facies are argillaceous facies, and the groups containing more silica then the formation average are assigned to the siliceous facies and the biogenic facies. The biogenic facies is somewhat of an anomaly in the siliciclastic facies because it is the only facies that is not detrital. The biogenic facies can be described using the XRF data, particularly silica's relationship to titanium and zirconium. Both of the latter elements are recognized as only detrital elements (Calvert and Pedersen, 2007). If the silica in the system were purely detrital, it is expected to co-vary with both titanium and zirconium; however, there is a sharp bend in the cross plots at high levels of silica content (above 25% silica) (Figure 16). This relationship is evidence that there is a biogenic component to the silica in the Cline Shale.

Calcareous facies were determined by distinguishing the dilution effect of calcium on TOC. As reported earlier, calcareous input dilutes TOC in the Cline Shale system. According to the TOC vs Ca cross plot, Ca in excess of 8% results in TOC values of generally less than 2% (Figure 15). The lack of organic matter in the mudrocks results in a different facies than what is apparent in the siliciclastic continuum. The 8% bulk Ca cutoff is roughly equivalent to 30% average 2XCaO lower cutoff for calcareous siliceous samples in the ternary mineralogy spectrum. The variance in the calcareous diluent required an intermediate cutoff to differentiate a calcareous siliceous facies, this was arbitrarily picked at 16% 2XCaO.

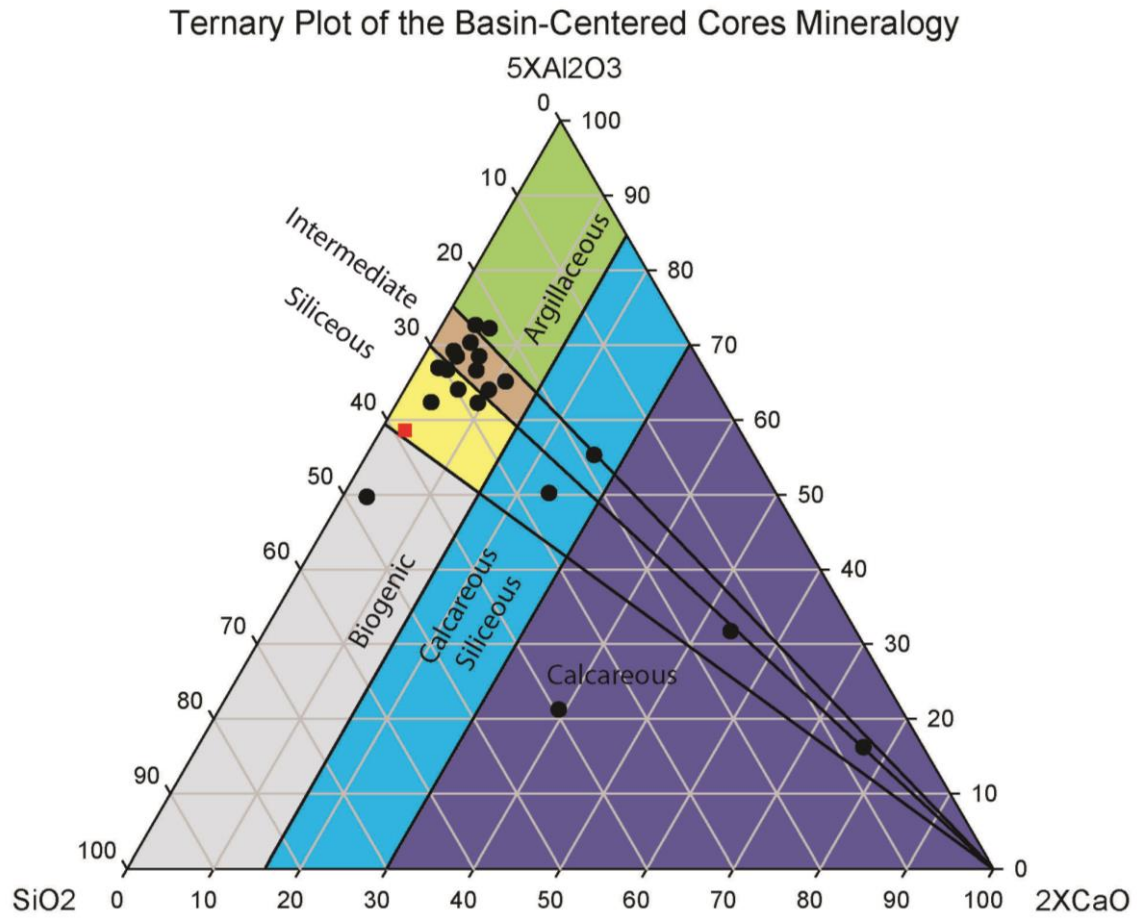

Figure 13: Ternary diagram of the basin-centered cores mineralogy. Elental oxides are used as proxies for minerals in this case (after Brumsack, 1989). The red square represents the average grey shale (Wedepohl, 1971). The black circles are the values of the cluster averages.

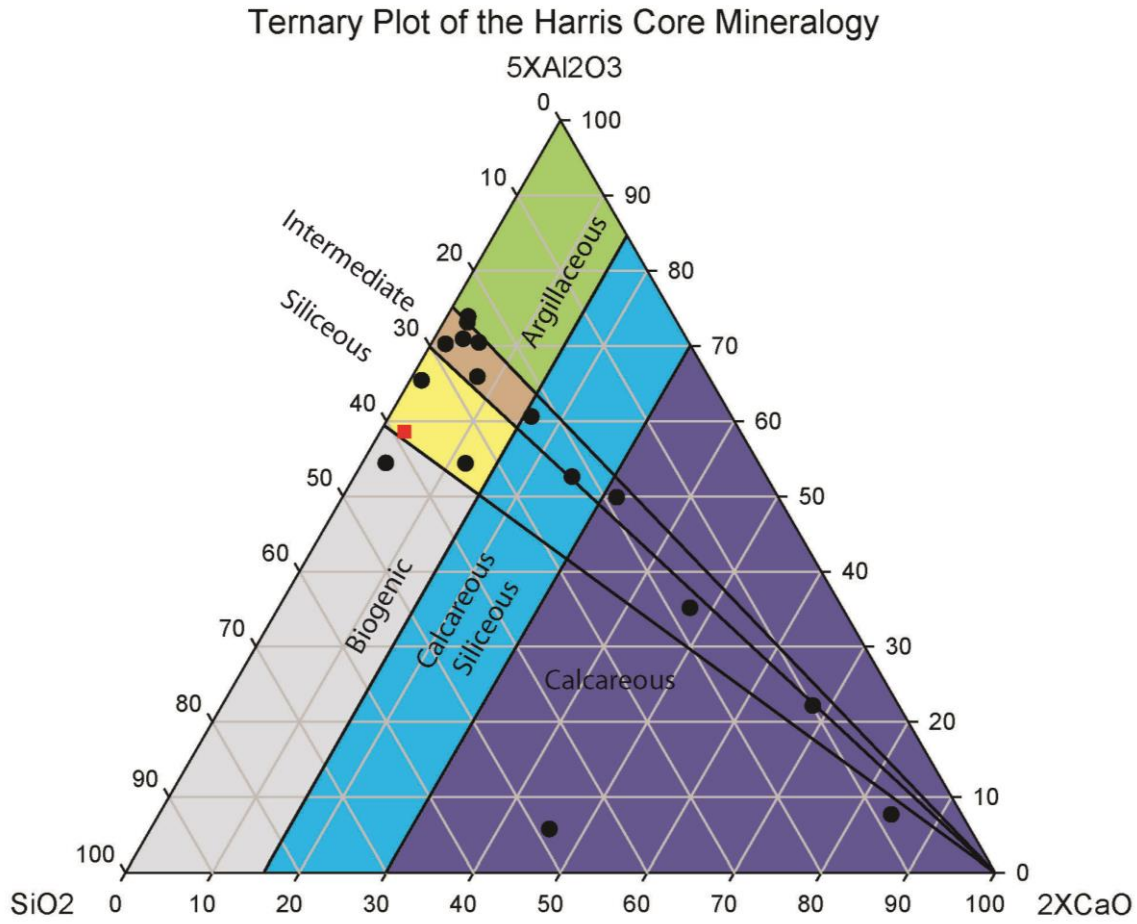

Figure 14: Ternary diagram of the Harris core mineralogy. Elemental oxides are used as proxies for minerals in this case (after Brumsack, 1989). The red square represents the average grey shale (Wedepohl, 1971). The black circles are the values of the cluster averages.

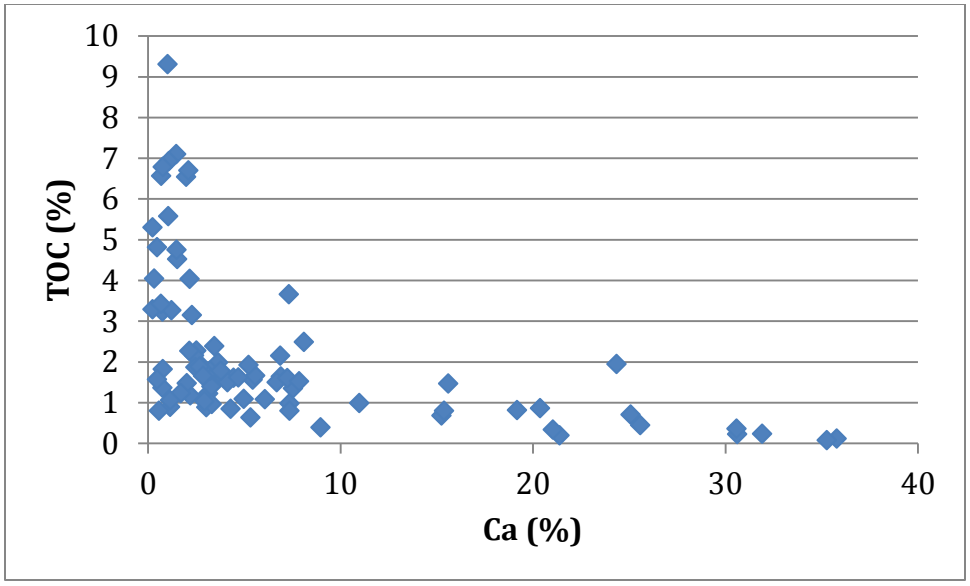

Figure 15: Plot of TOC (%) vs. Ca (%). As calicum increases, TOC decreases significantly.

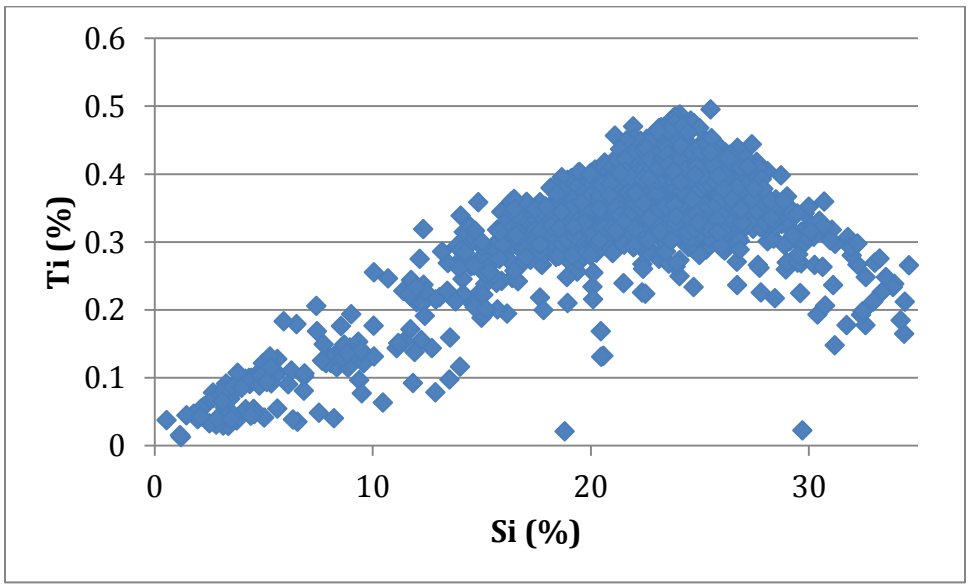

Figure 16: Plot of Ti (%) vs. Si (%). Titanium is always detrital; the sharp bend in the data at 25% Si is a result of biogenic silica being the most dominant type of silica in the system at levels above 25% Si.

Organic matter content is an important aspect of chemofacies distinction because it can be used to distinguish environments of deposition and it can be used to aid in hydrocarbon exploration and development techniques. Organic matter content is a product of a mass balance equation during deposition:

$$\frac{\text{organic matter production- organic matter destruction}}{\text{total rock volume}} = \text{TOC}$$

These three variables are all equally important in determining the organic matter content of a sample. However, organic matter production and destruction can be difficult to isolate. In general, XRF data can yield some insight into the variables of the organic matter equation, but the preconditioned water mass of the Pennsylvanian Midland Basin makes distinguishing the variables of the organic matter mass balance equation difficult. The preconditioned water mass eliminates the ability to discuss the redox state of basin bottom waters—a proxy for the degree of organic matter destruction. Elements that are commonly associated with the hydrogenous fraction of the redox-sensitive trace element (RSTE) input, such as molybdenum, are not enriched in these rocks (Calvert and Pedersen, 2007). Rather, the Cline Shale is enriched in elements such as Ni, Zn, V, Cr, and Co. These elements act as trace nutrients and are incorporated into the organic matter structure, and are therefore proxies for organic matter production (Piper and Calvert, 2009; Piper and Perkins, 2004; Piper, 1994). Distinguishing the influences of organic matter destruction is impossible in the Cline Shale; however, empirical evidence can be used to determine the bulk TOC of each XRF sample by cross plotting TOC and various RSTEs.

Empirical evidence suggests two different redox systems associated with the cores sampled in the basin. The basin-centered cores' TOC and RSTE relationships are different than those in the Harris core. The basin-centered core's best TOC covariables are Ni, Zn, and Co and there is a weak relationship with Mo. The Harris core's best TOC covariables are Ni, Cr, Zn, V, and Co, and there is no relationship to Mo.

The basin-centered wells and the Harris well have to be evaluated for TOC content individually. The RSTEs in these groups are different and produce different results. This is probably due to their different locations with respect to basin paleobathymetry. Cross plots of the relevant RSTEs and TOC were generated, cutoffs were delineated creating three facies; OM-Rich, OM-moderate, and OM-poor (Figure 17). These cutoffs are based on previous work by Boyer et al. (2006) and relate to TOC cutoffs of greater than 2% TOC for OM-rich, between 1% and 2% TOC for OM-moderate, and less than 1% TOC for OM-poor. Using multiple RSTE-TOC cross plots, the RSTE proxy for TOC can be determined and corroborated with multiple RSTE assemblages; providing a robust proxy system for TOC from the XRF data.

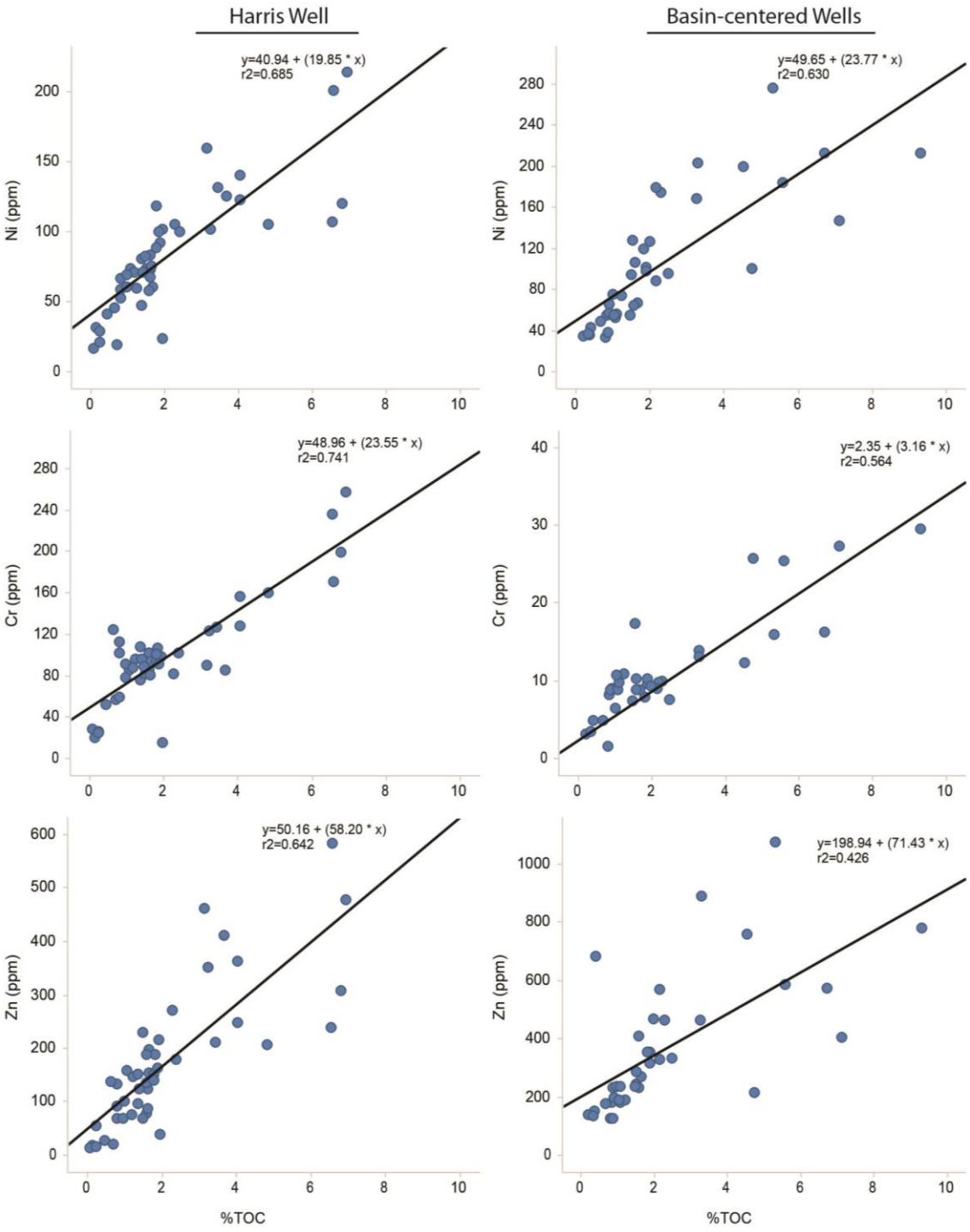
Harris Well
Basin-centered Wells
y=40.94 + (19.85 * x)
r2=0.685
y=49.65 + (23.77 * x)
r2=0.630
y=48.96 + (23.55 * x)
r2=0.741
y=2.35 + (3.16 * x)
r2=0.564
y=50.16 + (58.20 * x)
r2=0.642
y=198.94 + (71.43 * x)
r2=0.426
Ni (ppm)
Cr (ppm)
Zn (ppm)
%TOC

Figure 17: Cross plots of RSTEs vs. TOC. The Harris well and the basin-centered wells exhibit different relative concentrations of RSTEs, and therefore, must be clustered and interpreted separately. Relationships of TOC *versus* Ni, Cr, and Zn are used together to determine elemental proxies for TOC.

VISUAL LOG ANALYSIS

A visual core description was produced for each core. The visual core log has utility in distinguishing carbonate cementation from allochthonous carbonate deposits, discerning important contact surfaces for distinguishing sedimentary processes, and incorporating textures into the facies scheme. The visual core log is important to use in conjunction with the geochemical data to create comprehensive descriptions of the cores. From the four cores, five facies were distinguished; (1) allochthonous rudstone, (2) allochthonous grainstone, (3) allochthonous packstone, (4) microscopic wackestone, (5) mudstone with heavy calcite cement, and (6) mudstone. Each core was described using a hand lens and a low power reflected light microscope. Thin sections from each facies were described to discriminate and fully characterize each facies.

THIN SECTION ANALYSIS

Thin sections were taken from the Powell and Greer cores at exact locations of the XRF data. Each thin section was vacuum impregnated with blue fluorescent dye. These thin sections were used in conjunction with the high-resolution XRF dataset to distinguish textures associated with the geochemically derived facies.

ROCK PROPERTIES DATASET

The rock properties dataset is a comprehensive core-based dataset taken from the basin-centered wells. This dataset comprises of 65 sample locations containing XRD, porosity, permeability, rock-eval pyrolysis, TOC, bulk density, and thin-sections.

X-ray Diffraction (XRD) analyses of the samples were performed using a Siemens D500 automated powder diffractometer equipped with a copper X-ray source (40kV, 30mA) and a scintillation X-ray detector. The whole rock samples were analyzed over an angular range of five to sixty degrees two theta at a scan rate of one degree per minute, and the glycol-solvated oriented clay mounts were analyzed over an angular range of two to thirty six degrees two theta at a scan rate of one degree per minute.

Semiquantitative determinations of whole-rock mineral amounts were done using Jade Software (Materials Data, Inc.) with the Whole Pattern Fitting option. All quantitative data (including clay mineral amounts) come from the whole rock pattern. This was done by using Whole Pattern Fitting (WPF) and Rietveld refinement methods on the observed data. A diffraction model was fit to the measured pattern by non-linear least-square optimization in which certain parameters were varied to improve the fit of the model to the observed data. Modeling parameters included background, profile parameters, and lattice constants. For Rietveld refinement, a complete physics simulation was used in which crystal structures of the phases are required. Since the physics of scattering is well known, this method can be very exact and even allow adjustment of

atomic coordinates, occupancies, and thermal parameters (K-T Geoservices, Inc., personal communication)

Thin sections were prepared by first impregnating them with fluorescent dye spiked, (Columbia Blue by DayGlo Color Corp.), blue epoxy resin using vacuum and high pressure techniques. After initial sample preparation, specimens were mounted to slides using a light cure adhesive. Sections were then cut off and ground to final thickness using water or oil as appropriate. Samples were ground to 20 microns or less, to minimize grain overlap. The thin sections were then stained for calcite and ferroan carbonate minerals with Alizarin Red S and potassium ferricyanide in a 1/2% solution of HCl over 50% of the slide surface. Finally, a temporary cover slip was affixed to each section with Cargille type A immersion oil (Greg Vardilos, personal communication).

TOC was determined from crushed samples by acidifying 0.01g of sample in concentrated hydrochloric acid for a minimum of two hours, drying the sample at 110 degrees C for a minimum of one hour, and finally analyzing the sample with a LECO 600 Carbon Analyzer with detection limits of 0.01 wt. percent.

For rock-eval pyrolysis, the ground samples were heated in an inert environment to measure the S1, S2, and S3 peaks on a pyrogram (Peters, 1986). To obtain these peaks the sample was heated to 300 degrees C for 3 minutes (S1), then heated from 300 degrees C to 600 degrees C at a rate of 25 degrees C per minute and held at 600 degrees for 1 minute (S2), and S3 is trapped during heating between 300 and 390 degrees C.

The bulk density of the samples was measured using mercury immersion by volumetric or weight (Archimedes) displacement. The crushed rock permeability measurements were performed using a pressure decay system. The permeability method was adapted as standard methodology within the GRI crushed shale program. Porosity was determined by helium injection of a dried sample using the Boyle's Law method (Weatherford, description of selected experimental methods, personal communication).

REGIONAL STRATIGRAPHY

Correlation Process

A regional stratigraphic analysis was performed using as suite of over 350 raster logs using Petra (IHS, Inc) for interpretation. The stratigraphy was based primarily on work by Hamlin and Baumgardner (2012) and Brown et al. (1990). Four chronostratigraphic surfaces were delineated and mapped throughout the Midland Basin. The chronostratigraphic surfaces are commonly also lithostratigraphic surfaces. Widespread lithostratigraphic continuity has been documented in the Wolfberry deposits of the Midland Basin by Hamlin and Baumgardner (2012); the principal also applies to the Cline Shale.

Regional cross sections from Hamlin and Baumgardner (2012) were used as a guide for the regional stratigraphic correlation of the top of the Strawn Formation and the top of the Cline Shale surfaces. The top of the Lower Cline was picked with guidance from Tucker Hentz, and is based on correlations on the Eastern Shelf made by Brown et al. (1973, 1990) separating the Canyon and Cisco deposits (top of the Home Creek

Limestone). Chronostratigraphic surfaces on the shelf were correlated to the basin through the slope. However, the correlations contradict the sparse biostratigraphic data provided by Wahlman et al. (in preparation). According to the new biostratigraphic data, the Lower Cline is Missourian (Canyon), the Middle Cline is probably Missourian (Canyon) and Virgillian (Cisco), and the Upper Cline is probably Vigillian (Cisco). The Upper Cline and Middle Cline were separated based on zones of major TOC differences between and high-resolution XRF facies analysis differences in the Harris and the Powell wells (Figure 18).

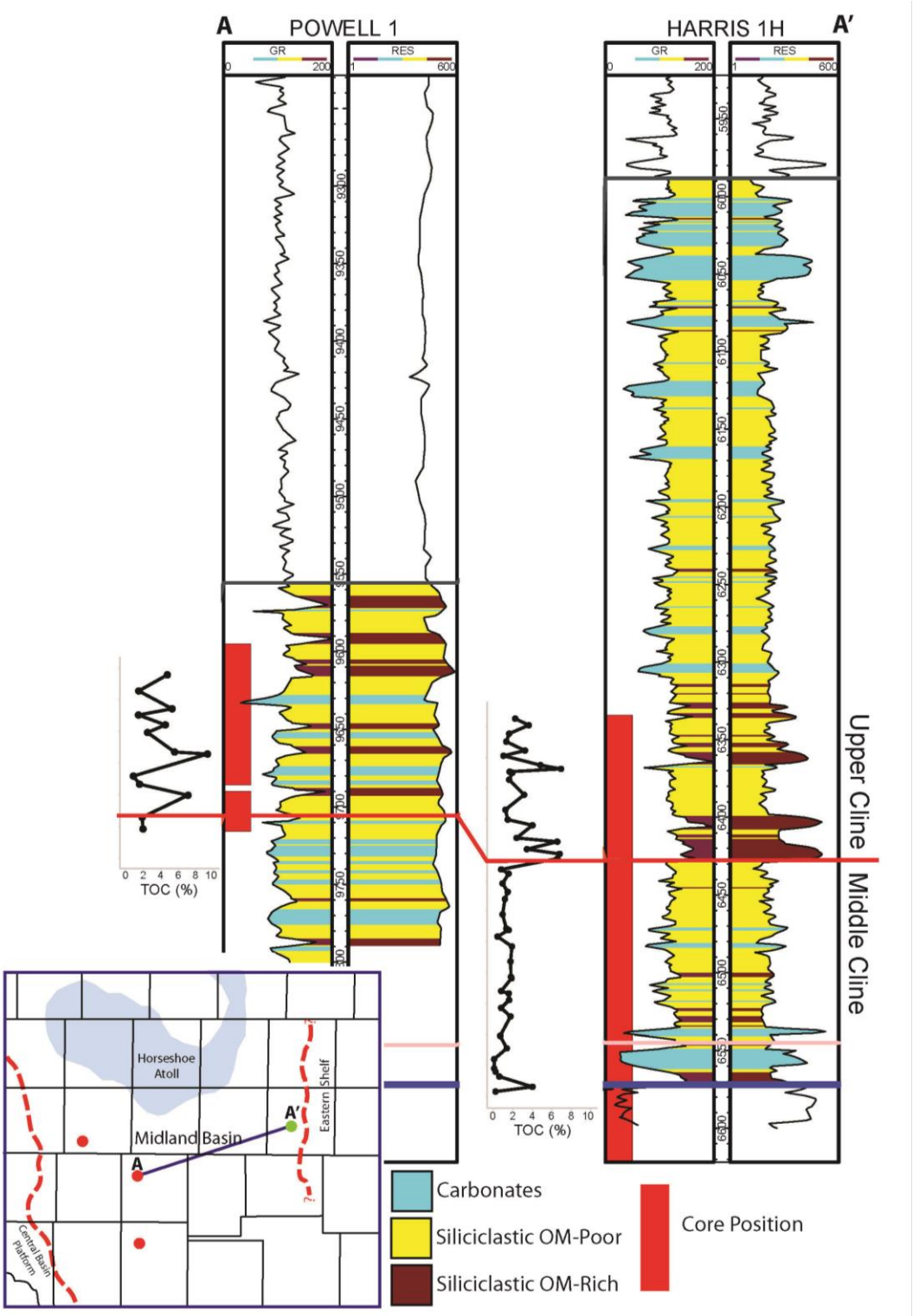
A
POWELL 1
GR
RES
HARRIS 1H
A'
TOC (%)
Upper Cline
Middle Cline
Horseshoe Atoll
Midland Basin
Eastern Shelf
Central Basin Platform
A
A'
Carbonates
Siliciclastic OM-Poor
Siliciclastic OM-Rich
Core Position

Figure 18: Cross section displaying the boundary surface of the Upper Cline and Middle Cline. The surface was initially delineated from an increase of TOC in the Harris core. The surface was mapped using wireline logs throughout the basin, and a similar increase in TOC was denoted in the Powell core. No other cores in this dataset contain this surface.

Structure Contour and Gross Isopach Maps

Structure contour maps and gross isopach maps were generated using the Petra least squares gridding algorithm. Structure contour maps were produced at the top of the Strawn, top of the Lower Cline, top of the Middle Cline, and top of the Upper Cline. The box size used for all of the grids was 2000X2000 feet, with 300X323 grid cells. To generate gross isopach maps, the lower surface of investigation was subtracted from the upper surface of investigation with each unit—this was performed using the isopach from grids tool in Petra.

Core-calibration of Well Logs

Calibrated well-log cutoffs were created using the XRF cluster analysis interpretation as a core-calibration tool of the gamma ray (GR) log (Figure 19). Three lithofacies were delineated from the XRF dataset that translated to the GR log— (1) carbonates, (2) siliciclastic OM-poor, and (3) siliciclastic OM-rich. Breyer (2012) documented sufficient contrast in mineral composition and TOC to affect the gamma ray log in mudrocks. Lüning and Kolonic (2003) discussed the relationship of TOC and uranium as being a very useful tool in conjunction with core calibrations—at high gamma ray values, uranium and by proxy, TOC, is the primary gamma ray influence in the Cline Shale. Carbonates tend to have a lower GR signature than shales and other siliciclastics, especially organic-rich shales (Dominguez and Samaniego, 1992) A caveat of the gamma ray log being used in this manner is the presence of diagenetic uranium in

carbonates (Lucia, 1999). In analyzing sparse spectral gamma ray control, no diagenetic uranium was detected in the Cline Shale.

The carbonates lithofacies consists of all calcareous and calcareous siliceous chemofacies, the siliciclastic OM-poor lithofacies consists of all of the OM-lean and OM-moderate siliciclastic chemofacies, and the siliciclastic OM-rich lithofacies consists of all of the OM-rich siliciclastic and biogenic OM-rich chemofacies.

Variability in wireline well logs is commonplace, where different contractors may produce slightly different log signatures depending on differences in software and tool design. This being the case, great attention must be placed on the logs being used to ensure consistent log signatures. Each gamma ray log was visually selected; older logs and poor quality logs were discarded. Each raster was digitized by the author. The gamma ray log was then normalized to the same minimum and maximum values of 0 to 200 API within the Cline Shale interval, minimizing internal, non-geologic variation. After the maps were computed, they were analyzed visually for non-geologic trends, and each well was visually inspected and discarded if it did not meet quality standards.

Quantitative cutoffs were determined from the data after normalization and quality controls were performed. The lithofacies cutoffs for the gamma ray log are GR<75 API for carbonates, 75<GR<120 API for siliciclastic OM-poor, and GR>120 API for siliciclastic OM-rich. The quantitative cutoff analysis was utilized for the Harris, Greer, and Powell wells (Figure 19). The Glass well was excluded from the analysis because the dataset does not contain a usable gamma ray log for the well (Figure 4). This

cutoff system is effective for two reasons— (1) the system is able to predict the presence of carbonates versus clastics and (2) the system is able to predict areas that are enriched in OM. Both of these reasons are important for proper reservoir development. These lithofacies maps are limited because clay distributions cannot be determined from gamma ray logs alone, a more robust petrophysical model must be utilized.

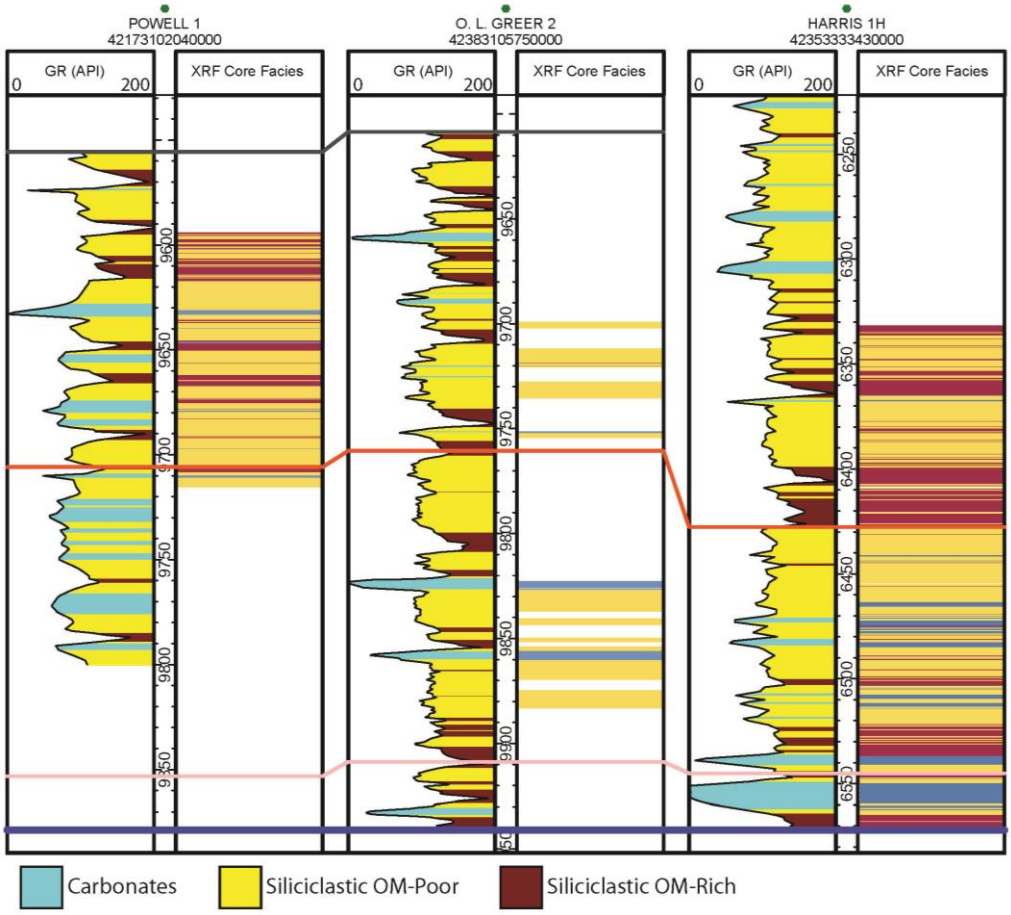

Figure 19: XRF Core facies to GR log cutoff lithofacies calibration. The GR logs were normalized to 0 to 200 API, and quantitative cutoff values were determined for carbonates, siliciclastic OM-poor, and siliciclastic OM-rich lithofacies.

Lithofacies Map Generation

Lithofacies maps were produced within the Cline by using core-calibrated gamma ray cutoffs. These maps are instrumental in evaluating regional lithofacies distributions. To take it a step furthur, four mapsets were created—maps of the Gross Cline, maps of the Lower Cline, maps of the Middle Cline, and maps of the Upper Cline. By separating

the Cline into these distinct chronostratigraphic units, lithofacies distributions were distinguished through time.

For each core-calibrated lithofacies (carbonates, siliciclastic OM-poor, and siliciclastic OM-rich) within each temporal mapset, a net thickness map and a net-to gross-map were produced. The lithofacies distribution maps provide a quick look at regional facies trends. They also provide insight into the sources of siliciclastic-enriched and carbonate-enriched mudrocks as well as distinguishing OM-enriched areas. For this, net footages and net-to-gross values of each lithofacies within all four intervals were computed within Petra. These values were then gridded with Petra using the least squares gridding algorithm and grid cell size of 2000X2000 feet with 300X323 box grid cells.

Regional Cross Sections

Regional cross sections were generated to display the variability associated with the Cline deposits. Three east-west sections and three north-south sections were created. Each cross section displays the Lower Cline, Middle Cline, and Upper Cline contacts as well as the same core-calibrated lithofacies cutoffs as the facies distribution maps.

Composite lithofacies Distribution Maps

Composite lithofacies distribution maps were synthesized utilizing individual lithofacies distribution maps. Cutoffs were mapped from the net-to-gross lithofacies maps to create the composite maps; greater than 0.6 net-to-gross siliciclastic OM-poor

deposits were mapped, greater than 0.4 net-to-gross Carbonate deposits were mapped, and greater than 0.2 net-to-gross siliciclastic OM-rich deposits were mapped. The cutoffs were based on facies distribution lithofacies cutoffs that denoted enrichment in that lithofacies. These composite facies distribution maps can be utilized to discuss regional lithofacies heterogeneity through the Canyon, Lower Cisco, and Upper Cisco, as well as delineate source areas and their dominant sediment types.

Results

HIGH-RESOLUTION XRF ANALYSIS

From the high-resolution XRF analysis, fourteen geochemically derived facies were distinguished. Each chemofacies has its own intrinsic properties and was based on mineralogy and organic matter content.

Chemofacies

Argillaceous OM-Lean

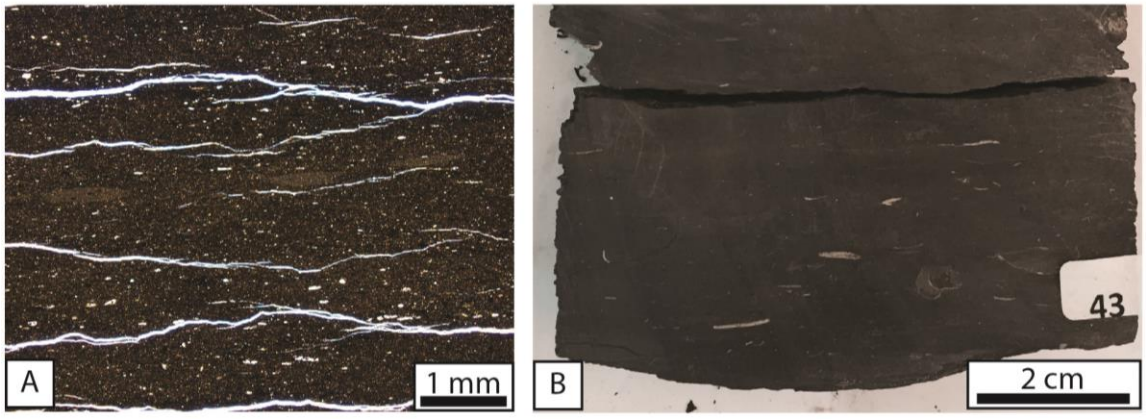

Figure 20: Photographs of the argillaceous OM-lean chemofacies.

(A) Photomicrograph containing recrystallized calcareous fragments, agglutinated foraminifera, and aligned clays, Greer Well, 9860.9'; (B) Slabbed core photo showing rare calcareous allochems in a dark matrix, Powell Well, 9617.6'.

The argillaceous OM-lean chemofacies is defined geochemically as XRF clusters that contain, in a ternary system, less than 16% 2XCaO, a SiO_2 to $5XAl_2O_3$ ratio of less than 0.33 (represented by a calcium dilution line), and TOC of less than 1%. The average mineralogy of the argillaceous OM-lean chemofacies is 27.3% quartz, 21.6% kaolinite

and illite, 22.6% calcite and dolomite, and 28.5% other minerals. Argillaceous OM-lean samples only occur in the basin-centered cores, and they are 6.3% of the total samples taken from all of the cores.

The chemofacies is commonly a mudrock in hand sample; there are rarely distinguishable depositional features seen with a hand lens and rare allochems (Figure 20). In thin section, the facies contains abundant agglutinated foraminifera and common uniserial foraminifera and calcareous fragments. There are rare phosphatic grains and ostracods and common burrows present as well. Burrows are a qualitative proxy for organic matter destruction—generally the greater the burrow abundance, the less OM remains in the deposits.

Argillaceous OM-Moderate

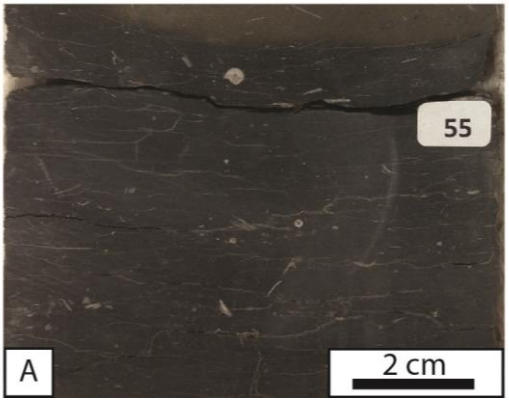

Figure 21: Photograph of argillaceous OM-moderate chemofacies.

(A) Slabbed core photo showing rare to common calcareous allochems in a dark matrix with no distinguishable depositional features.

The argillaceous OM-moderate chemofacies is defined geochemically as XRF clusters that contain, in a ternary system, less than 16% 2XCaO, a SiO_2 to $5XAl_2O_3$ ratio of less than 0.33 (represented by a calcium dilution line), and TOC of 1-2%. The average mineralogy of the argillaceous OM-moderate chemofacies is 32.9% quartz, 23.7% kaolinite and illite, 20.1% calcite and dolomite, and 23.3% other minerals. Argillaceous OM-moderate samples only occur in the Harris core, and they are 8.2% of the total samples taken from all of the cores.

Argillaceous OM-moderate mudrocks are mudstones to packstones in hand sample with common bivalves and crinoids (Figure 21). There are few depositional features in this chemofacies besides thin (cm scale) dilute debris flows.

Biogenic OM-Rich

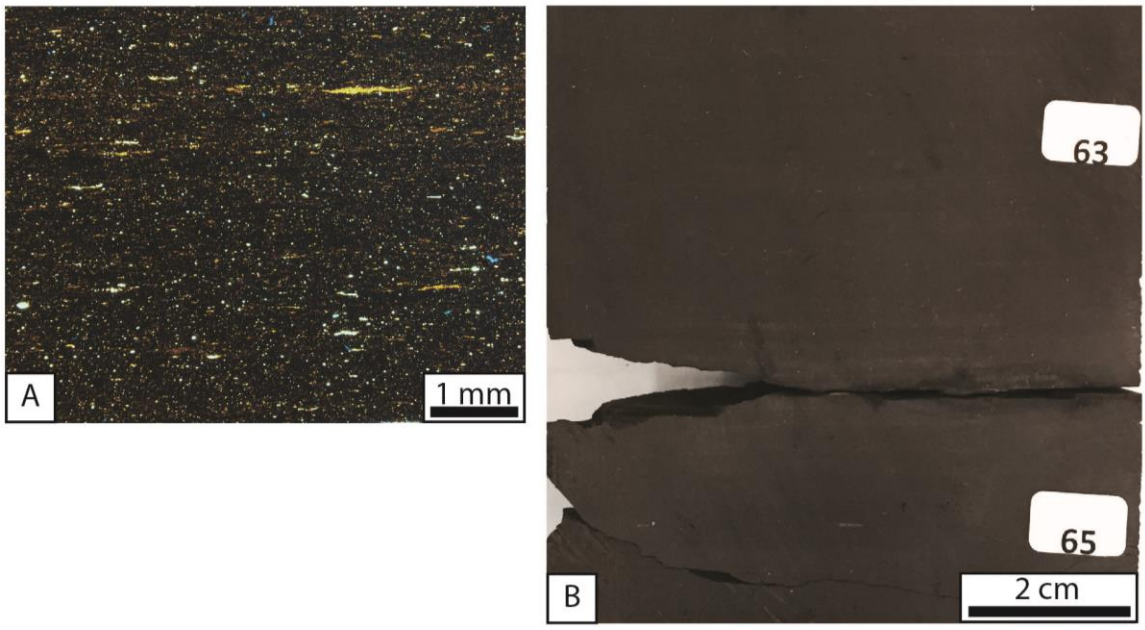

Figure 22: Photographs of the biogenic OM-rich chemofacies.

(A) Photomicrograph containing common 0.1 to 0.2 mm long agglutinated foraminifera, and less than 1 mm long aligned clay floccules, Powell Well, 9614.3'; (B) Slabbed core sample containing a distinct lack of macroscopic carbonate debris, Powell Well, 9606.3.

The biogenic OM-rich chemofacies is defined geochemically as XRF clusters that contain, in a ternary system, less than 16% 2XCaO, a SiO_2 to $5XAl_2O_3$ ratio of greater than 0.72 (represented by a calcium dilution line), and TOC of more than 2%. The average mineralogy of the biogenic OM-rich chemofacies is 45.4% quartz, 15.5% kaolinite and illite, 19.2% calcite and dolomite, and 19.9% other minerals. Biogenic OM-rich samples occur in both the Harris core and the Powell core, and they are 2.4% of the total samples taken from all of the cores. The chemofacies occurs in distinct zones on the order of a foot thick where present.

The biogenic OM-rich chemofacies is a mudstone in hand sample, with no visible allochems to the naked eye, and a lack of internal depositional features (Figure 22). In thin section, the chemofacies contains abundant agglutinated foraminifera and aligned clays. The chemofacies is very dark in thin section, probably from the concentrated OM in the sample.

Calcareous Siliceous OM-Lean

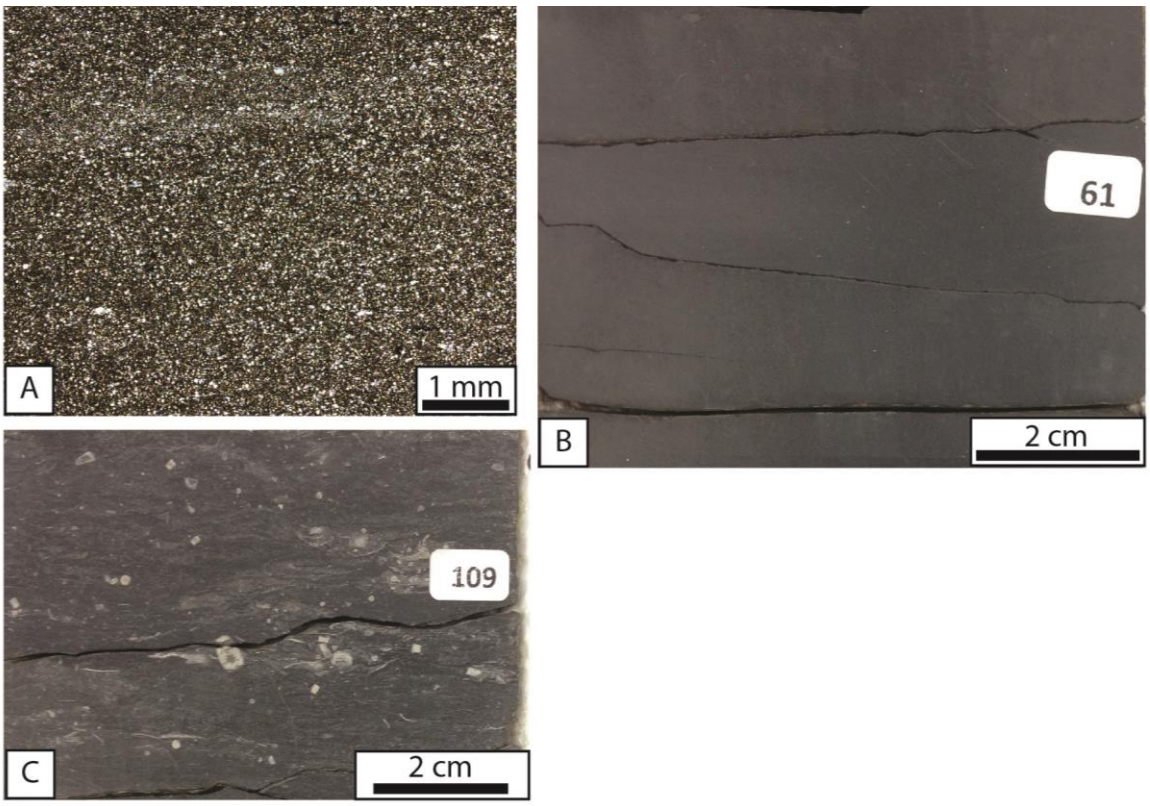

Figure 23: Photographs of the calcareous siliceous OM-lean chemofacies.

(A) Photomicrograph displaying ankerite crystals in a mud matrix, Greer Well, 9859.8'; (B) Slabbed core photo showing a sample similar to that of "A", with considerable carbonate input from diagenetic recrystallization, Harris Well,

6427.1'; (C) Slabbed core photo showing a carbonate debris flow, Harris Well, 6481.1'.

The calcareous siliceous OM-lean chemofacies is defined geochemically as XRF clusters that contain, in a ternary system, between 16% and 30% 2XCaO and TOC of less than 1%. The average mineralogy of the calcareous siliceous OM-lean chemofacies is 20.6% quartz, 16.7% kaolinite and illite, 42.6% calcite and dolomite, and 20.1% other minerals. Calcareous siliceous OM-lean samples occur in the Harris core, Powell core, and Greer core, and they are 3.8% of the total samples taken from all of the cores.

The calcareous siliceous OM-lean chemofacies can occur as a semi-concentrated debris flow, where allochthonous allochems makeup the large carbonate content, or as a recrystallized microspar or ankerite crystals (Figure 23). In the former instance, the hand sample is quite distinguishable, as there are common bivalves and crinoids and horizontal bedding features. The latter example has no distinguishable features in hand sample, other than the generally lighter color from the ankerite. In thin section, the recrystallized microspar is random, and it is floating in a clay-rich matrix.

Calcareous Siliceous OM-Moderate

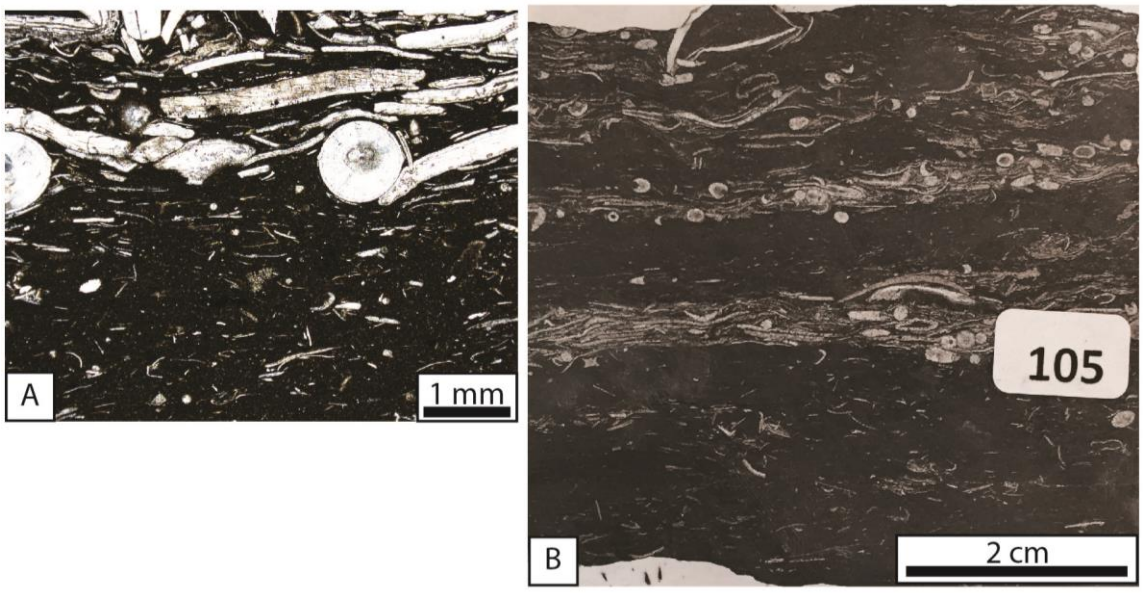

Figure 24: Photographs of the calcareous siliceous OM-moderate chemofacies.

(A) Photomicrograph of a bivalve, belemnite, and shell fragment debris flow, Powell Well, 9631.8'; (B) Slabbed core photo showing the same debris flows from "A". The debris flows are interbedded with high-OM mudrocks.

The calcareous siliceous OM-moderate chemofacies is defined geochemically as XRF clusters that contain, in a ternary system, between 16% and 30% 2XCaO and TOC between 1% and 2%. The average mineralogy of the calcareous siliceous OM-lean chemofacies is 24.4% quartz, 14.9% kaolinite and illite, 40.9% calcite and dolomite, and 19.8% other minerals. Calcareous siliceous OM-moderate samples occur only in the basin-centered cores; they represent 0.6% of the total samples taken from all of the cores.

The calcareous siliceous OM-Moderate chemofacies is rare. The texture of the facies is interbedded (cm scale) debris flows with organic-rich mudrock (Figure 24). In this case, the debris flow was sampled with the XRF gun. The XRF is evenly spaced, and

moving the XRF gun a centimeter above or below the sample location would result in a completely different elemental assemblage—this is a rare case where the heterogeneity of the rock is greater than the sampling rate of the XRF data. There are common horizontal lamina approximately one centimeter thick. The debris flows contain common bivalves, belemnites, and other fossil fragments.

Calcareous OM-Lean

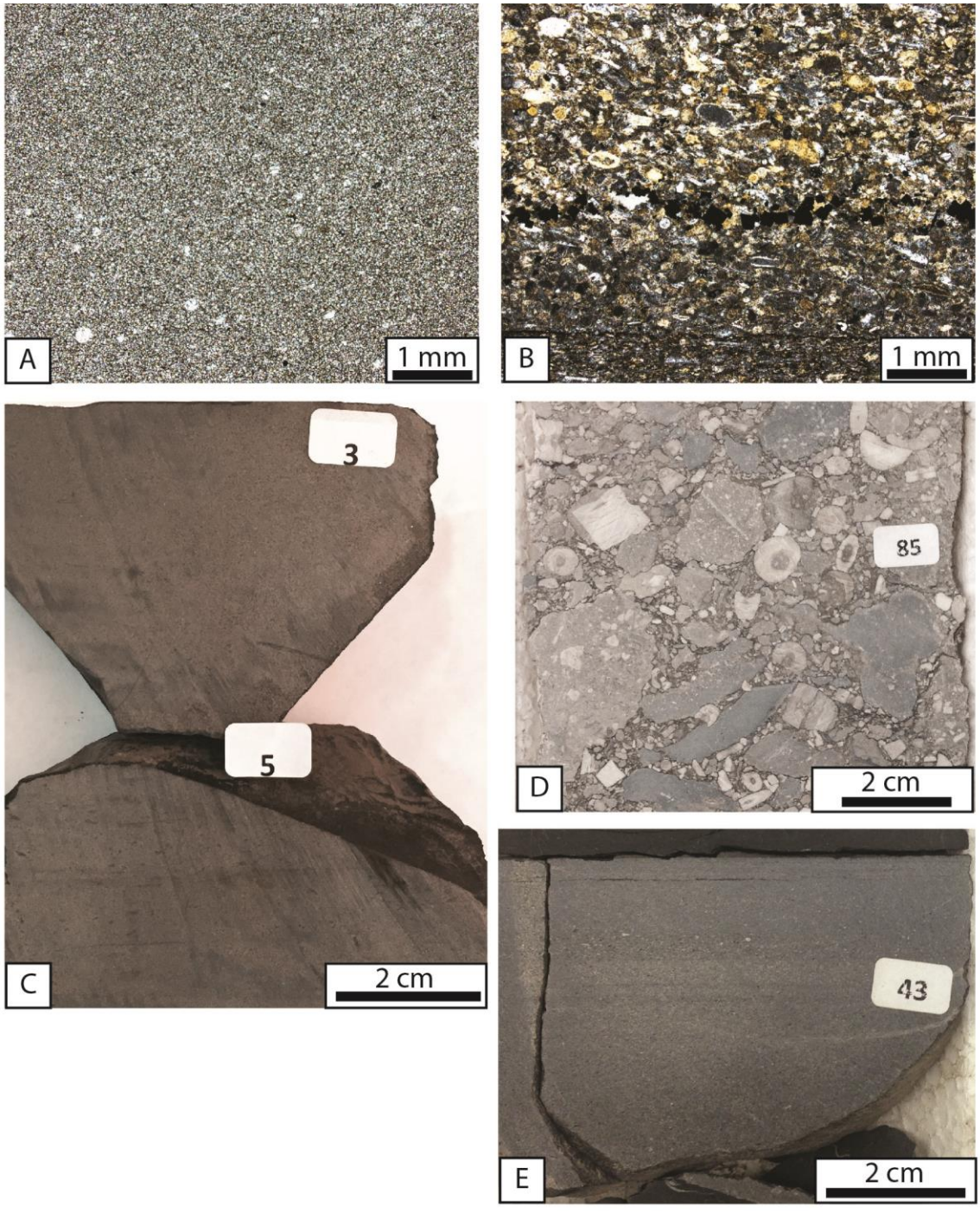

Figure 25: Photographs of the calcareous OM-lean chemofacies.

(A) Photomicrograph containing a subhedral ankerite microspar with recrystallized calcispheres, Greer Well, 9825.0'; (B) Photomicrograph containing a contourite with concentrated calcareous microfossils and a band of euhedral pyrite, there is a sharp contact near the base of the photomicrograph that separates two distinctly sized assemblages of allochems, Greer Well, 9718.1'; (C) Slabbed core photograph of recrystallized facies similar to "A". (D) Encrinite rudstone near the base of the Harris Well, 6561.1';(E) Slabbed core photo of a fine-grained contourite with faint, planar internal bedding and a sharp contact at the top.

The calcareous OM-lean chemofacies is defined geochemically as XRF clusters that contain, in a ternary system, more than 30% 2XCaO and TOC of less than 1%. The average mineralogy of the calcareous OM-lean chemofacies is 8.9% quartz, 9.6% kaolinite and illite, 62.1% calcite and dolomite, and 19.4% other minerals. Calcareous OM-lean samples occur all of the cores that were studied, and they constitute 6.2% of the total samples taken from all of the cores.

The calcareous OM-lean chemofacies has many morphologies. The facies can be an allochthonous rudstone or grainstone, a contourite, or a mudrock with recrystallized ankerite cement (Figure 25). The concentrated debris flows rarely show sorting or internal bedding features, though they are readily distinguishable in core. The contourites are also quite distinguishable in hand sample; they are generally less than 1 foot thick, commonly have internal bedding features, and have distinct, abrupt contacts. The ankerite recrystallized mudstone is much more difficult to assess in hand sample, as the only difference from that of a siliciclastic mudrock is that it is lighter in color and macroscopic allochems are uncommon.

Intermediate OM-Lean

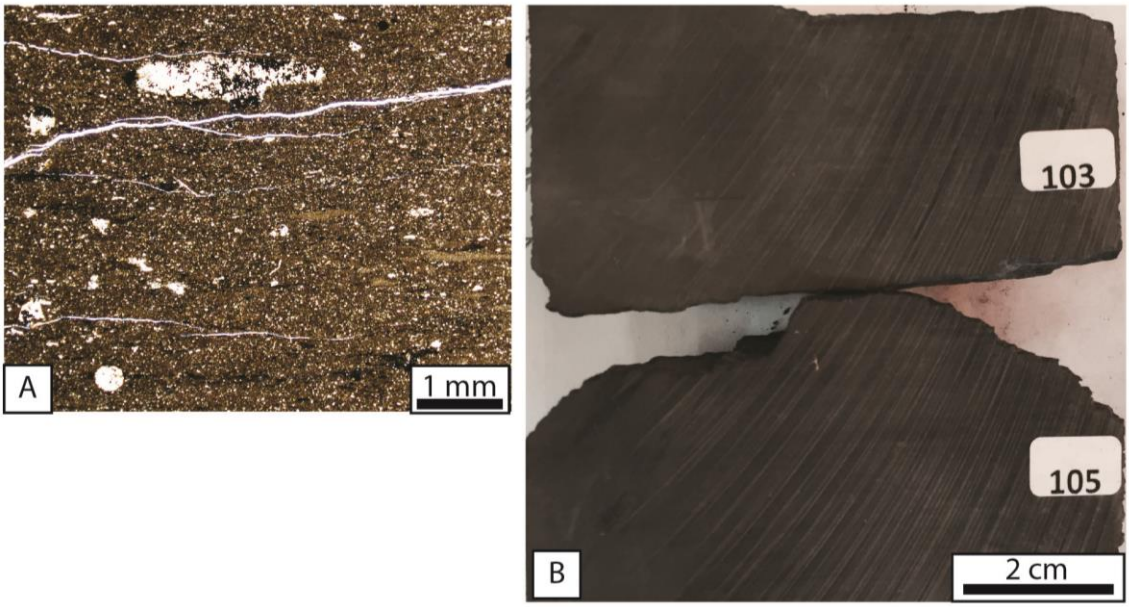

Figure 26: Photographs of the intermediate OM-lean chemofacies.

(A) Photomicrograph containing a bryozoan crinoid wakestone, showing replacement of crinoid allochems with heavy minerals. Clays are mostly aligned, Greer Well, 9855.5'; (B) Slabbed core photo of an allochem-free interval of the intermediate OM-lean facies. There are no discernible features in hand sample from this photo, Powell Well, 9683.7'.

The intermediate OM-lean chemofacies is defined geochemically as XRF clusters that contain, in a ternary system, less than 16% 2XCaO, a SiO_2 to $5XAl_2O_3$ ratio between 0.33 and 0.43 (represented by calcium dilution lines), and TOC of less than 1%. The average mineralogy of the intermediate OM-lean chemofacies is 26.3% quartz, 19.3% kaolinite and illite, 25.1% calcite and dolomite, and 29.3% other minerals. Intermediate OM-lean samples occur in all three of the basin centered wells, and they are 6.9% of the total samples taken from all of the cores.

The intermediate OM-lean chemofacies has common crinoids and bivalves in thin section (Figure 26). The allochems are partially replaced by heavy minerals and poorly imbricated. There are rare to common horizontal burrows present and poorly aligned clays. In hand sample, the facies is a mudrock to wackestone with rare discernible allochems.

Intermediate OM-Moderate

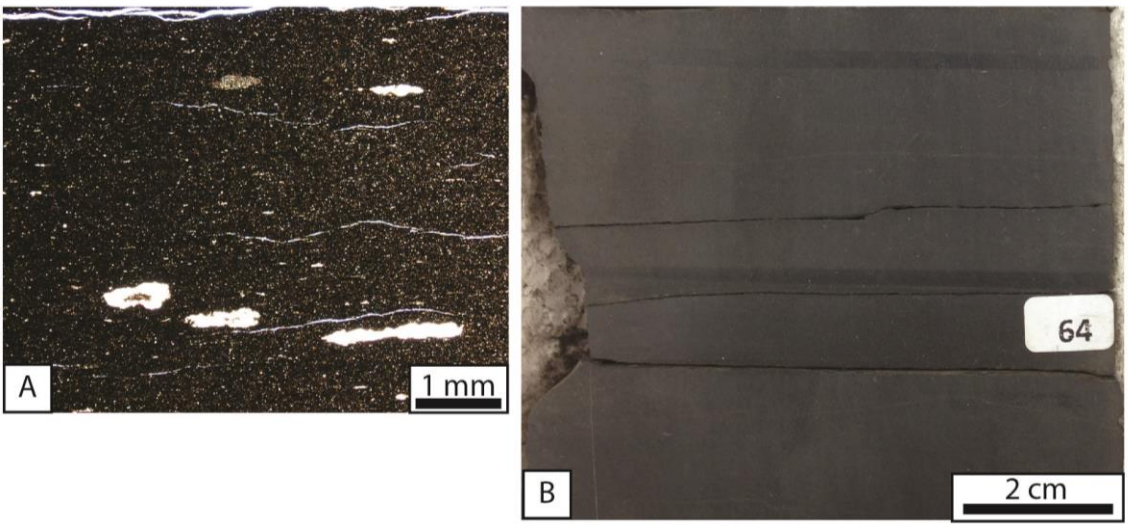

Figure 27: Photographs of the intermediate OM-moderate chemofacies.

(A) Photomicrograph showing large aligned agglutinated foraminifera tests and aligned clays, Greer Well, 9731.9'; (B) Slabbed core sample of the facies with no visible allochems. There are two visible horizontal nodular facies in the photo; one near the top and the other just above the 64 sticker, Harris Well, 6427.3'.

The intermediate OM-moderate chemofacies is defined geochemically as XRF clusters that contain, in a ternary system, less than 16% 2XCaO, a SiO_2 to $5XAl_2O_3$ ratio between 0.33 and 0.43 (represented by calcium dilution lines), and TOC of between 1% and 2%. The average mineralogy of the intermediate OM-moderate chemofacies is

31.1% quartz, 20.5% kaolinite and illite, 24.8% calcite and dolomite, and 23.6% other minerals. Intermediate OM-moderate samples occur in all of the cores, and they comprise 35.1% of the total samples taken from all of the cores. The intermediate OM-moderate chemofacies is the most common facies among the dataset.

The intermediate OM-moderate chemofacies contains rare allochems in hand sample and is usually a mudstone (Figure 27). The chemofacies contains large imbricated agglutinated foraminifera, and rare burrows in thin section. The clays are poorly aligned.

Intermediate OM-Rich

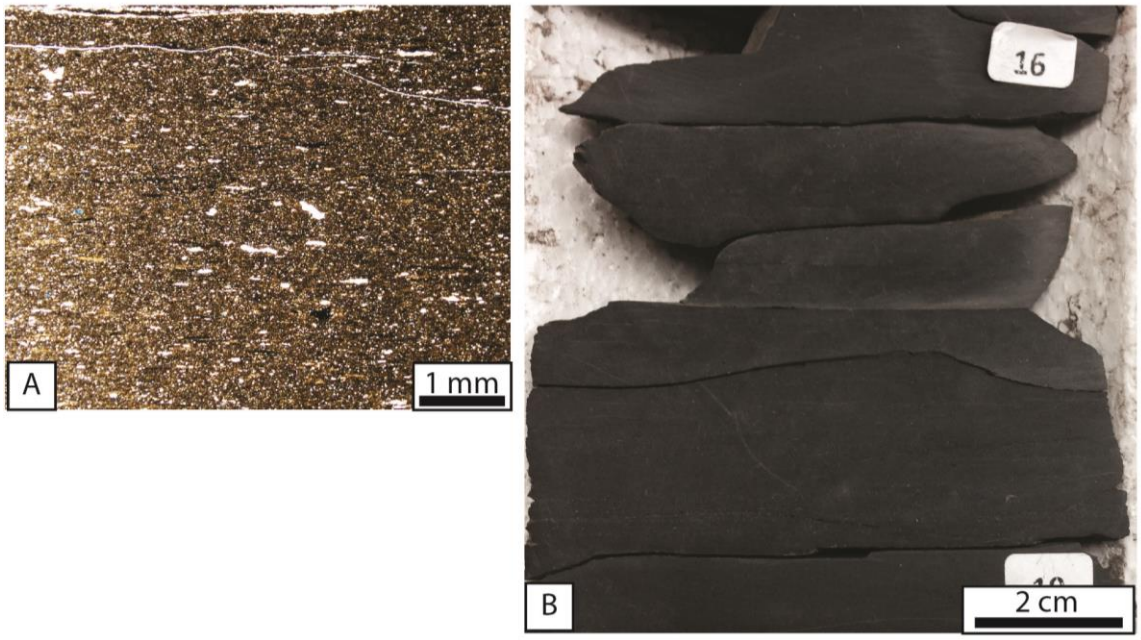

Figure 28: Photographs of the intermediate OM-rich chemofacies.

(A) Photomicrograph containing poorly aligned, less than 0.5 mm in length agglutinated foraminifera and aligned clays, Harris Well, 6362.8'; (B) Slabbed

Core photo of the facies with no distinguishable features present, Harris Well, 6574.5'.

The intermediate OM-rich chemofacies is defined geochemically as XRF clusters that contain, in a ternary system, less than 16% 2XCaO, a SiO_2 to $5XAl_2O_3$ ratio between 0.33 and 0.43 (represented by calcium dilution lines), and TOC greater than 2%. The average mineralogy of the intermediate OM-rich chemofacies is 33.8% quartz, 21.2% kaolinite and illite, 20.0% calcite and dolomite, and 25.0% other minerals. Intermediate OM-rich samples occur in all of the cores; although they are much more common in the Harris core than the basin-centered cores. The chemofacies comprises 13.0% of the total samples taken from all of the cores; this is the second most common chemofacies in the dataset.

The intermediate OM-rich chemofacies is an indistinguishable mudstone in hand sample. In thin section, the chemofacies has abundant small agglutinated foraminifera and well aligned clays (Figure 28).

Siliceous OM-Lean

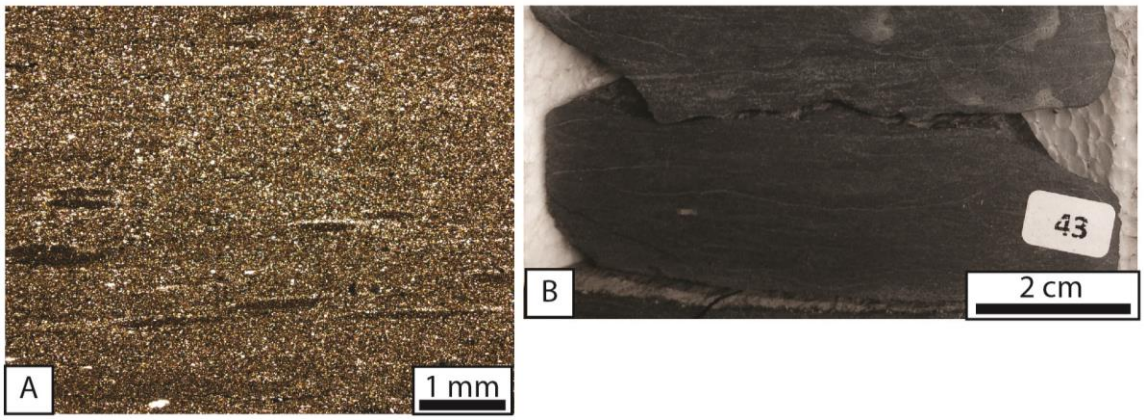

Figure 29: Photographs of the siliceous OM-lean chemofacies.

(A) Photomicrograph displaying abundant silica grains, and common burrows, Greer Well, 9834.8'; (B) Slabbed core photo showing light streaks (zones of very high silica content) within the darker mudrock host, Harris Well, 6566.6'.

The siliceous OM-lean chemofacies is defined geochemically as XRF clusters that contain, in a ternary system, less than 16% 2XCaO, a SiO_2 to $5XAl_2O_3$ ratio between 0.43 and 0.72 (represented by calcium dilution lines), and TOC less than 1%. The average mineralogy of the siliceous OM-lean chemofacies is 33.0% quartz, 17.1% kaolinite and illite, 28.5% calcite and dolomite, and 21.4% other minerals. Siliceous OM-lean samples occur in all of the cores; the facies comprises 3.8% of the total samples taken from all of the cores.

The siliceous OM-lean chemofacies is distinguished in hand sample as a microscopic wackestone (Figure 29). The microscopic grains are lenses of detrital quartz. In hand sample, the chemofacies has rare fossiliferous allochems, and contains

abundant horizontal burrows. In thin section, lamina of increased detrital quartz grains are apparent with abundant horizontal burrows.

Siliceous OM-Moderate

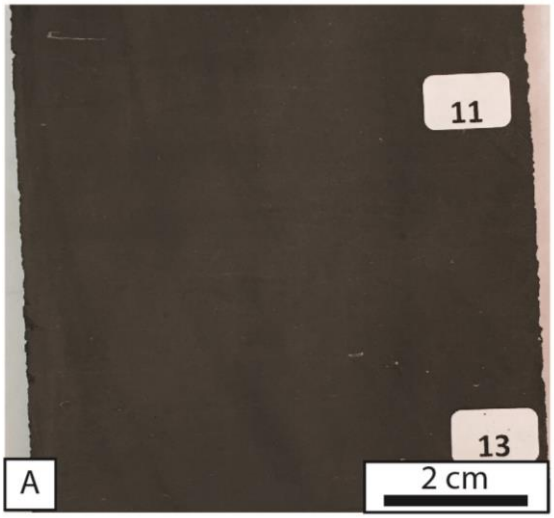

Figure 30: Photograph of the siliceous OM-moderate chemofacies.

(A) Core slab photograph showing absence of internal features and the rare calcareous allochems visible in hand sample for this facies, Powell Well, 9602.1'.

The siliceous OM-moderate chemofacies is defined geochemically as XRF clusters that contain, in a ternary system, less than 30% 2XCaO, a SiO_2 to $5XAl_2O_3$ ratio between 0.43 and 0.72 (represented by calcium dilution lines), and TOC between 1% and 2%. The average mineralogy of the siliceous OM-moderate chemofacies is 30.9% quartz, 18.0% kaolinite and illite, 23.2% calcite and dolomite, and 27.9% other minerals. Siliceous OM-moderate samples occur in the basin-centered cores only; the chemofacies comprises 5.5% of the total samples taken from all of the cores.

Siliceous OM-moderate samples are indistinguishable from many other geochemically derived facies in hand sample (Figure 30). The facies is dark mudrock with rare fossiliferous allochems.

Siliceous OM-Rich

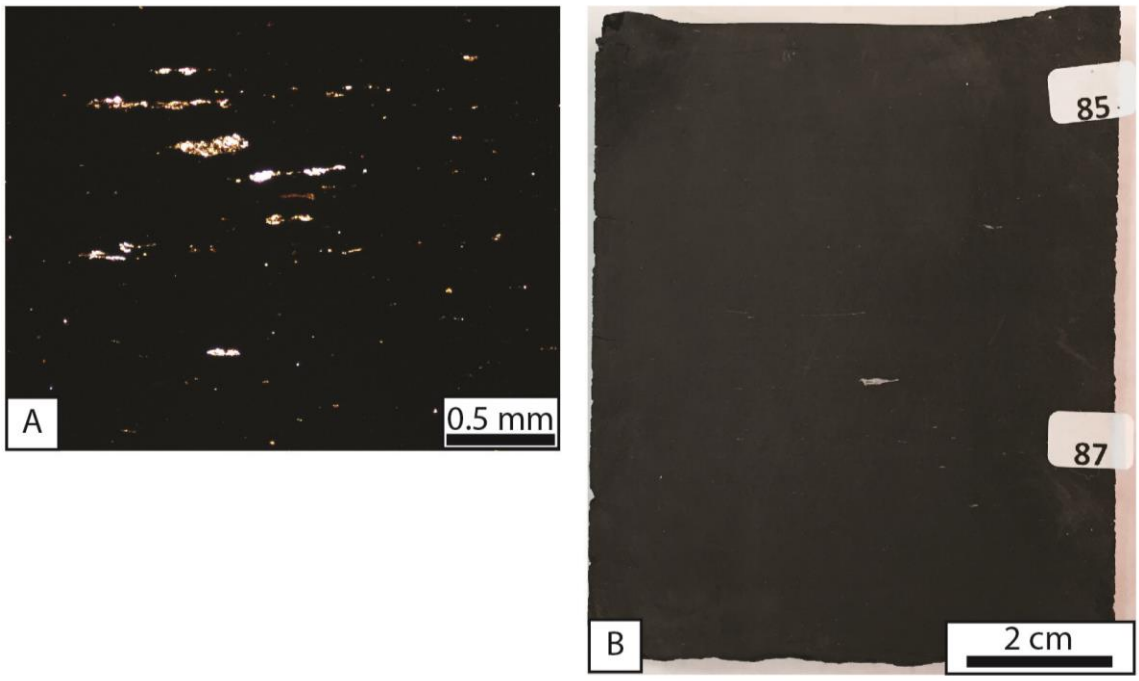

Figure 31: Photographs of the siliceous OM-rich chemofacies.

(A) Photomicrograph containing aligned agglutinated foraminifera in a very dark matrix, Powell Well, 9661.3'; (B) Slabbed core photo showing the dark matrix and rare calcareous allochems, Powell Well, 9604.2'.

The siliceous OM-rich chemofacies is defined geochemically as XRF clusters that contain, in a ternary system, less than 30% 2XCaO, a SiO_2 to $5XAl_2O_3$ ratio between 0.43 and 0.72 (represented by calcium dilution lines), and TOC greater than 2%. The average mineralogy of the siliceous OM-moderate chemofacies is 36.9% quartz, 19.2%

kaolinite and illite, 19% calcite and dolomite, and 24.9% other minerals. Siliceous OM-rich samples occur in all of the cores, but the chemofacies is most common within the Upper Cisco portion of the section. The chemofacies comprises 7.7% of the total samples taken from all of the cores.

The siliceous OM-rich facies is a mudrock with rare allochems in hand sample, making it nearly indistinguishable from other chemofacies (Figure 31). In thin section, the matrix is very dark and indistinguishable; there are common agglutinated foraminifera and rare shell fragments.

Nodule

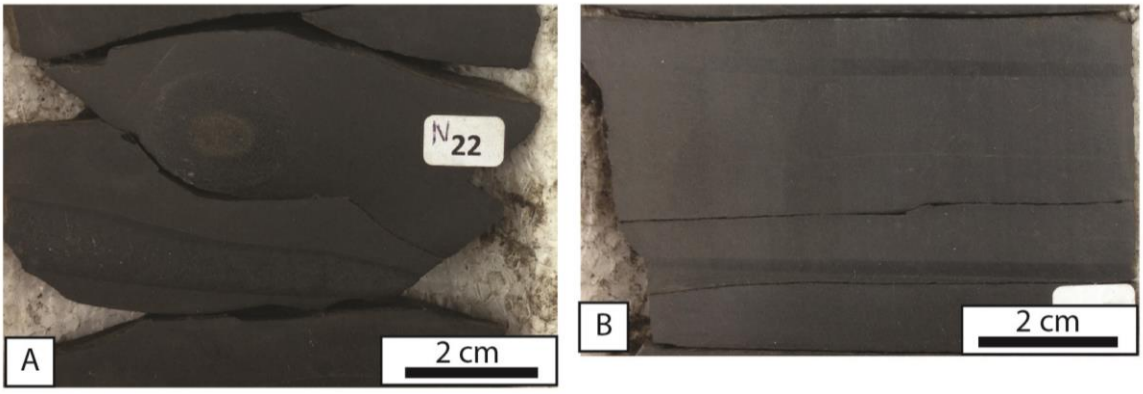

Figure 32: Photographs of the nodule chemofacies.

(A) Slabbed core photo of a rounded nodule with a pyrite-dominated core and a slightly elongated nodule below, Harris Well, 6423.9'; (B) Slabbed core photo of elongate horizontal nodules, Harris Well, 6427.3'.

The nodule chemofacies is defined both geochemically and visually. The nodules do not plot on the traditional ternary diagram. Most of the nodules are phosphatic; the exception being one sample with high cobalt concentrations. The facies is easily

distinguished visually in the core as nodules. They occur in all of the cores, but they are most abundant in the Harris and Powell cores. Nodules comprise of 0.5% of the total sample set; making them the most insignificant facies in distribution.

The nodule chemofacies is readily distinguishable in hand sample (Figure 32). They are commonly spherical, elliptical, or lenticular. Nodules are commonly smaller in thickness than the resolution of XRF investigation (2 to 3 inches). Visual recognition of the nodule facies is important with regards to chemofacies association because it typically occurs near OM-rich facies.

Stratigraphic Chemofacies Distribution from Core

Investigating chemofacies distributions and chemofacies stacking patterns is an important asset to building a stratigraphic architecture. To do this, we can take a one-dimensional look at the chemofacies in each core and compare to the other cores in the basin. A facies key was developed for both the geochemically derived chemofacies and visual log facies (Figure 33). Each chemostratigraphic plot has four columns: the first column is the visual log, the second Colum is the chemostratigraphic log, the third column is the chemostratigraphic log sorted by mineralogy, and the fourth column is the chemostratigraphic log sorted by OM content (Figures 34-37). The visual, mineralogical, OM variations can be assessed readily using all four columns together.

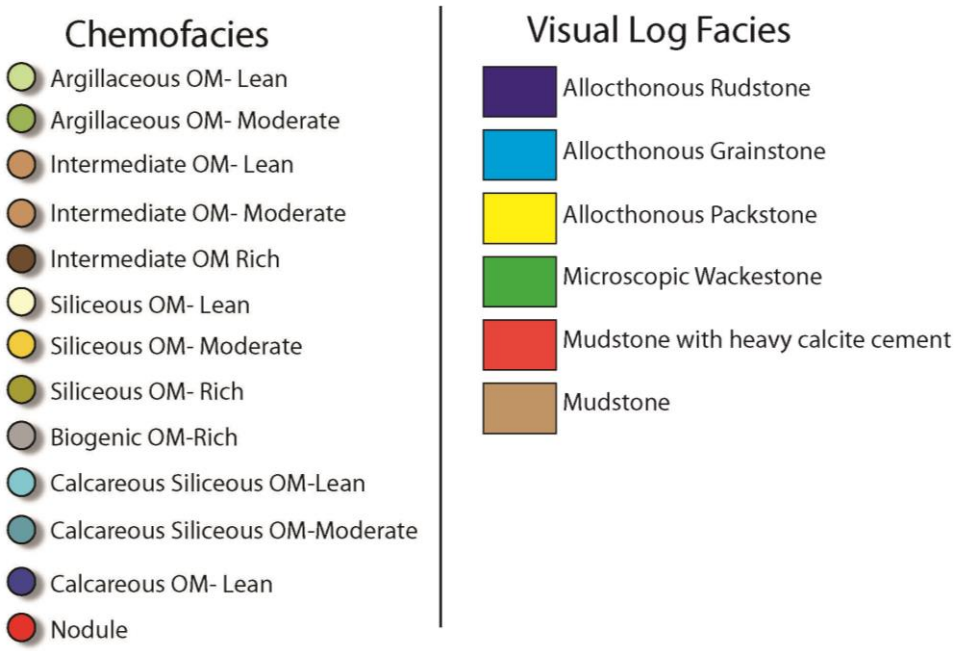

Figure 33: Geochemical facies and visual log facies keys.

Harris Core

The Harris core is the most complete Cline core in this dataset (Figure 34). The core includes all of the Lower and Middle Cline sections, and is missing only the top quarter of the basinal Upper Cline section. This core is also important for comparing to the other cores because it is from the eastern margin of the basin, whereas the other cores are located near the basin axis (Figure 1).

The Lower Cline section of the Harris well is dominated by allochthonous carbonates and organic-rich intermediate chemofacies, and it is punctuated by siliceous chemofacies. The section is 45 feet in thickness. The carbonate and siliceous

chemofacies are OM-lean. This basal section contains the thickest and cleanest carbonate deposits of the dataset, and it contains an eight-foot, predominantly crinoid rudstone. These deposits are interbedded with intermediate OM-rich chemofacies.

The Middle Cline section of the Harris well is characterized by a vertical succession grading from OM-rich intermediate chemofacies to OM-moderate argillaceous chemofacies with common carbonate and carbonate siliceous components. The carbonaceous chemofacies are concentrated into three horizons in the Middle Cline section. The unit is about 110 feet thick. There is about a foot of OM-poor siliceous rocks near the base of the section. However, siliceous chemofacies do not exist throughout the rest of the section.

The Upper Cline consists of cycles of OM-rich siliceous, biogenic, and intermediate chemofacies grading into OM-moderate argillaceous chemofacies. The Harris core does not contain the top 30 feet of the basinal Cline section, but the cored section of the Upper Cline is 95 feet thick. The base of the unit consists of a biogenic siliceous unit that is anomalously high in TOC. The OM-rich clusters at the base of the Upper Cline also contain common phosphate nodules. Carbonate chemofacies are rare in the section. However, there are thin carbonate deposits.

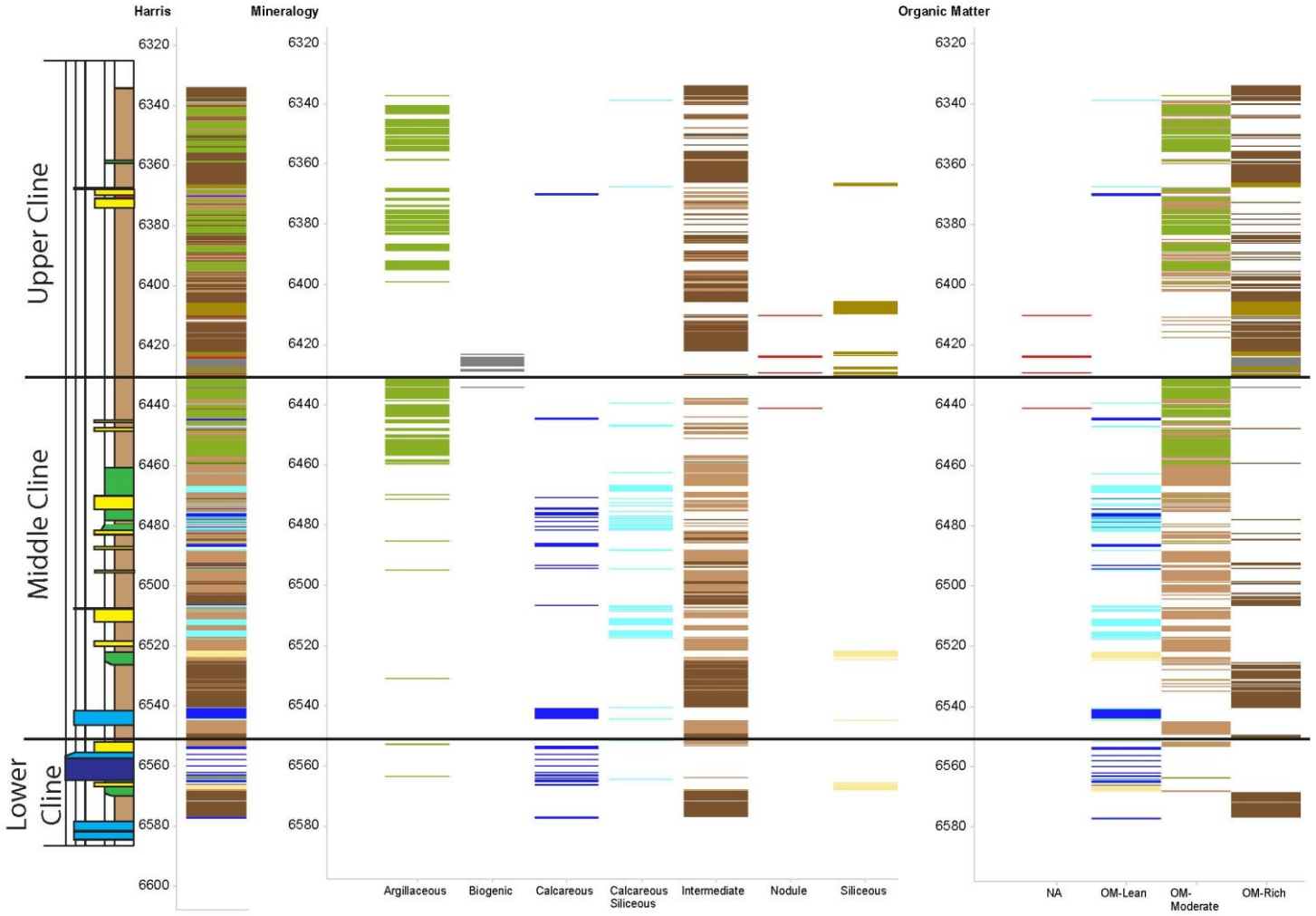

Figure 34: Chemostratigraphic interpretation of the Harris core. The plots from left to right are (1) visual log, (2) chemostratigraphic plot, (3) chemostratigraphic plot displayed by mineralogy, and (4) chemostratigraphic plot displayed by OM content.

Powell Core

The Powell core contains predominantly the OM-moderate intermediate chemofacies, but there are common siliceous chemofacies and calcareous chemofacies throughout the core (Figure 35). The heterogeneity is commonly on the order of less than a foot. There are rare argillaceous chemofacies, but they are more common vertically through the core. The argillaceous, calcareous siliceous, and calcareous chemofacies are generally OM-lean; the siliceous chemofacies is commonly OM-rich. There is a 10-foot biogenic zone near the top of the core, and it is OM-rich as well. Phosphate nodules are common in association with the biogenic zone and OM-rich siliceous samples. This core contains the uppermost seven feet of the Middle Cline; from the small snapshot seen in core, there is no major facies difference associated with the change. However, there are no OM-rich rocks present in the Middle Cline.

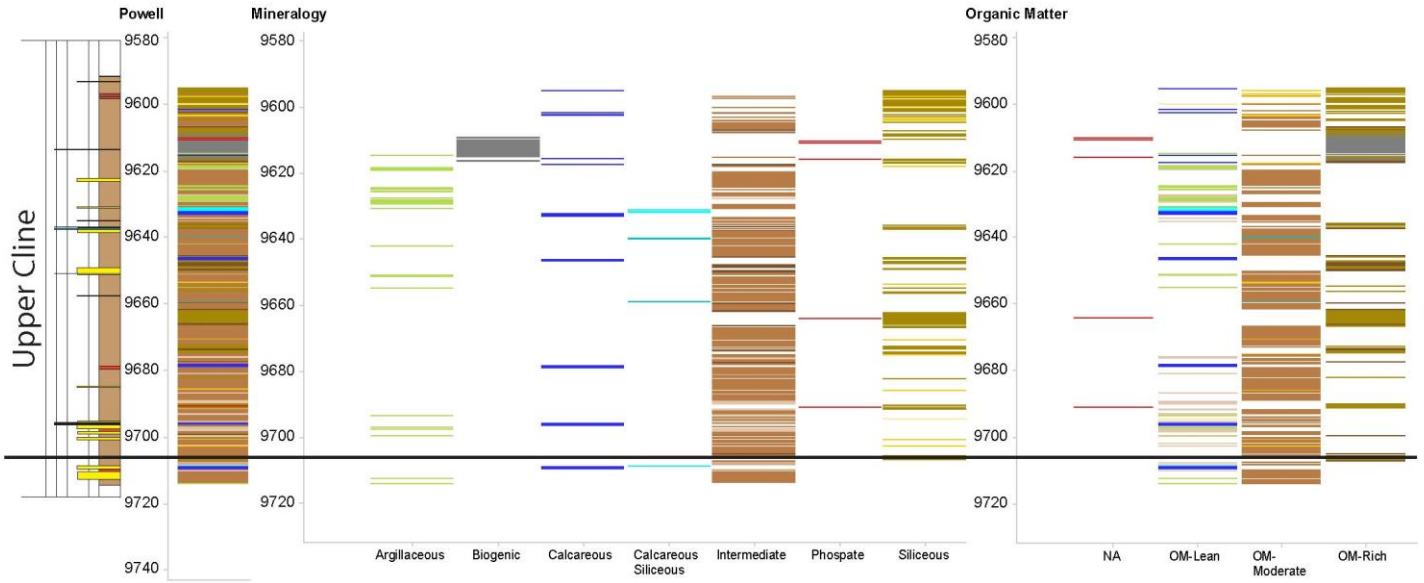

Figure 35: Chemostratigraphic interpretation of the Powell core. The plots from left to right are (1) visual log, (2) chemostratigraphic plot, (3) chemostratigraphic plot displayed by mineralogy, and (4) chemostratigraphic plot displayed by OM content.

Greer Core

The Greer core is the most discontinuous core in the dataset, making it difficult to discern vertical changes throughout the core; however, it contains a range of facies from the Middle Cline and the Upper Cline (Figure 36). The OM-rich chemofacies are not cored in the Greer well (Figure 4). The Middle Cline contains OM-lean argillaceous, calcareous, calcareous siliceous, intermediate, and siliceous chemofacies, as well as OM-moderate intermediate and siliceous chemofacies. OM-rich chemofacies are absent in the Middle Cline portion of the Greer core. The calcareous chemofacies are present as rare debrites and turbidities, but the thickest calcareous deposits in the section (about four feet thick) are mudstones with early calcareous cementation of ankerite.

The total cored section of the Upper Cline is less than 30 feet, and the core is in four discontinuous pieces—this makes it very difficult to assume that the Greer core is representative of the diversity of the Upper Cline samples. The chemofacies in the Upper Cline are much less diverse. The cores are dominated by OM-moderate and OM-lean intermediate chemofacies. There are rare thin carbonates and siliceous chemofacies, and only four sample points are OM-rich.

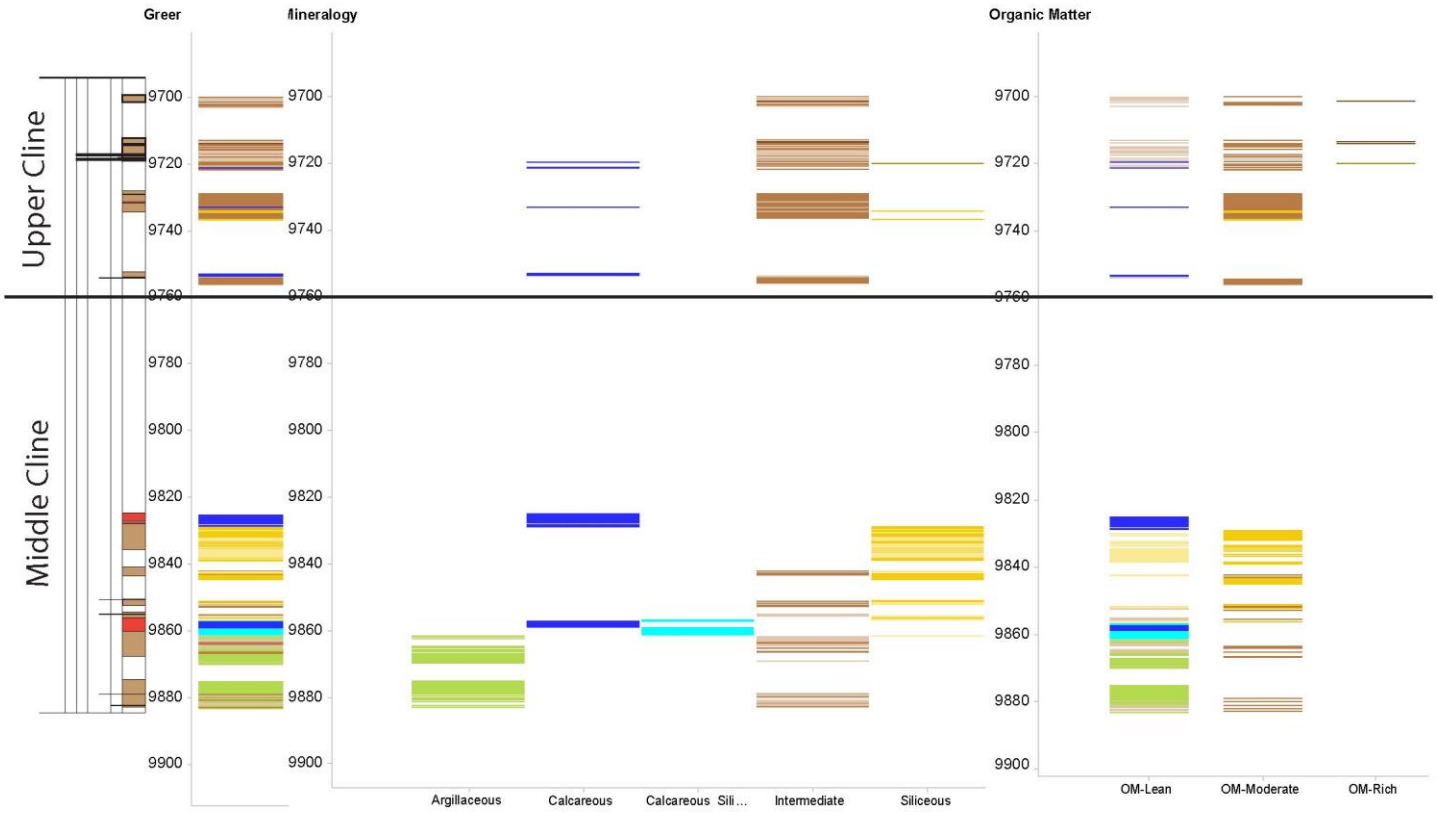

Figure 36: Chemostratigraphic interpretation of the Greer core. The plots from left to right are (1) visual log, (2) chemostratigraphic plot, (3) chemostratigraphic plot displayed by mineralogy, and (4) chemostratigraphic plot displayed by OM content.

Glass Core

The Glass core is continuous and short core that contains the uppermost three feet of the Lowe Cline section and the bottom 50 feet of the Middle Cline unit (Figure 37). The core is heterogeneous, and is more silica dominated than the other cores in the study. The Lower Cline-Middle Cline boundary is evident from thin (less than one foot) carbonate debrites in the uppermost Lower Cline. The core is predominantly OM-lean and OM-moderate, with rare OM-rich siliceous chemofacies. The calcareous and argillaceous chemofacies are both mostly OM-lean, and OM-lean and OM-moderate intermediate chemofacies are also common.

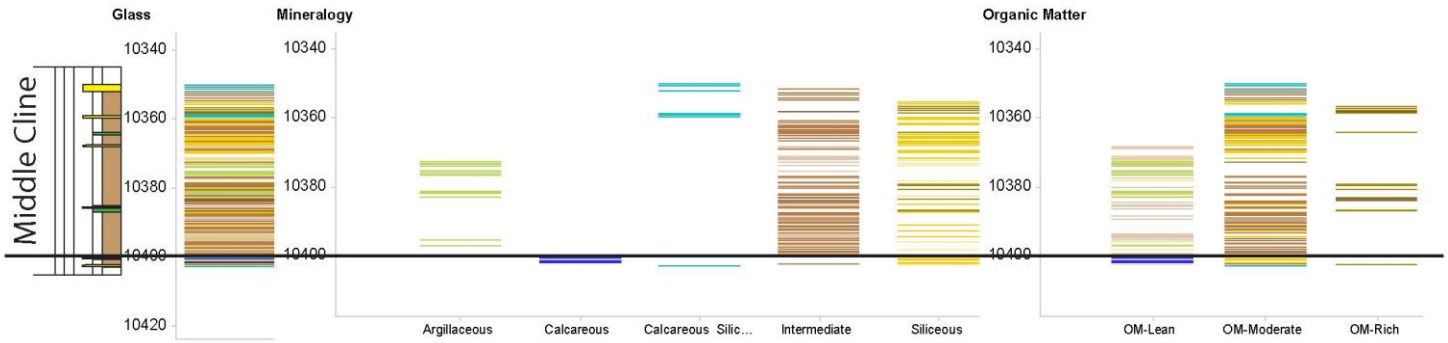

Figure 37: Chemostratigraphic interpretation of the Glass core. The plots from left to right are (1) visual log, (2) chemostratigraphic plot, (3) chemostratigraphic plot displayed by mineralogy, and (4) chemostratigraphic plot displayed by OM content.

Conclusion of High-Resolution XRF Results

The basin-centered wells can be treated as a single dataset. They are all near the basin axis, and although there are differences, the wells can be compiled stratigraphically to represent one composite well. The Glass well core contains the base of Middle Cline, the Greer core contains the middle of the Middle Cline, and the Powell core contains the Upper Cline. The Lower Cline deposits are not represented in the basin-centered dataset. When these three cores are analyzed together, a distinct difference in mineralogy and TOC is evident. The Middle Cline is more siliceous and lower in organics than the Upper Cline. The Upper Cline contains siliceous and biogenic chemofacies that are OM-rich and a larger percentage of argillaceous deposits, uncommon in the Middle Cline interval of the wells.

The basin-centered wells and the Harris well can be compared to determine the geochemical facies difference between the basin center and the eastern margin of the basin in the Middle and Upper Cline. The Harris well has more argillaceous chemofacies and thicker carbonate deposits. Biogenic zones occur in the Upper Cline in both the basin center and the eastern margin, though as chronostratigraphically distinct deposits. The Upper Cline has greater organic matter content than the Middle Cline as well. The carbonates in the Harris well are allochthonous in nature as evidenced in core from the visual log analysis, and much more common, where the thicker carbonate sections of the basin centered cores are associated with early carbonate cementation, though this may due to fluids occurring from proximal allochthonous deposits.

ROCK PROPERTIES DATASET

Mineralogy

The Cline Shale exhibits a predominant ternary mineralogical system consisting of carbonates, clays, and quartz, as is common in most mudrock systems. The data are plotted on a ternary diagram along with other important shale plays across North America (Figure 38). The formation is predominantly siliciclastic, with commonly equal parts quartz and feldspars and clays, but the formation experiences carbonate dilution because of dilute debris flows or high levels of carbonate cement. Biogenic or diagenetic quartz and carbonates are also present but rare. The diagenetic carbonates are predominately ankerite in composition, and are interpreted to be early diagenetic features of little lateral importance, similar to diagenetic nodules (Harry Rowe, personal communication). The mineralogy of the Cline shale has direct importance to the amount of total organic carbon (TOC) in the system. Carbonates serve as diluents to the TOC in the system (Figure 39). If the total carbonates in the sample exceed 30%, the TOC drops consistently below 2%—a boundary that commonly separates a good mudrock from a fair mudrock (Boyer et al, 2006).

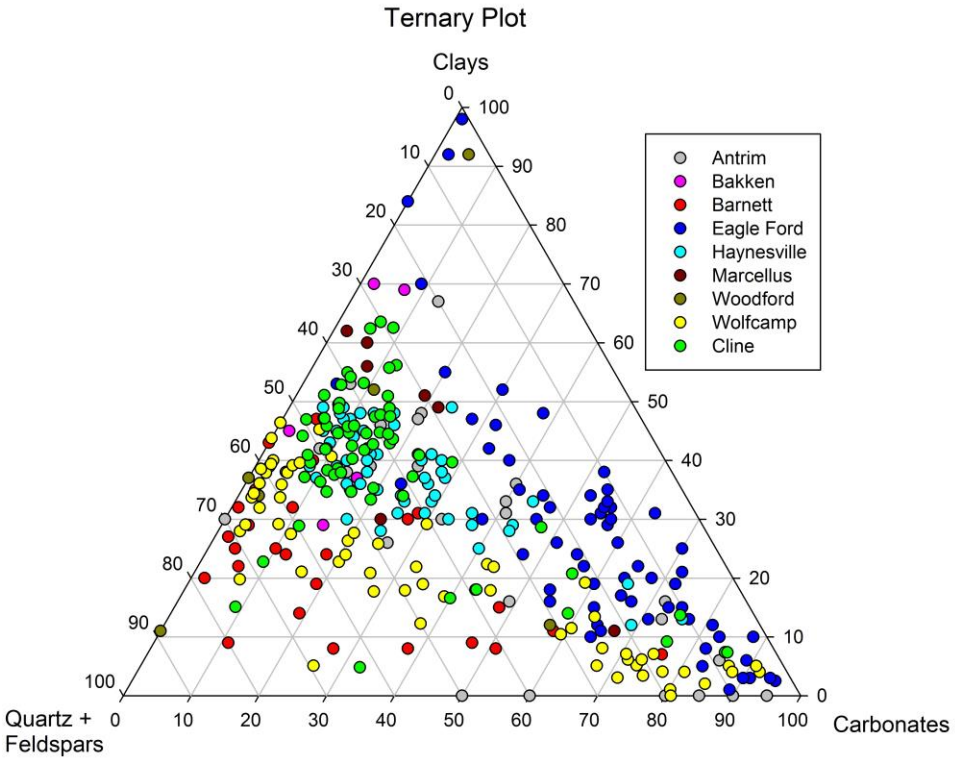

Figure 38: Ternary diagram of multiple shale mineralogies. All data except for the Cline (from this study) and the Wolfcamp (displayed with permission from Robert Baumgardner) are taken from Chermak and Schreiber (2014).

The ternary diagram presents a comparison of the Cline mineralogy to other important shale plays. The Cline Shale plots as an argillaceous mudrock with minor carbonate content. The argillaceous data points have a negative impact on the mechanical rock properties with regards to brittleness and hydraulic fracturing (Binnion, 2012). The mineralogy of the Cline is similar to that of the Haynesville, a highly studied mudrock formation that may be useful as an analog formation. The Wolfcamp mineralogy is more quartz and feldspar rich common carbonate dilution. The Wolfcamp was deposited

directly above the Cline Shale; based on the mineralogy, the Cline Shale and Wolfcamp are two distinct shale systems.

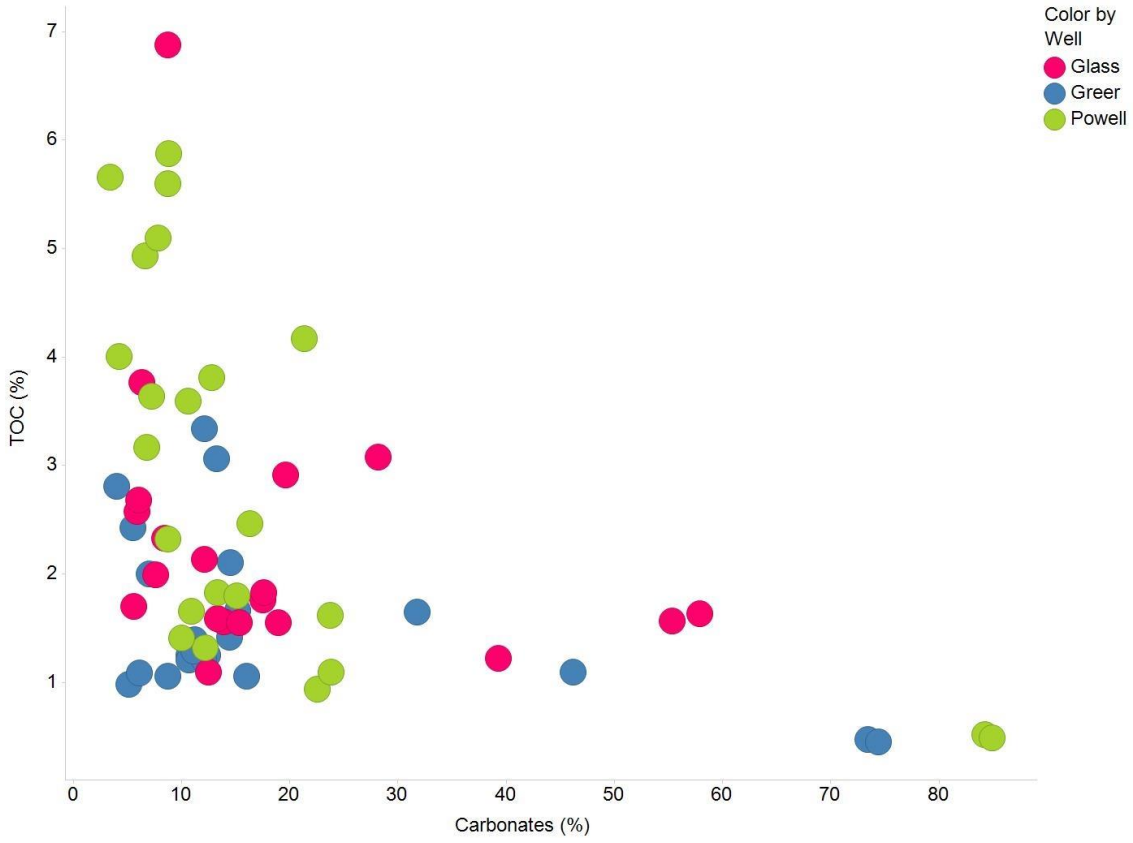

Figure 39: Plot of TOC (%) vs. carbonates (%). TOC decreases significantly with increasing carbonate input.

Kerogen Type and Thermal Maturity

The Cline shale consists of types I, II, and III kerogen and is currently in the oil window to early condensate window. Rock-eval is a three step process: S1 corresponds to the process of thermal distillation, S2 corresponds to the process of pyrolytic

degredation on kerogen (Tmax is determined at the time when the maximum amount of hydrocarbons are being generated from S2), and S3 corresponds to carbon dioxide generation during heating up to 390°C. The hydrogen index (HI) is a ratio of pyrotyzable organic compounds in S2 to the TOC in the same sample, and the oxygen index (OI) is a ratio of the carbon dioxide from S3 to the TOC in the same sample (Peters, 1986). A plot of HI vs OI is used to discern kerogen type in mudrocks (Boyer et al, 2006). The Cline Shale has a range of type I, II, and III kerogen (Figure 40). The Glass and Powell wells contain predominately types I, and II kerogen. The Greer well contains predominantly type III kerogen. The cored intervals of the wells allows for relating kerogen type to temporal changes in deposition. The base of the Lower Cisco (Glass well) is type I and II, the upper portion of the Lower Cisco (Greer well) is Type III, and the Upper Cisco (Powell well) is again type 1 and II. The change in kerogen type can be related to the source of OM (Langford and Blanc-Valleron, 1990). The base of the Lower Cisco kerogen is marine in origin, the top of the Lower Cisco is mostly woody material of continental origin, and the Upper Cisco is mostly lacustrine and marine in origin again.

A plot of HI vs Tmax is used to determine thermal maturity (Figure 41). Tmax values are correlated to thermal maturity (Peters, 1986). Tmax values below 435 degrees Celsius are immature, Tmax values between 435 and 455 degrees celcius are in the oil window, Tmax values between 455 and 475 are in the condensate window, and Tmax values above 475 are in the dry gas window. The Cline Shale is in the oil window and the early condensate window. The Glass and Powell wells are in the oil window, and he

Greer well is in the oil window and early condensate window. The rocks from these wells were deposited near the basin axis, the deepest part of the basin during deposition, and are currently near the greatest depth of burial in the basin; therefore, the samples from these wells are probably some of the most thermally mature samples from the basin. Local differences in burial depth and heat flow are probably the primary contributors to the slight maturity differences in these samples.

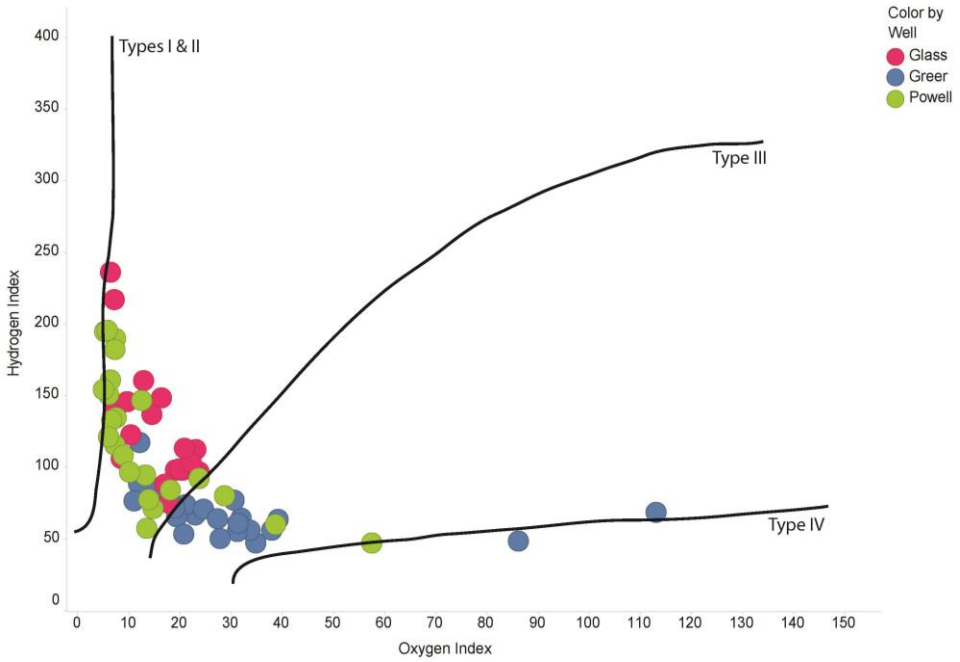

Figure 40: Plot of HI vs. OI displaying the kerogen type of the Cline Shale.

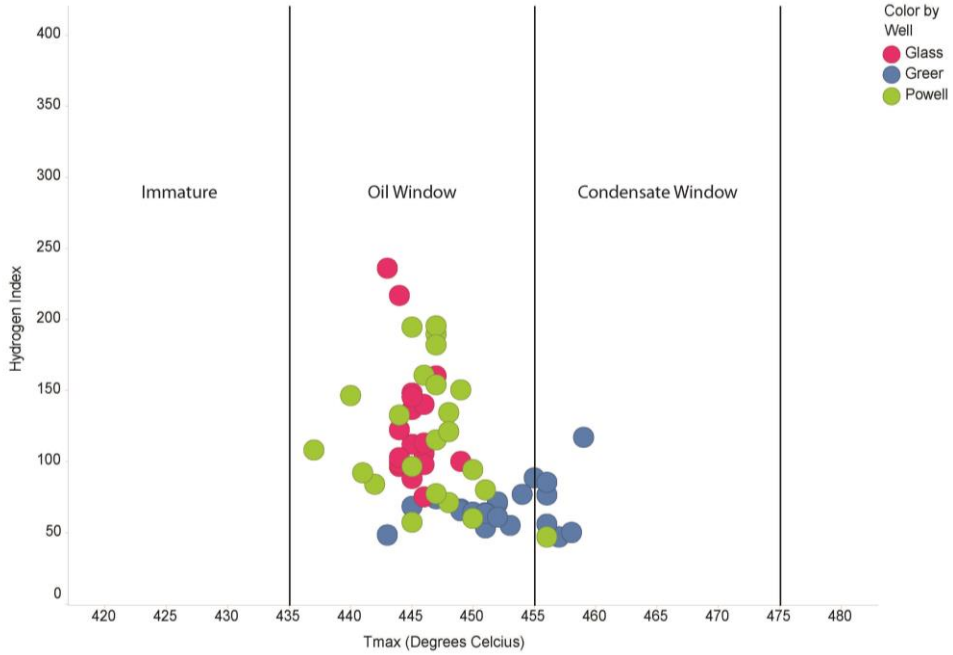

Figure 41: Plot of HI vs. Tmax (degrees Celsius) displaying the thermal maturity of the Cline Shale.

Empirical Relationships of Rock Properties

This dataset is important for characterizing the Cline shale because empirical relationships can be developed by cross plotting the rock properties. TOC has a positive correlation with porosity, TOC has a negative correlation with grain density, and permeability has a positive correlation with thermal maturity (Tmax).

TOC and porosity exhibit a positive correlation (Figure 42). This is probably related to the organic matter (OM) hosted porosity in the system. As OM is added to the system, it adds porosity through OM matter pores and contributes to the total pore system in the mudrock. OM porosity is any porosity within organic matter and has been documented in rocks in the oil window and at higher thermal maturities (Loucks et al., 2012). Positive correlations between OM and porosity have been previously recorded (Passey et al., 2010; Milliken et al., 2012; Milliken et al., 2013). A study on the Marcellus Formation showed good correlation of TOC and porosity up to 5.5% TOC, above that threshold there is no correlation (Miliken et al., 2013). In this Cline Shale dataset, TOC values rarely exceed 5.5%. The positive empirical relationship between TOC and porosity also shows that rocks with good TOC will have better porosity, two very important factors in shale reservoir evaluation. A positive correlation between the two factors has a positive effect on the reservoir evaluation.

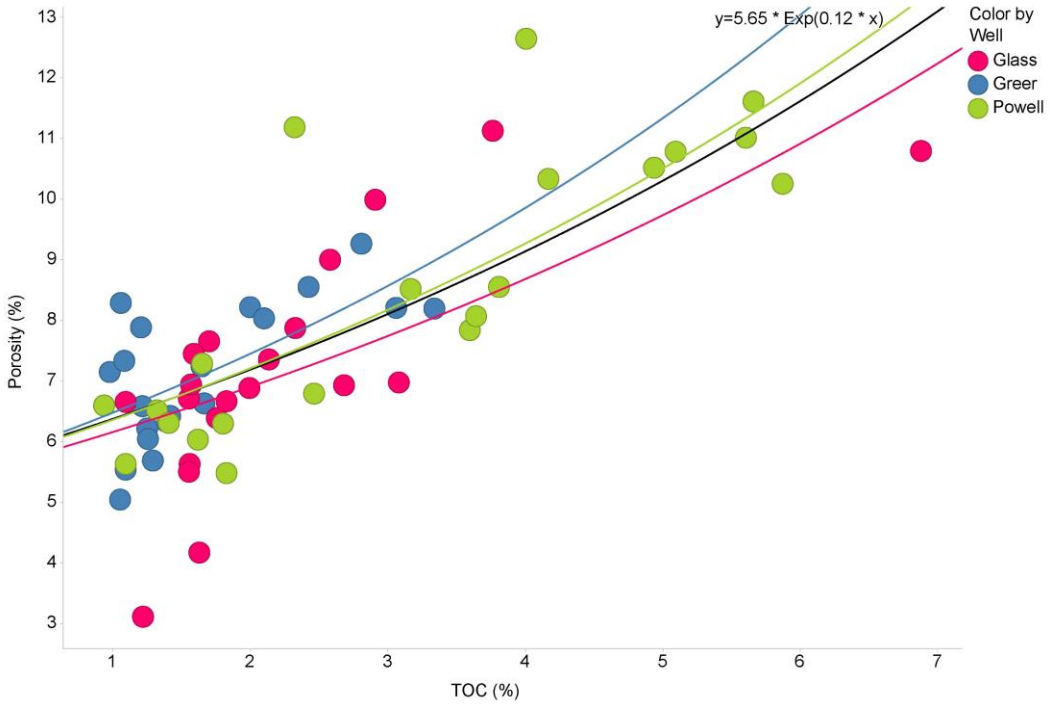

Figure 42: Plot of porosity (%) vs TOC (%) exhibiting a positive exponential relationship.

TOC and grain density exhibit a negative correlation (Figure 43). This is important because of petrophysical implications. Well logs can directly measure density; if there is a direct correlation of density and TOC, calculating TOC throughout the basin becomes a much simpler task. This petrophysical relationship has been established in previous work (Ferti and Chilingar, 1988).

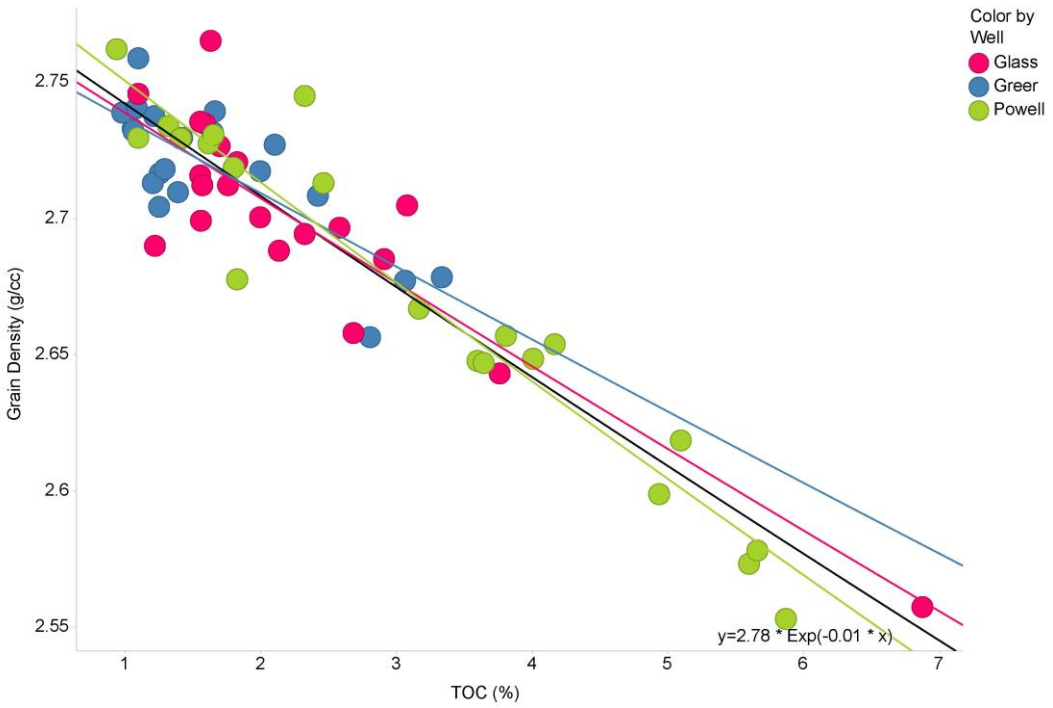

Figure 43: Plot of grain density (g/cc) vs TOC (%) exhibiting a negative exponential relationship.

Permeability and thermal maturity (Tmax) exhibit a positive correlation (Figure 44). This relationship shows the importance of OM hosted porosity on pore systems, and the degree of maturity that is necessary to create connected pore systems in OM. The Cline shale is a relatively immature unconventional reservoir having the most mature samples in the early condensate window and the majority of samples in the oil window. Loucks et al. (2009) suggest that because most pores are associated with OM, that the permeability should be greatly influenced by the OM properties. The low maturity of the Cline lends itself to the incipient expulsion of hydrocarbons as the dominant creator of porosity in organic matter, and can greatly increase the permeability through connected

OM hosted pore networks. Therefore, thermal maturity is an important controlling factor on permeability development.

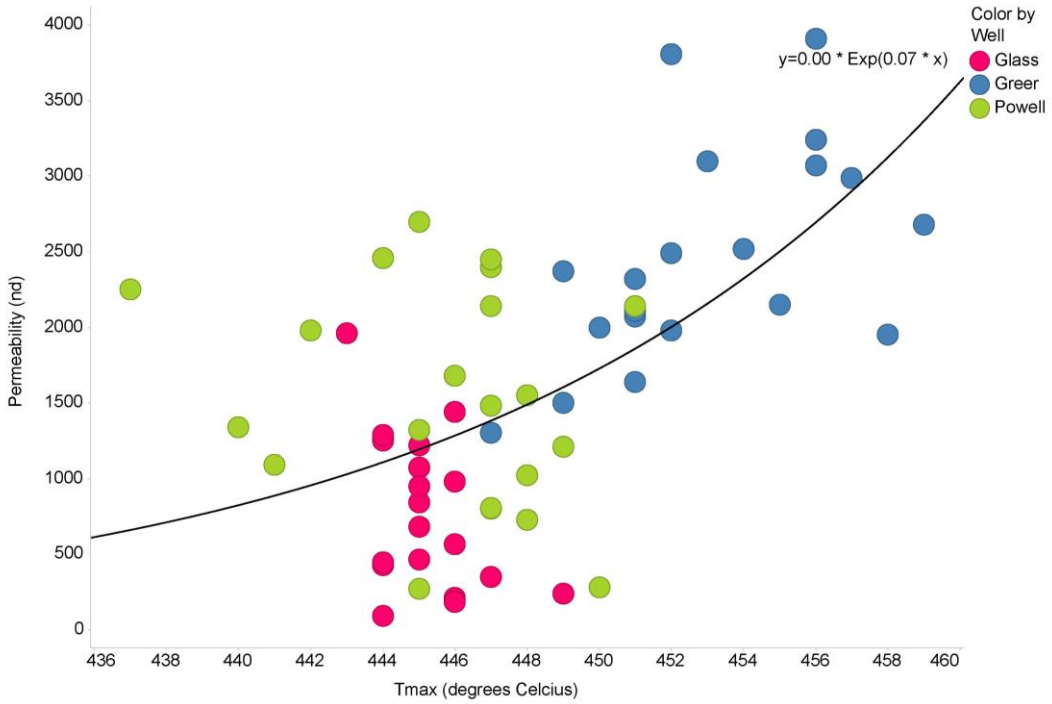

Figure 44: Plot of permeability (nd) vs Tmax (degrees Celsius) exhibiting a positive exponential relationship.

Conclusion of Rock Properties Results

1. The Cline shale has a dominantly siliciclastic mineralogy with minor carbonate components.
2. Kerogen in the Cline Shale is Types I, II, and III. The Cline Shale is currently in the oil window and the early condensate window.
3. Direct correlations exist between TOC and grain density, TOC and porosity, and Thermal Maturity (Tmax) and Permeability. These correlations can be used to build a robust petrophysical model of the Cline Shale.

REGIONAL STRATIGRAPHY

Structure Contour Maps

Four structure contour maps were made; one at each major horizon within the Cline Shale—top of the Strawn, top of the Lower Cline, top of the Middle Cline, and top of the Upper Cline (Figures 45 – 48). There are minor variations between the maps, but the most striking observation is the similarity of the four maps. Each map displays a gentle dip to the west, highlighting the asymmetry of the Midland Basin. The deepest part of the basin is currently in the western side of the basin running north-south through Martin and Midland counties; this could be influenced by later subsidence and tectonics after Cline deposition. There is a relative structural high in the form of an arch in northern Midland County that does persist throughout deposition; this structural feature affects the facies distributions presented later in this study. Carbonate facies tend to have a higher net-to-gross across the high than adjacent parts of the basin.

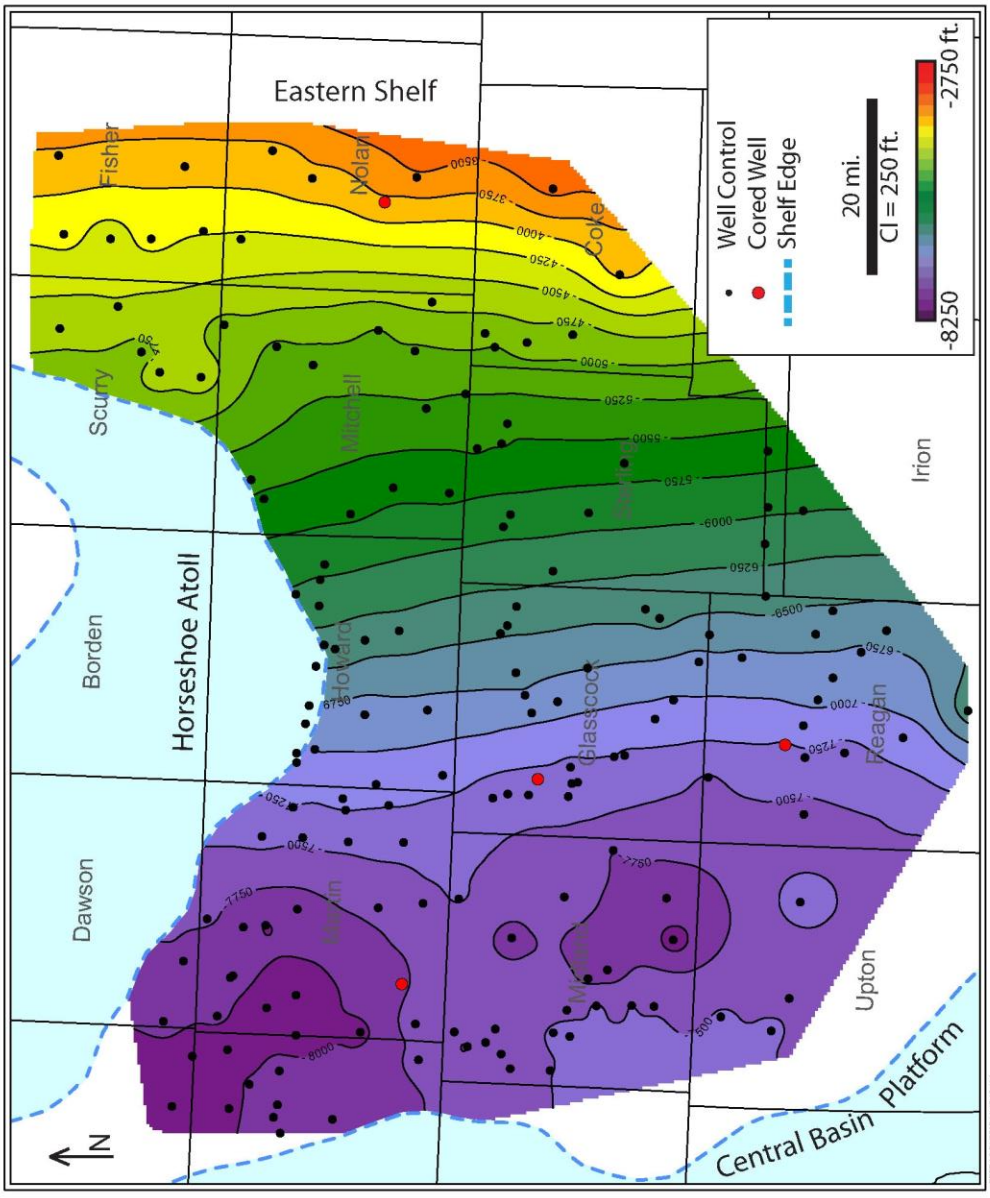

Figure 45: Structure contour map of the top of the Strawn Formation. The basin is dipping shallowly to the west.

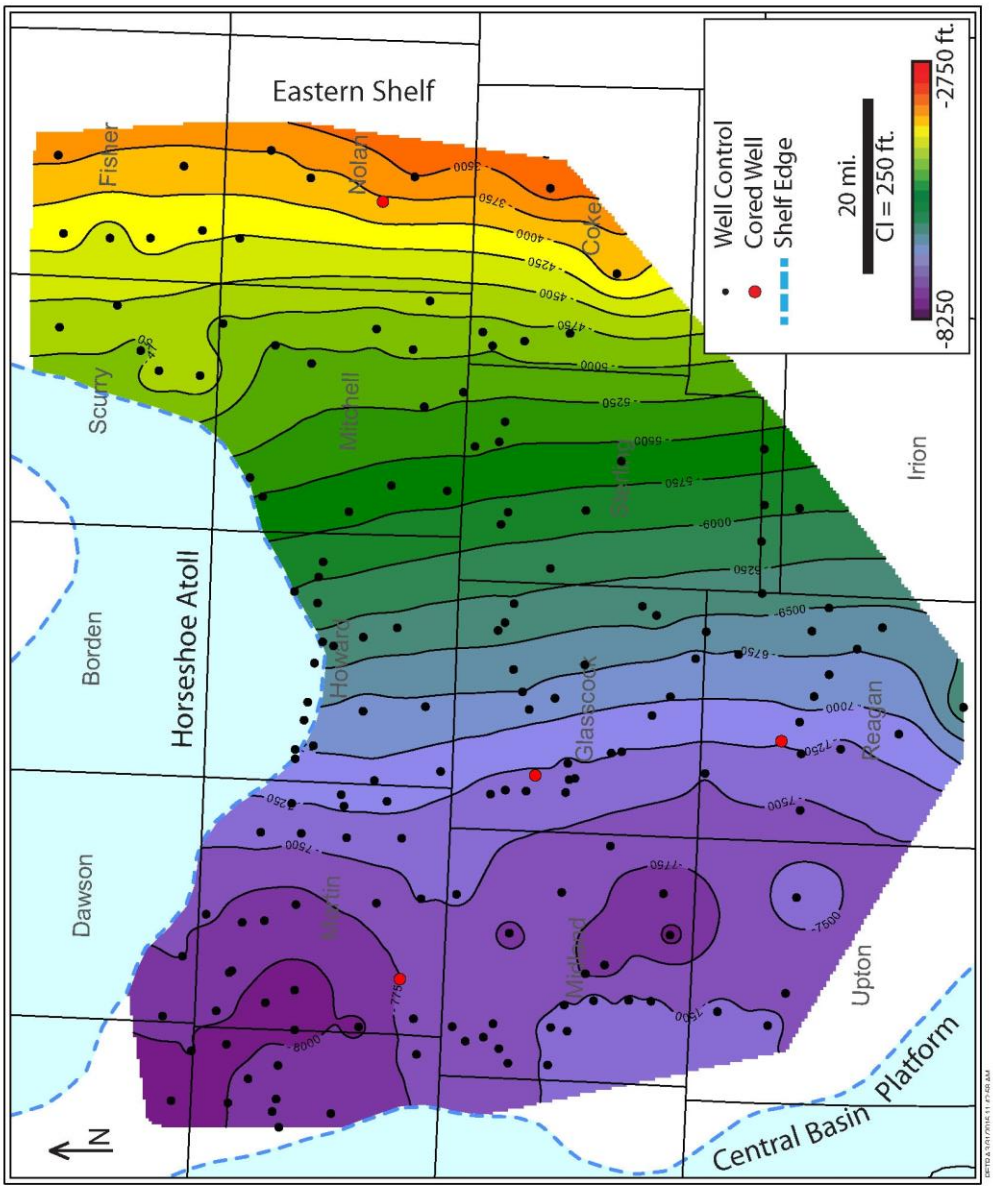

Figure 46: Structure contour map of the top of the Lower Cline. The basin is dipping shallowly to the west. There is an arch in northern Midland County

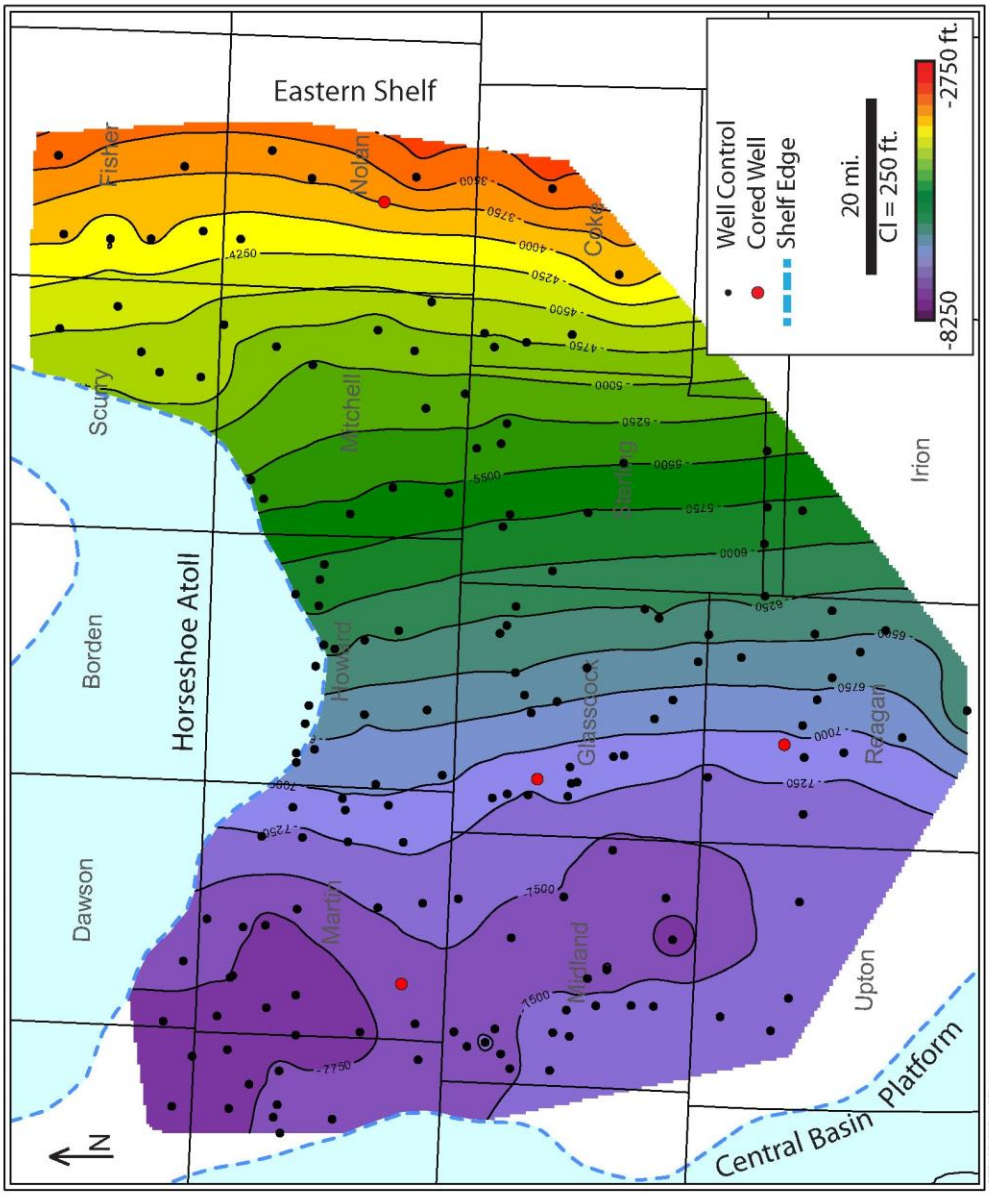

Figure 47: Structure Contour map of the top of the Middle Cline. The Basin is dipping shallowly to the west. The deepest part of the basin is in the northwest.

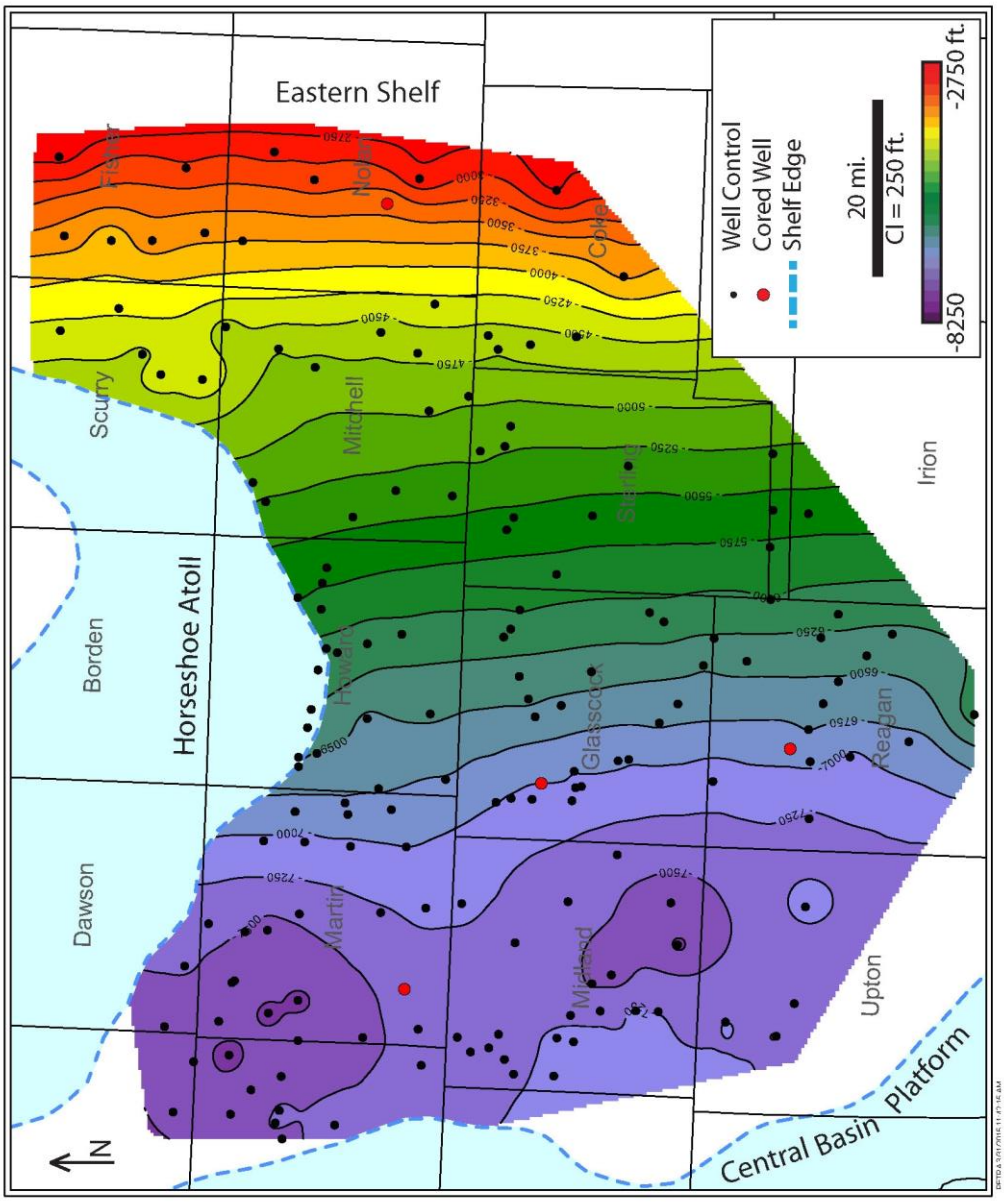

Figure 48: Structure contour map of the top of the Upper Cline. The basin is dipping shallowly to the west. There is an arch in northern Midland County.

Isopach Maps

Four gross isopach maps were created; a gross isopach of the entire Cline section and gross isopach maps of the Lower Cline, Middle Cline, and Upper Cline (Figures 49-52). The gross Cline isopach maps shows overall depositional trends. The Cline Shale is 200 to 425 feet thick in the Southern Midland Basin (Figure 49). The thickest parts of the Cline Shale are associated with major potential sediment source areas in the basin. Andrews County, near the Central Basin Platform has total thicknesses greater than 400 feet. Martin County, adjacent to and southwest of the Horseshoe Atoll, also features thickness values greater than 400 feet. In Mitchell County, proximal to the Eastern Shelf, thicknesses values are greater than 325 feet. Reagan County, proximal to the Ozona Uplift, also contains thicknesses of more than 375 feet. The Cline is the thinnest near the southern portion of the Central Basin Platform where it is commonly less than 225 feet thick.

The Lower Cline is thin, with thicknesses ranging from under 25 feet to just over 50 feet (Figure 50). The Lower Cline does not exhibit much thickness variation across the basin. It is sheet-like and does not appear to be influenced by source proximity. There is an anomalous depositional thick in Mitchell County, near the Eastern Shelf boundary.

The Middle Cline interval exhibits linear zones of large thickness and similar zones of thin values (Figure 51). It is between 50 feet and 225 feet in thickness. The thinnest positions of the Middle Cline are in Mitchell County, near the northern end of

the Eastern Shelf, and in Midland County, proximal to the Central Basin Platform. There is a weak linear trend that extends out to the basin. Conversely, the thickest parts of the Middle Cline are in the northwestern and southeastern corners; linear thickness trends striking NW-SE are prevalent in both areas and thin towards the center of the basin.

The Upper Cline is the thickest unit within the Cline with thicknesses in excess of 275 feet on the southwest flank of the Horseshoe Atoll (Figure 52). Areas of great thickness also occur in Mitchell County, Ector and Midland Counties, and NW-SE trends of great thickness occur in Reagan and Glasscock counties. The thinnest area of Upper Cline deposition is the southwest portion of the basin. The Upper Cline also contains the most basinward deposits of the slope associated with the Eastern Shelf in Fisher, Nolan, and Coke Counties (Brown et al., 1990).

These isopach maps show important changes in regional areas of depositional influence. The Lower Cline exhibits a sheet like geometry with a slightly increased thickness to the northeast. The Middle Cline contains a NW-SE thickness trend across the basin, with a small influence from the Horseshoe atoll and little deposition from the northeast and southwest. The Upper Cline shows a continuation of the NW-SE trending thick, but there are increased influences from the SW of the Horseshoe Atoll, the Central Basin Platform, and the northeast section of the basin.

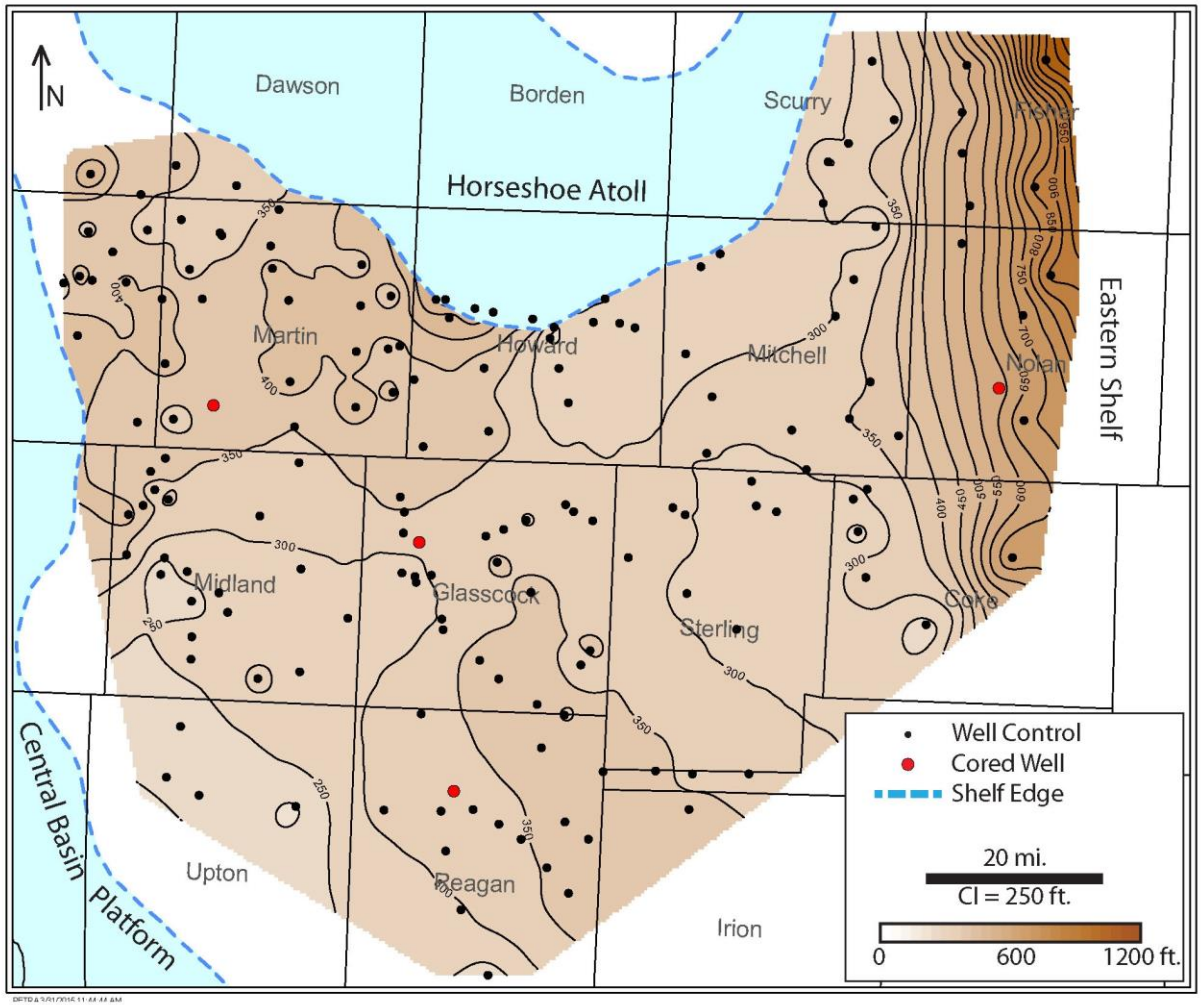

Figure 49: Isopach map of the gross Cline. There is a thick fairway in Irion, Reagan and Glasscock counties, and another thick fairway in Martin and Andrews Counties.

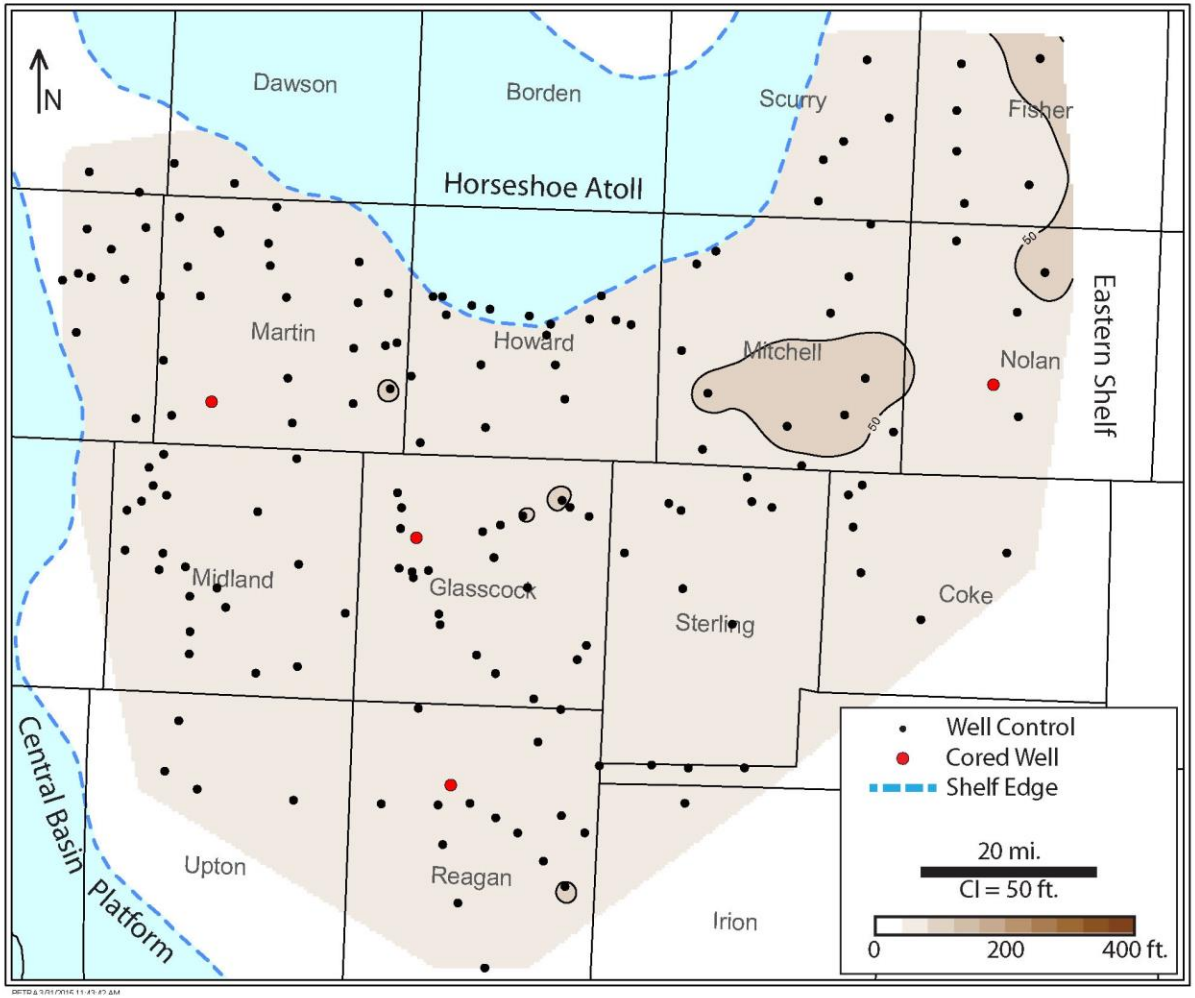

Figure 50: Isopach map of the Lower Cline. This interval was deposited as a thin sheet. There is an area of increased thickness in Mitchell County.

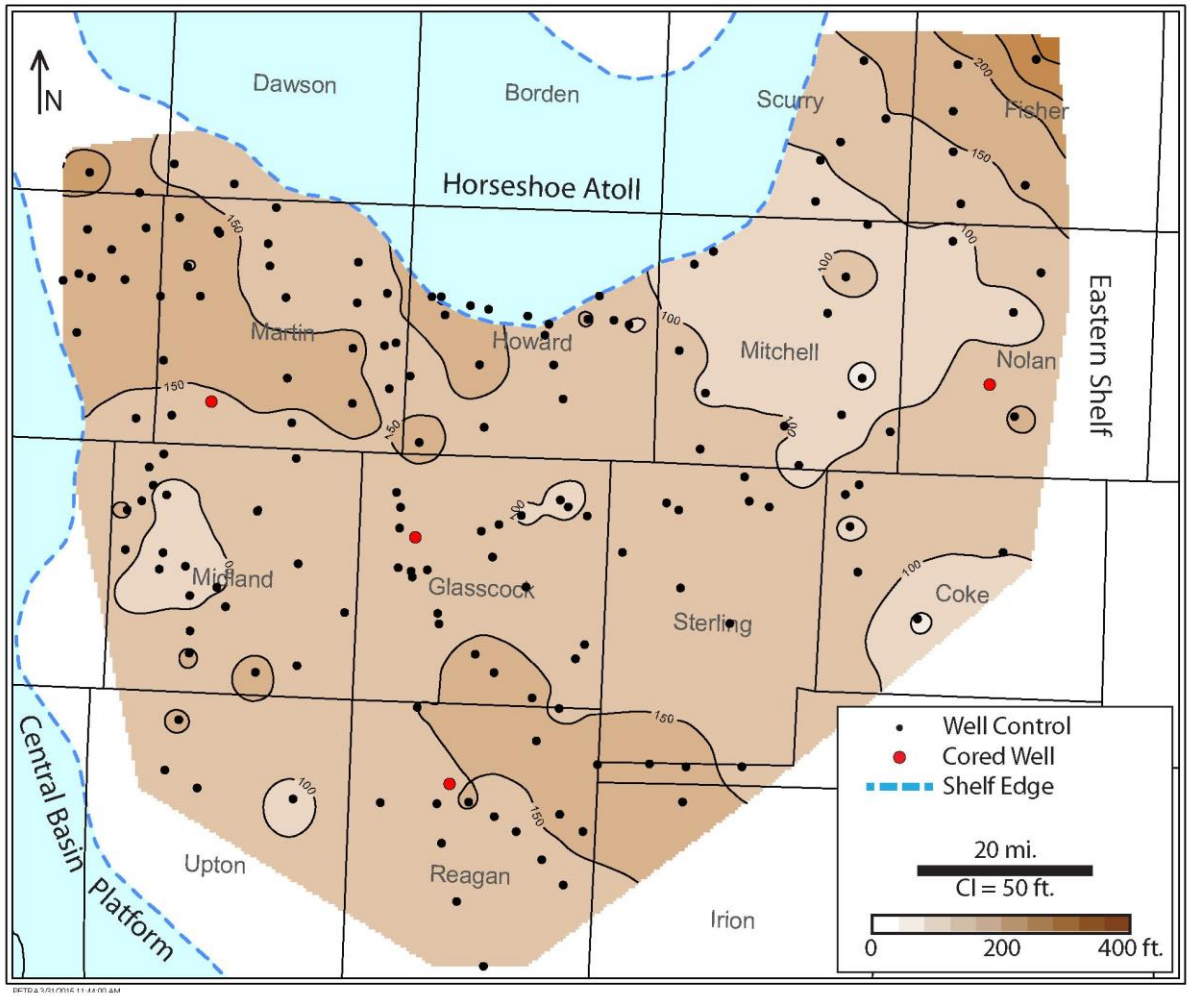

Figure 51: Isopach map of the Middle Cline. There is a fairway of thin deposits in Mitchell and Nolan Counties, and a fairway of thick deposits in Martin and Andrews Counties.

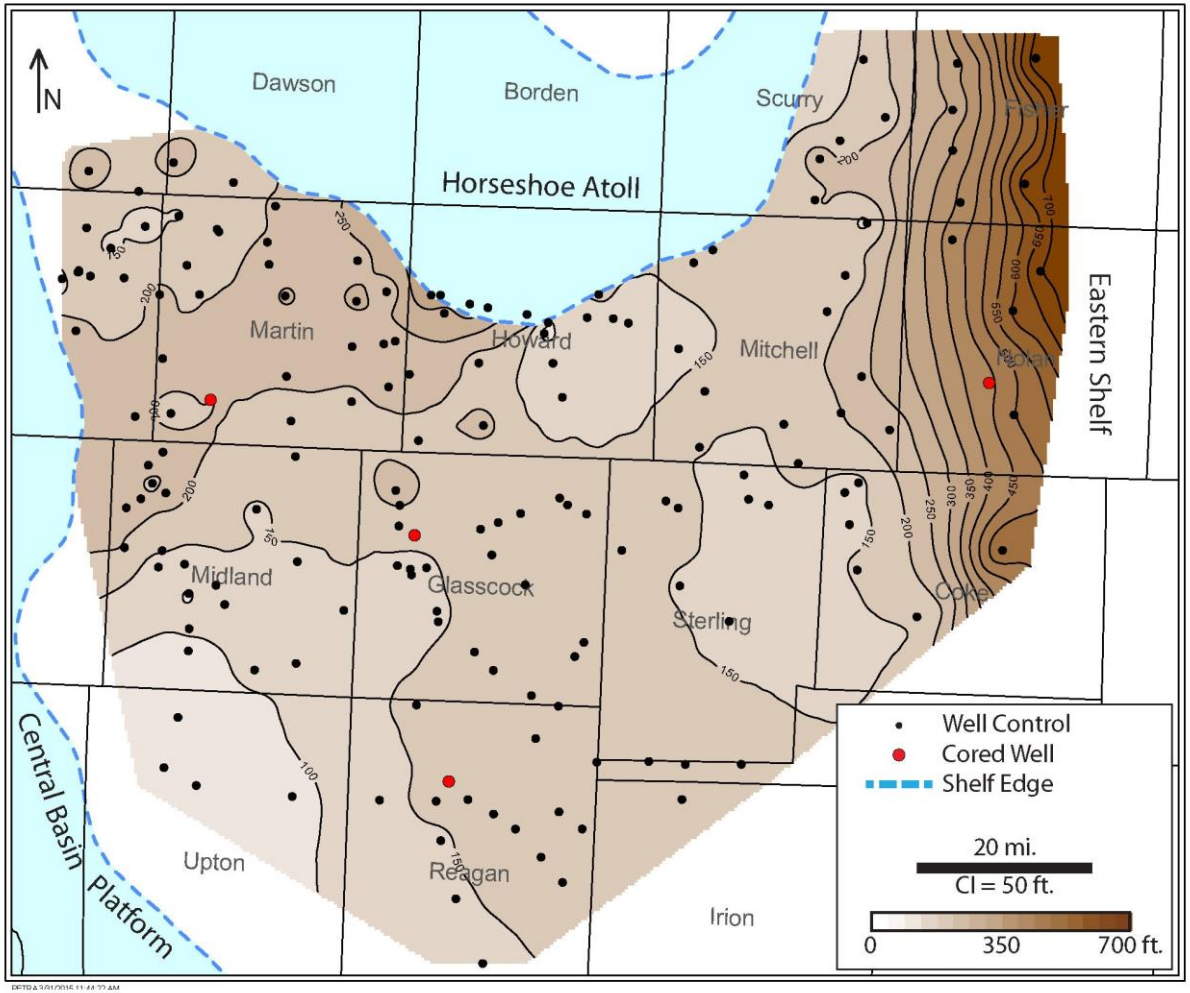

Figure 52: Isopach map of the Upper Cline. The thick in the east side of the study area is associated with time-equivalent slope deposits from the Eastern Shelf.

Lithofacies Distribution Maps

Gross Cline Lithofacies Distribution Mapset

The lithofacies distributions across the entire Cline Shale section exhibit generalized regional trends (Figures 53-58). The carbonates lithofacies is thickest and has the greatest net-to-gross values along the boundaries of the Central Basin Platform and the Horseshoe Atoll and in the Northwestern portion of the Basin (Figures 53 and 54). The siliciclastic OM-poor lithofacies is thickest in the southeast portion of the basin, in southeast Mitchel County, and in the basin to the northeast (Figure 55). Carbonate dilution diminishes the influence of the siliciclastic OM-poor lithofacies to the northwest; the same is true for the siliciclastic OM-rich lithofacies—carbonates act as diluents in the northwest as well (Figure 56). The siliciclastic OM-rich lithofacies exhibits a sheet-like geometry with thinner deposits to the southwest and thicker deposits in the northeast portion of the study area (Figure 57). There is a fairway of high net-to-gross siliciclastic OM-rich lithofacies (greater than 0.2 net-to-gross) trending northwest-southeast through Mitchell, Sterling, and Coke counties (Figure 58).

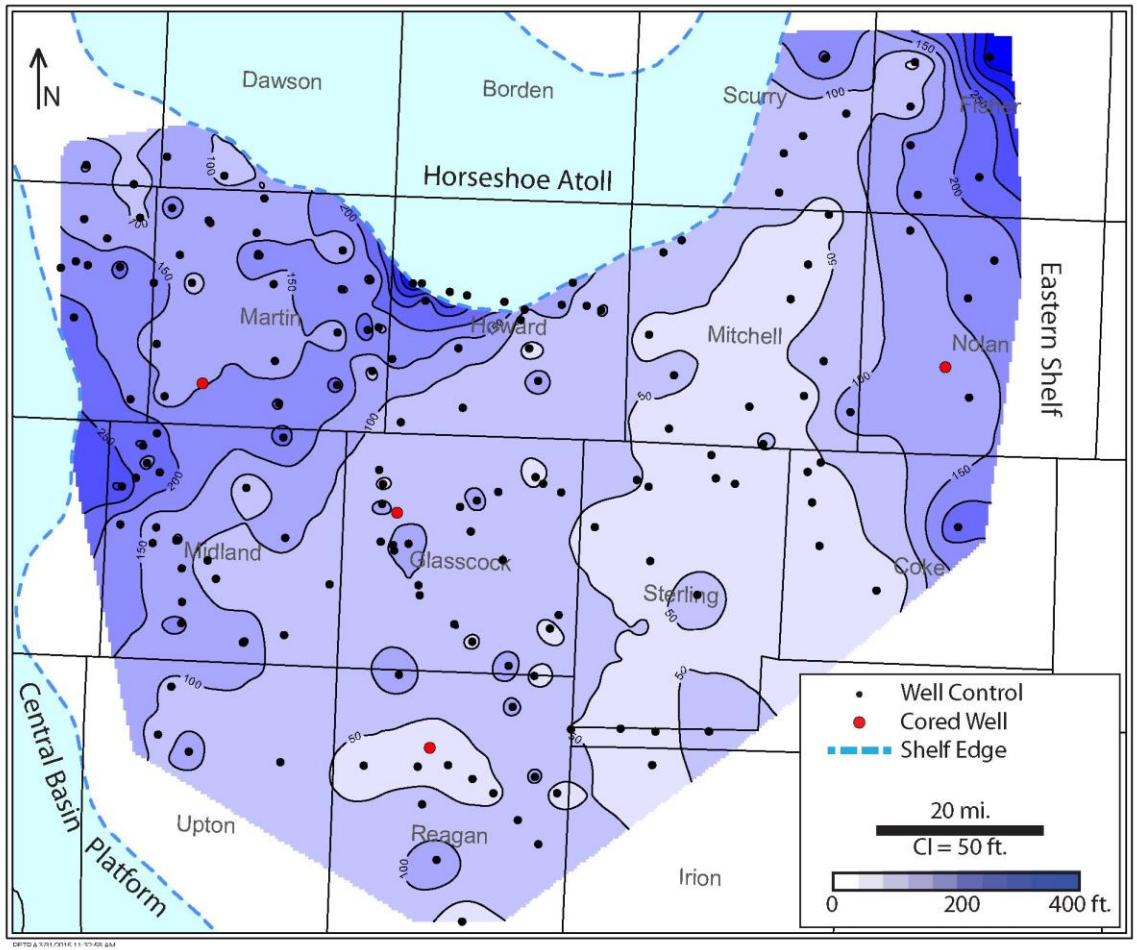

Figure 53: Gross Cline net carbonate lithofacies distribution. Thick carbonate deposits are located proximal to the shelf edges, and in the northwestern half of the study area.

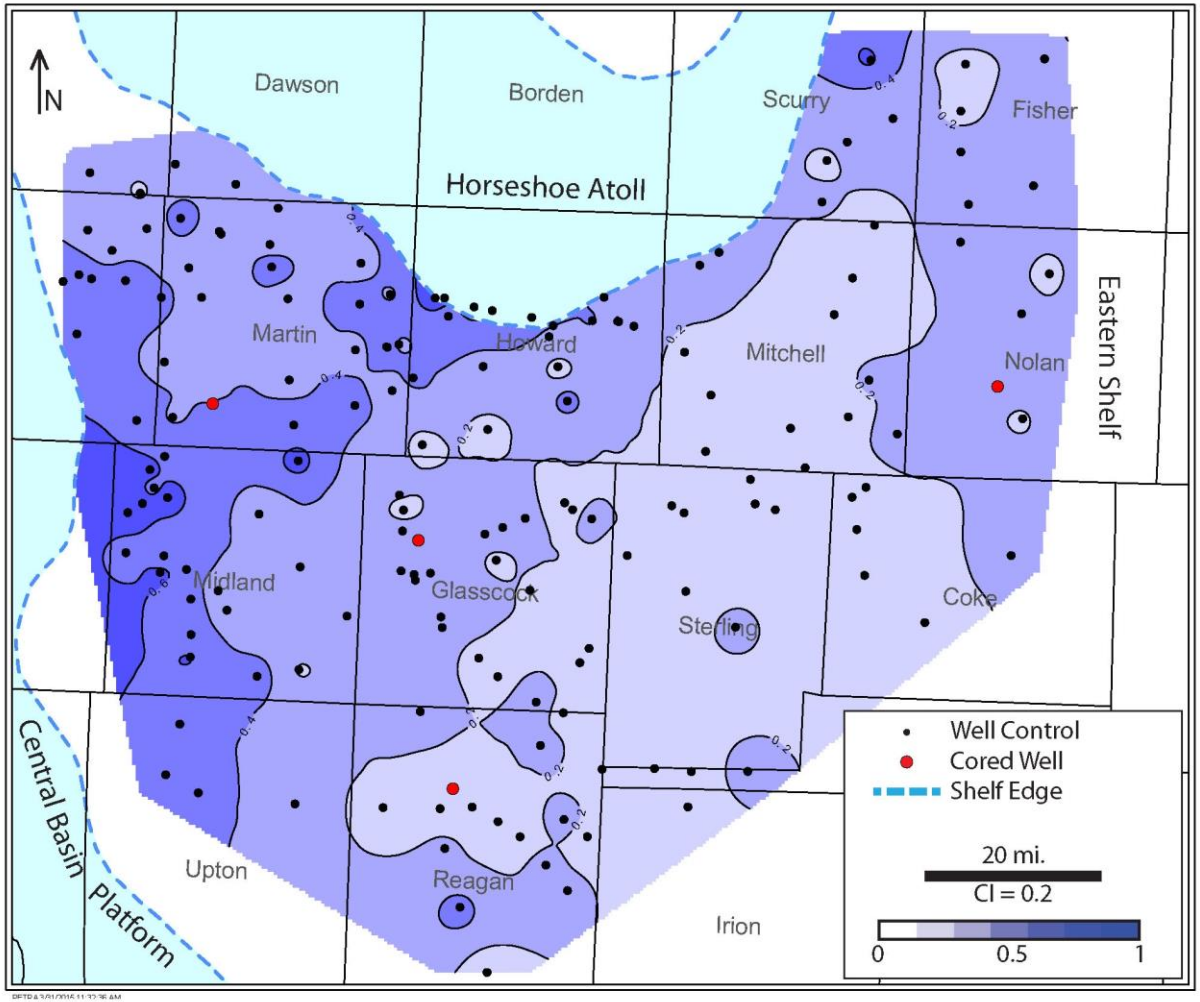

Figure 54: Gross Cline net-to-gross carbonate lithofacies distribution. Largest net-to-gross values occur proximal to the Horseshoe Atoll and Central Basin Platform, two carbonate platforms.

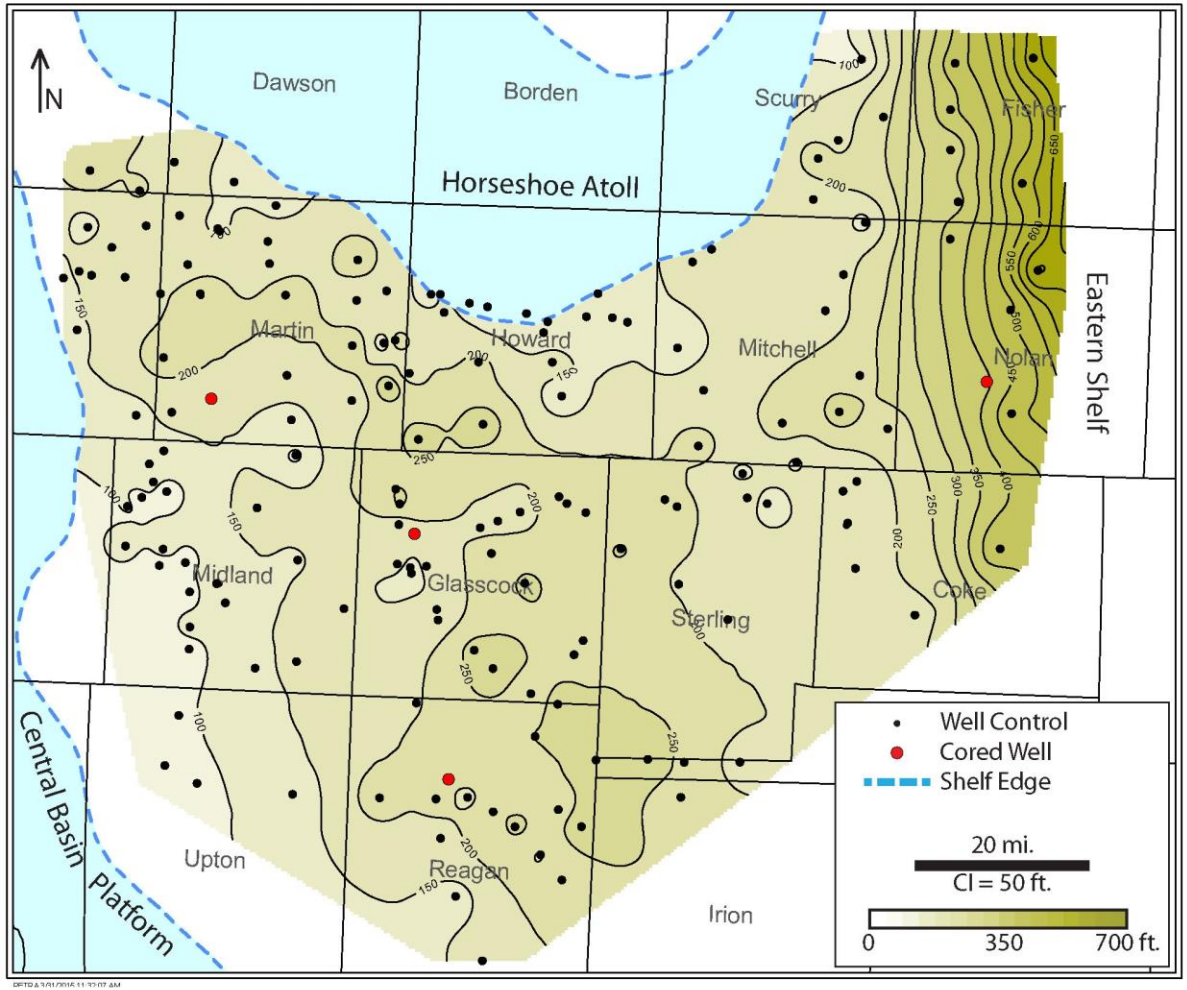

Figure 55: Gross Cline net siliciclastic OM-poor lithofacies distribution. The thickest deposits are located near the Eastern Shelf and in the basin center.

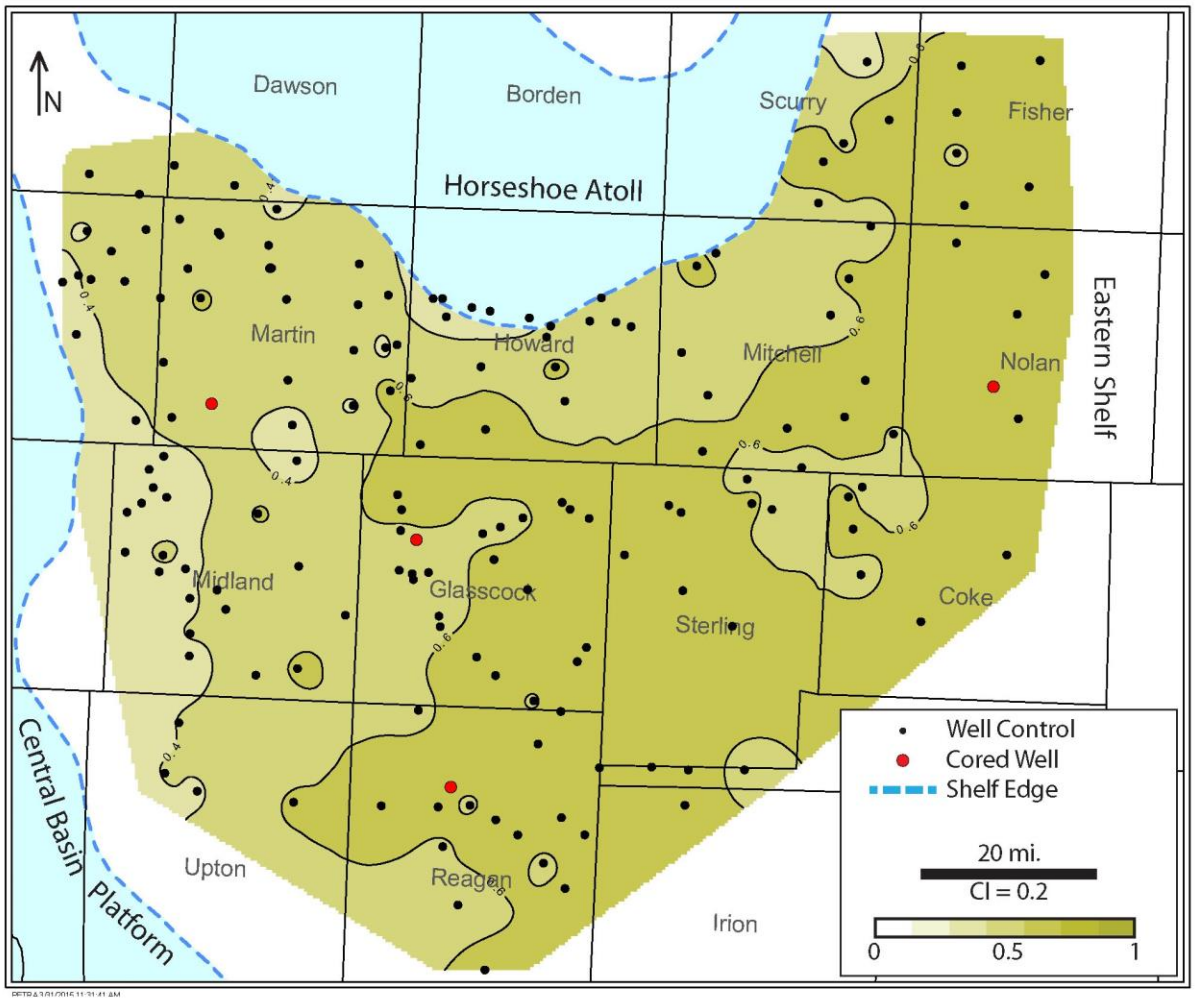

Figure 56: Gross Cline net-to-gross siliciclastic OM-poor lithofacies distribution. The largest net-to-gross values are located in the southeast half of the study area.

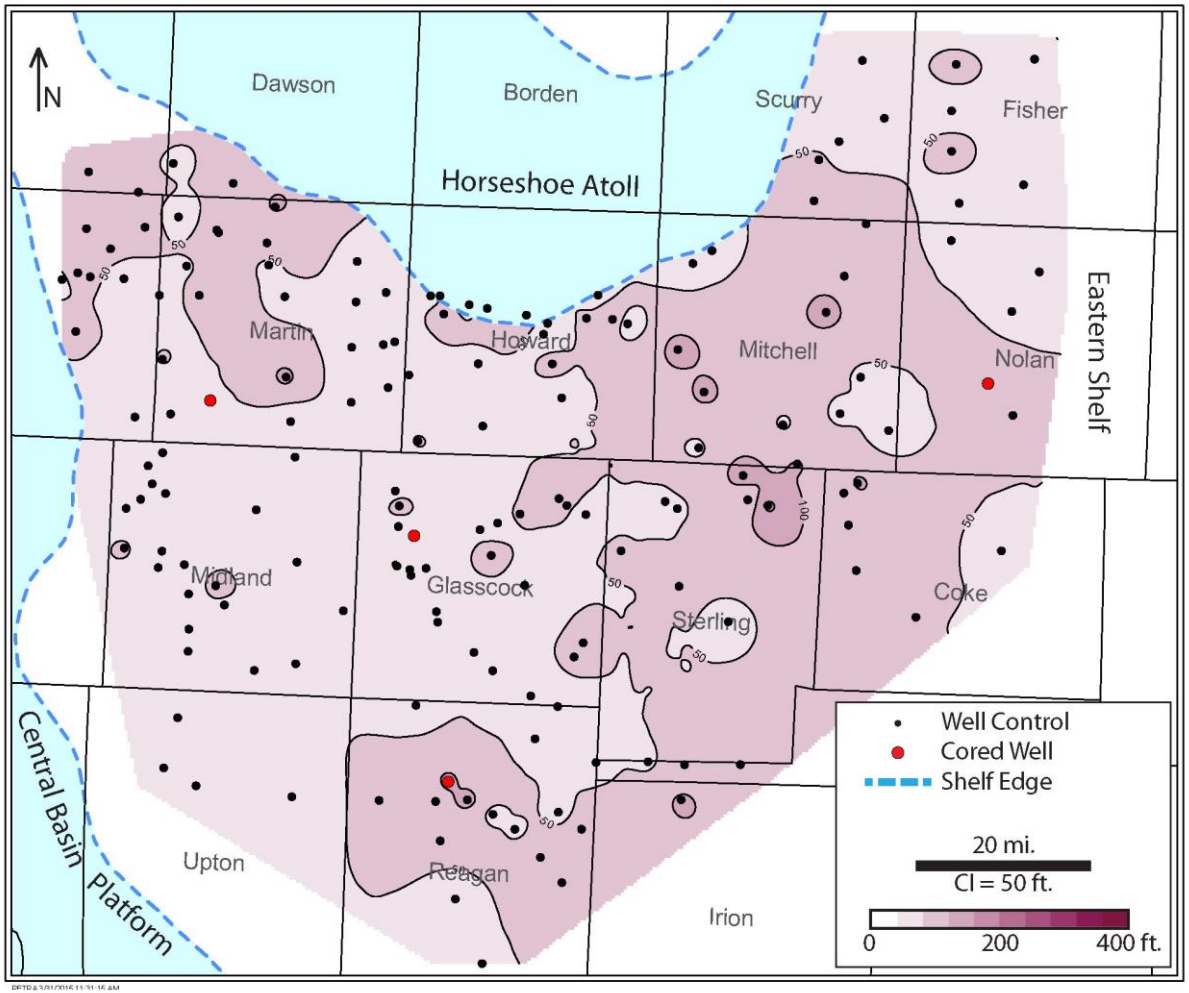

Figure 57: Gross Cline net siliciclastic OM-rich lithofacies distribution. The thickest deposits are concentrated in a fairway in Mitchell, Coke, and Sterling Counties, and in the northwest corner of the study area.

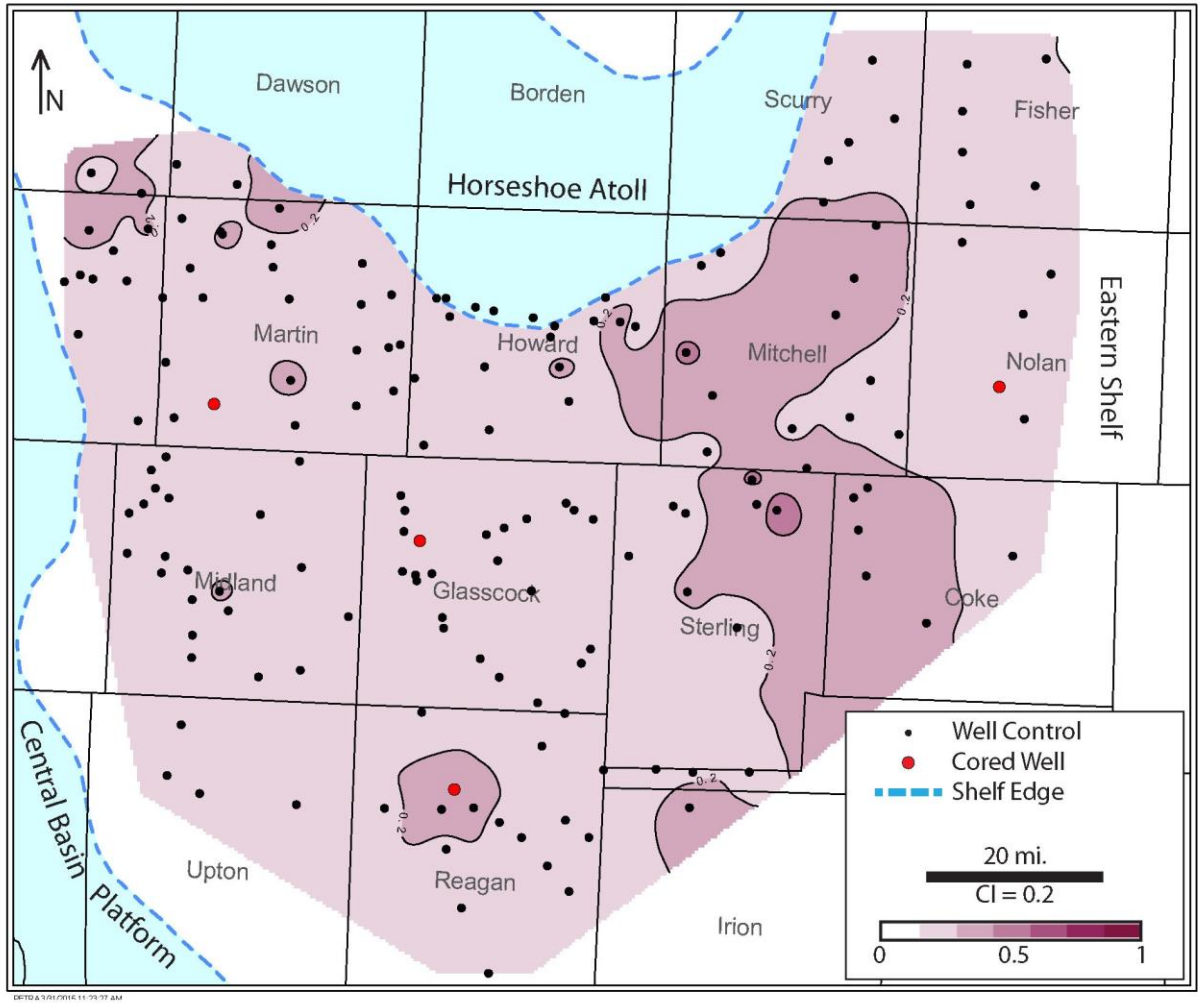

Figure 58: Gross Cline net-to-gross siliciclastic OM-rich lithofacies distribution. Largest net-to-gross values are located in Mitchell, Sterling, and Coke Counties.

Lower Cline Lithofacies Distribution Mapset

The Lower Cline deposits of the Southern Midland Basin are thin and sheetlike, commonly less than 50 feet thick (Figure 50). Because of the thin nature of these lithofacies, the net-to-gross maps useful in determining lithofacies distributions—especially in evaluating the relative importance of each lithofacies.

The carbonate lithofacies of the Lower Cline are mostly sheet-like in the basin, with areas of greatest thickness restricted to the basin edges, proximal to the source areas (Figures 59 and 60). The exception to this rule occurs in Glasscock County where there is an extensive, anomalous thick area.

The siliciclastic OM-poor lithofacies was deposited as a sheet in the basin probably from turbiditic or hemipelagic deposition; there are two small thick depocenters in the eastern and southeastern limits of the study (Figure 61). The net-to-gross map exhibits a distinct trend where greater than 0.4 net-to-gross siliciclastic OM-poor lithofacies are restricted to the southeastern half of the study area, with a small influence from the northeastern corner of the study area (Figure 62).

The siliciclastic OM-rich lithofacies has the largest relative thickness in the Lower Cline section (Figure 63). The net-to-gross of the siliciclastic OM-rich lithofacies commonly exceeds 0.4 (Figure 64). There does not seem to be a depositional trend associated with this lithofacies distribution, as it was deposited both in the basin and along the basin edges.

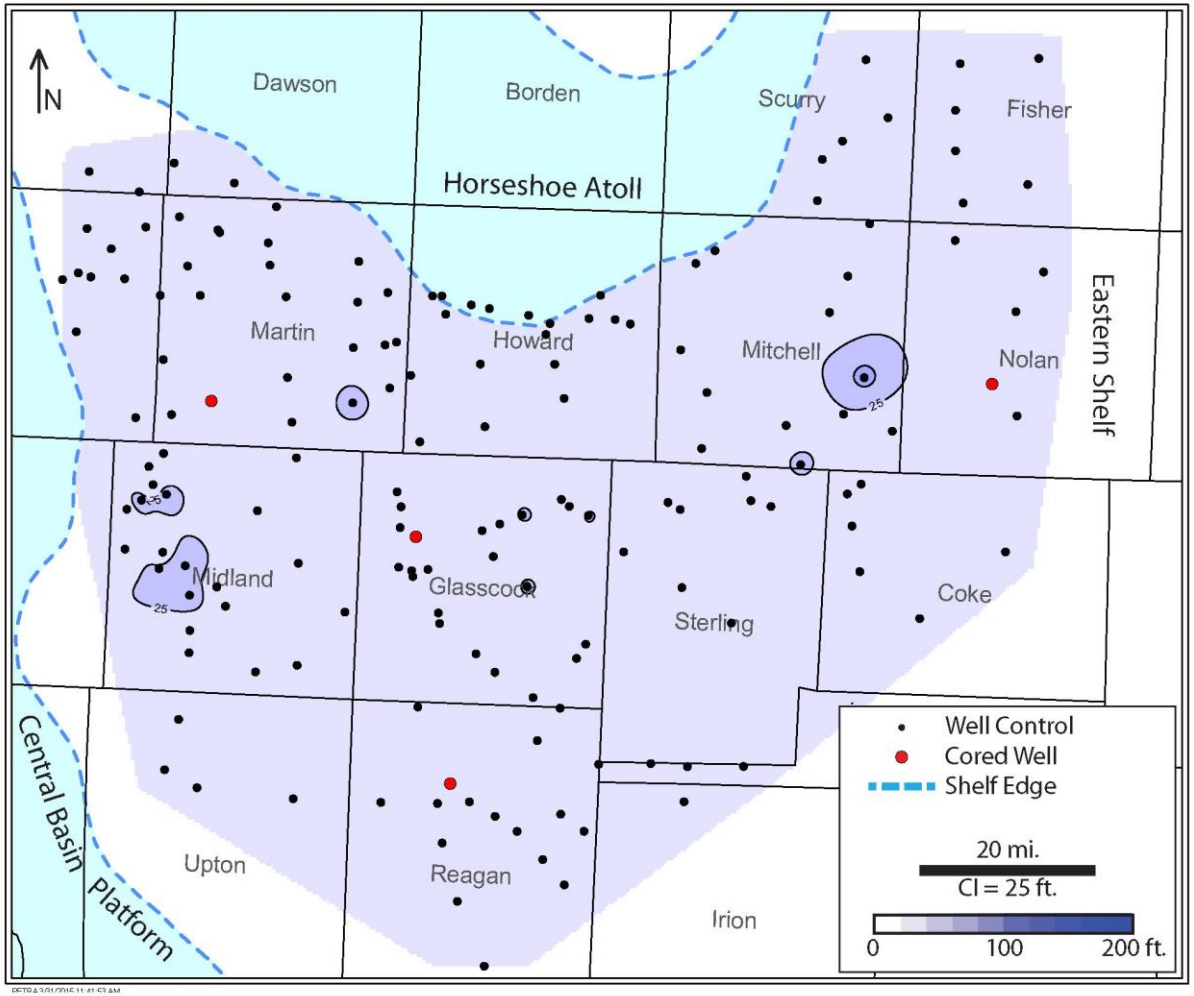

Figure 59: Lower Cline net carbonate lithofacies distribution. Small thicks are apparent in Mitchell and Midland Counties.

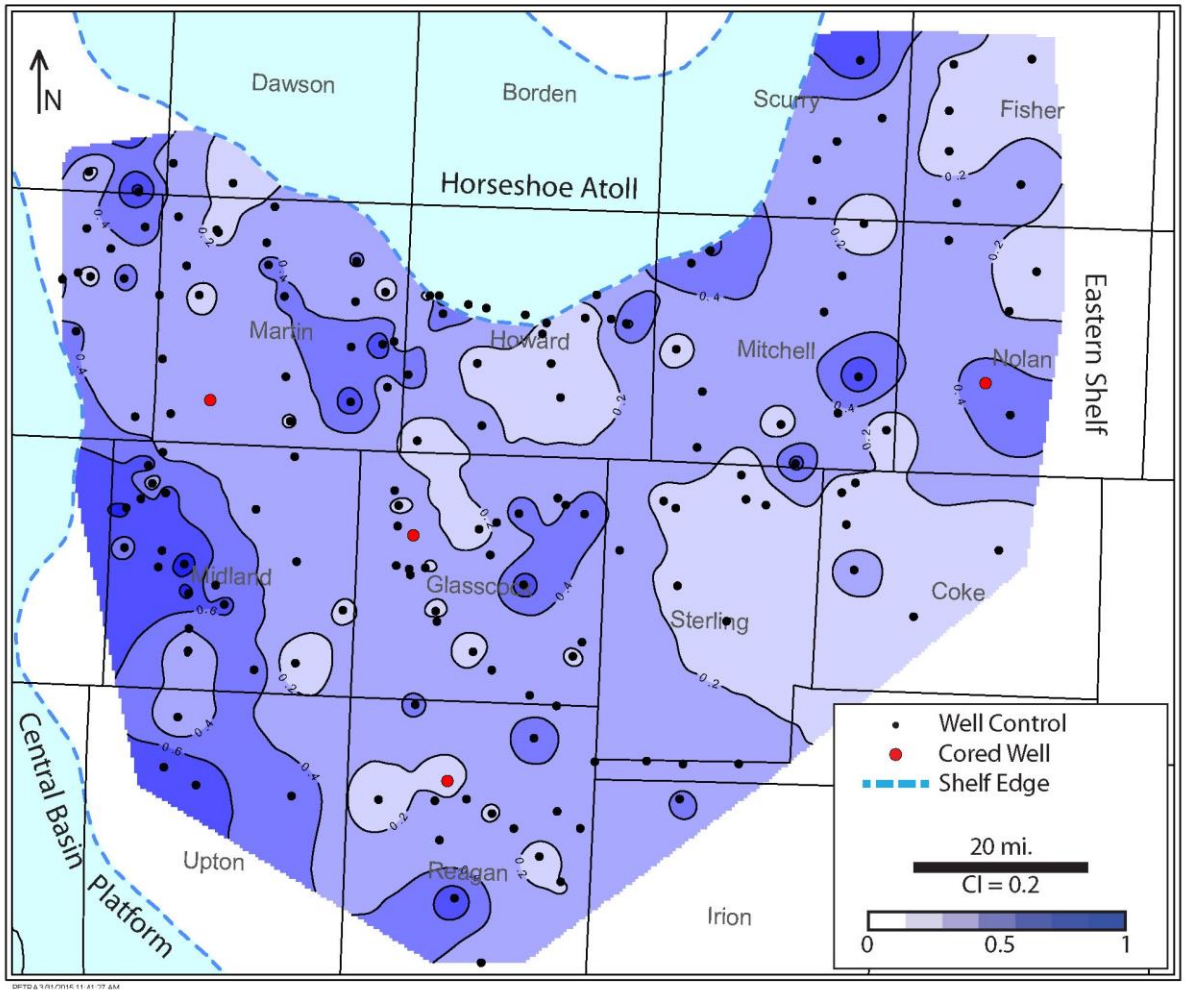

Figure 60: Lower Cline net-to-gross carbonate lithofacies distribution. Large net-to-gross values are detected proximal to the Central Basin Platform and sporadically throughout the basin.

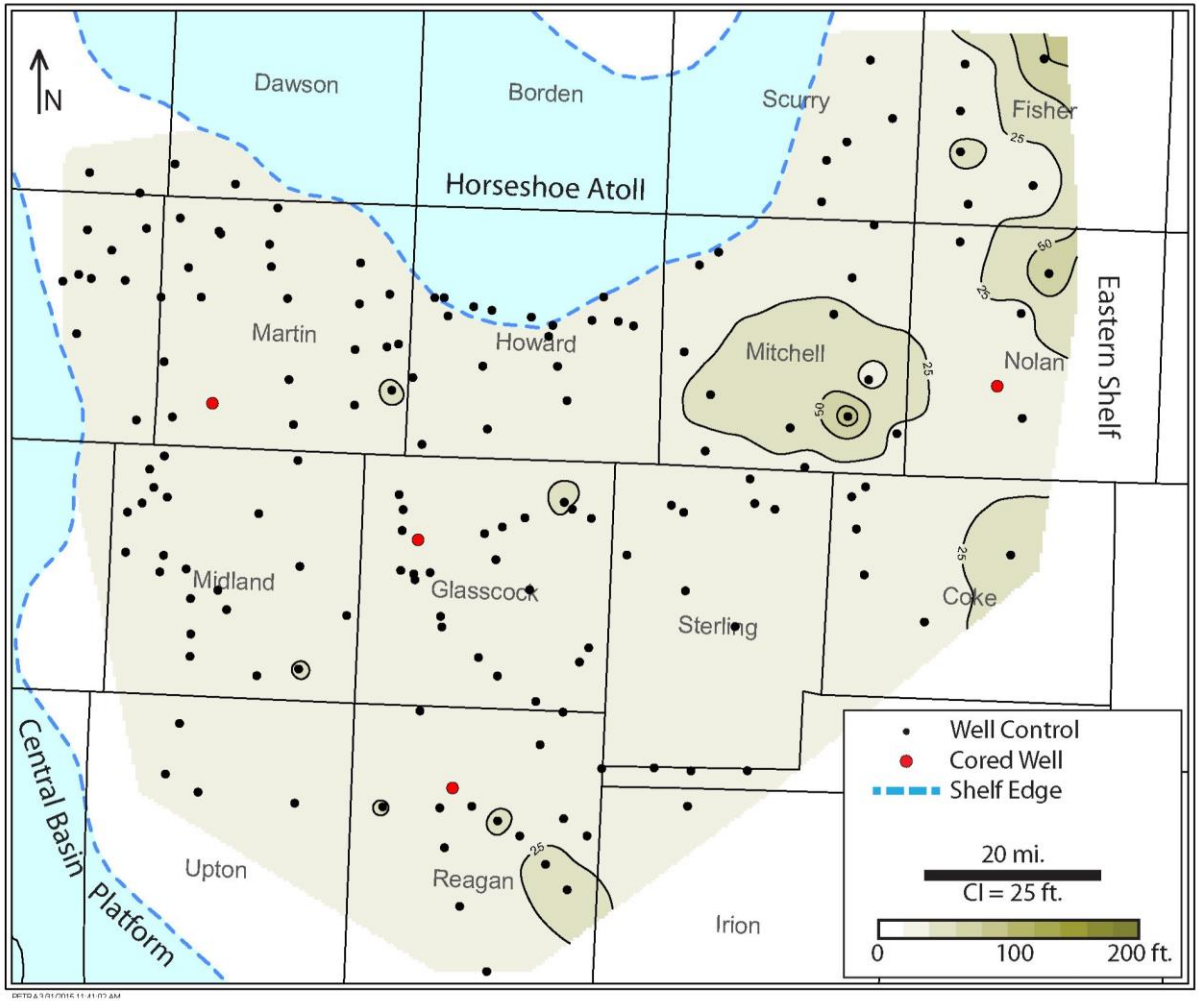

Figure 61: Lower Cline net siliciclastic OM-poor lithofacies distribution. Mitchell County contains a thick deposit.

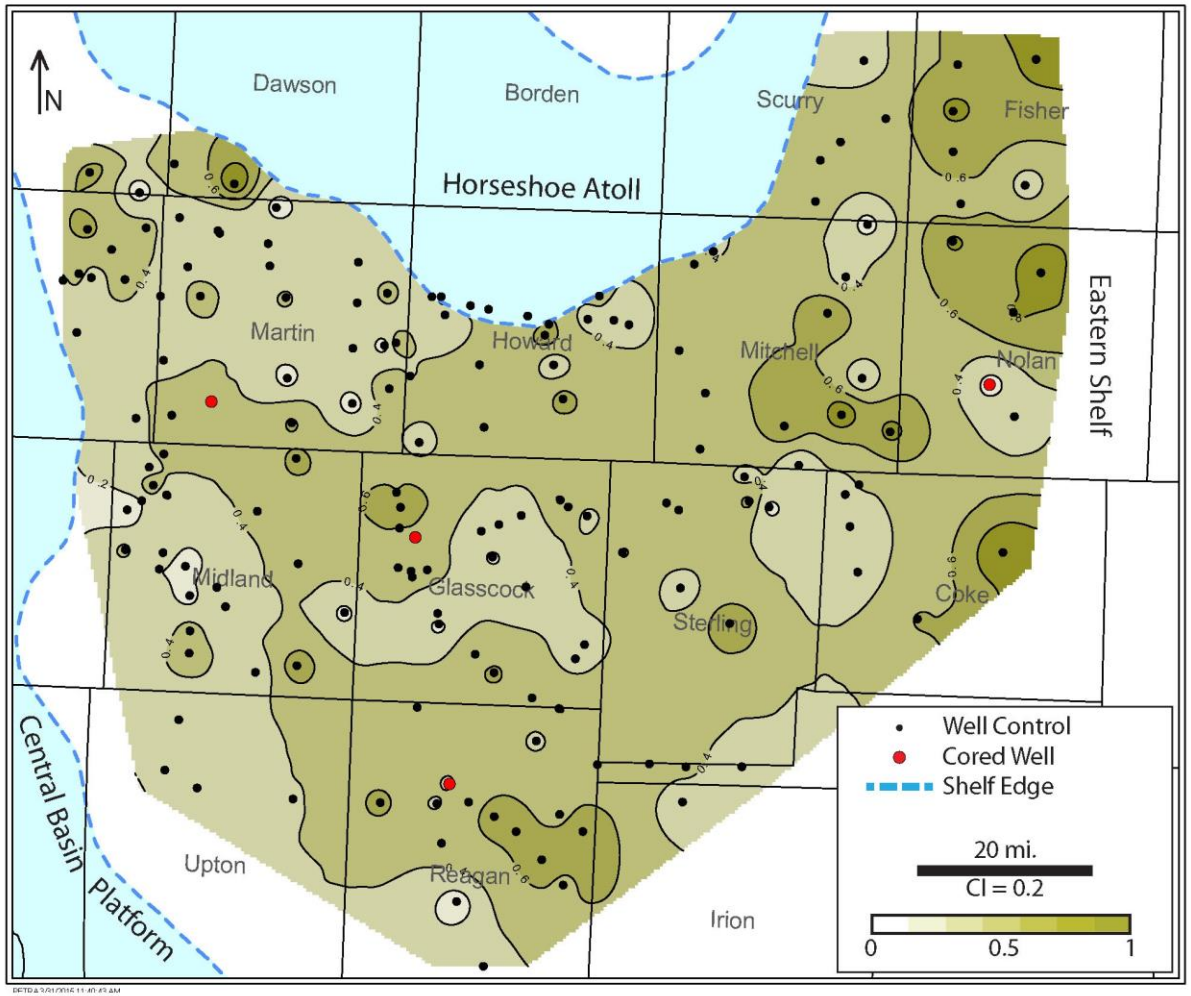

Figure 62: Lower Cline net-to-gross siliciclastic OM-poor lithofacies distribution. No facies trends are apparent.

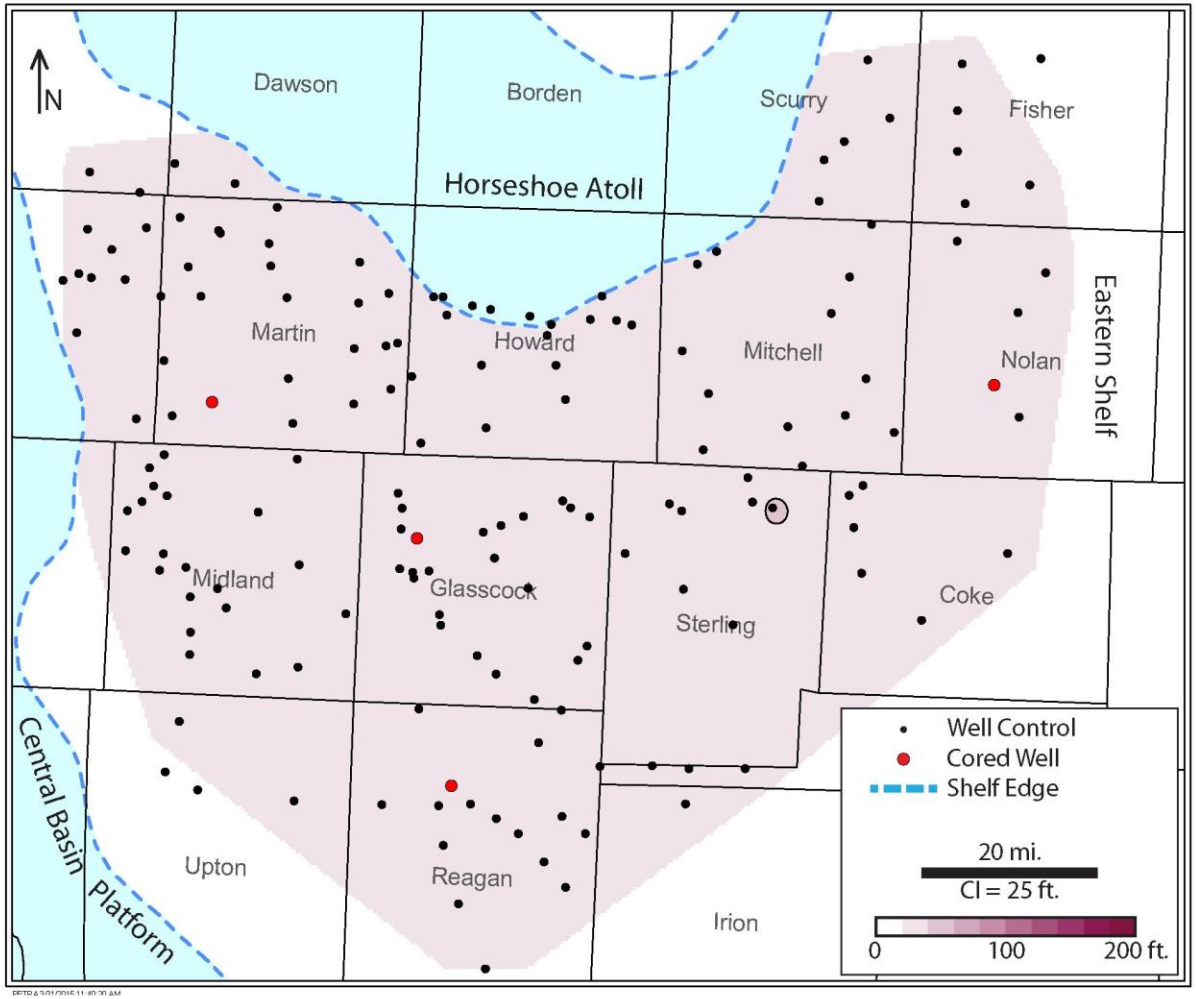

Figure 63: Lower Cline net siliciclastic OM-rich lithofacies distribution. All OM-rich lithofacies are less than 25 net feet in the Lower Cline except a small area in Sterling County.

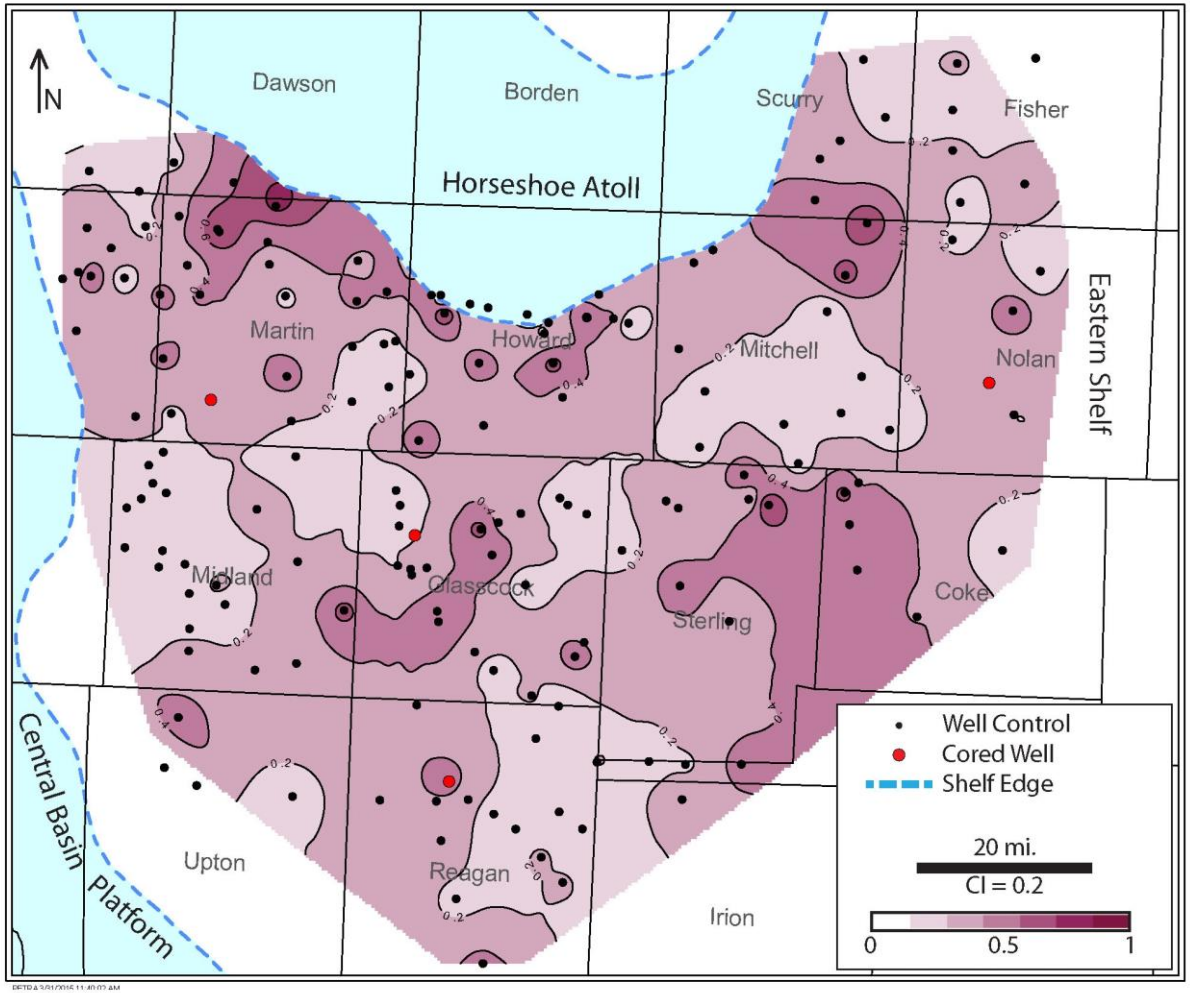

Figure 64: Lower Cline net-to-gross siliciclastic OM-rich lithofacies distribution. There is no apparent trend in the facies distribution.

Middle Cline Lithofacies Distribution Mapset

The Middle Cline interval marks a time of mixed clastics and carbonates. A line can be drawn from the southwest to the northeast that separates siliciclastic dominated lithofacies to the south and the east from carbonate dominated lithofacies from the west and north.

Thickest carbonate deposits are restricted to the edges of the basin during deposition of the Middle Cline (Figures 65-66). They are mostly associated with the boundaries of the Central Basin Platform and the Horseshoe Atoll—two well established carbonate sources (Vest, 1970; Waite, 1993; Saller, 1994).

The net lithofacies distribution of the Middle Cline siliciclastic OM-poor lithofacies is dominated by a linear thickness trend from the southeast to the northwest (Figure 67). Though this net thickness trend extends into the northwest portion of the study area, the relative importance of the siliciclastic OM-poor lithofacies diminishes in the northwest half (Figure 68). This is because the siliciclastic OM-poor lithofacies was diluted by the carbonate lithofacies. The influence of carbonate dilution restricts the siliciclastic OM-poor lithofacies to the southeastern half of the basin.

There are three main areas with thicker net sections of the siliciclastic OM-rich lithofacies in the Middle Cline. The largest concentration is in the northeast section of the study area, and there are also areas of great thickness in the southeast and northwest corners of the study area (Figure 69). The area of great thickness to the northeast is reinforced by the map of relative abundance of the siliciclastic OM-rich lithofacies

(Figure 70). There is an absence of deposition of carbonates and siliciclastic OM-poor lithofacies in this area, resulting in a relative concentration of OM-rich lithofacies.

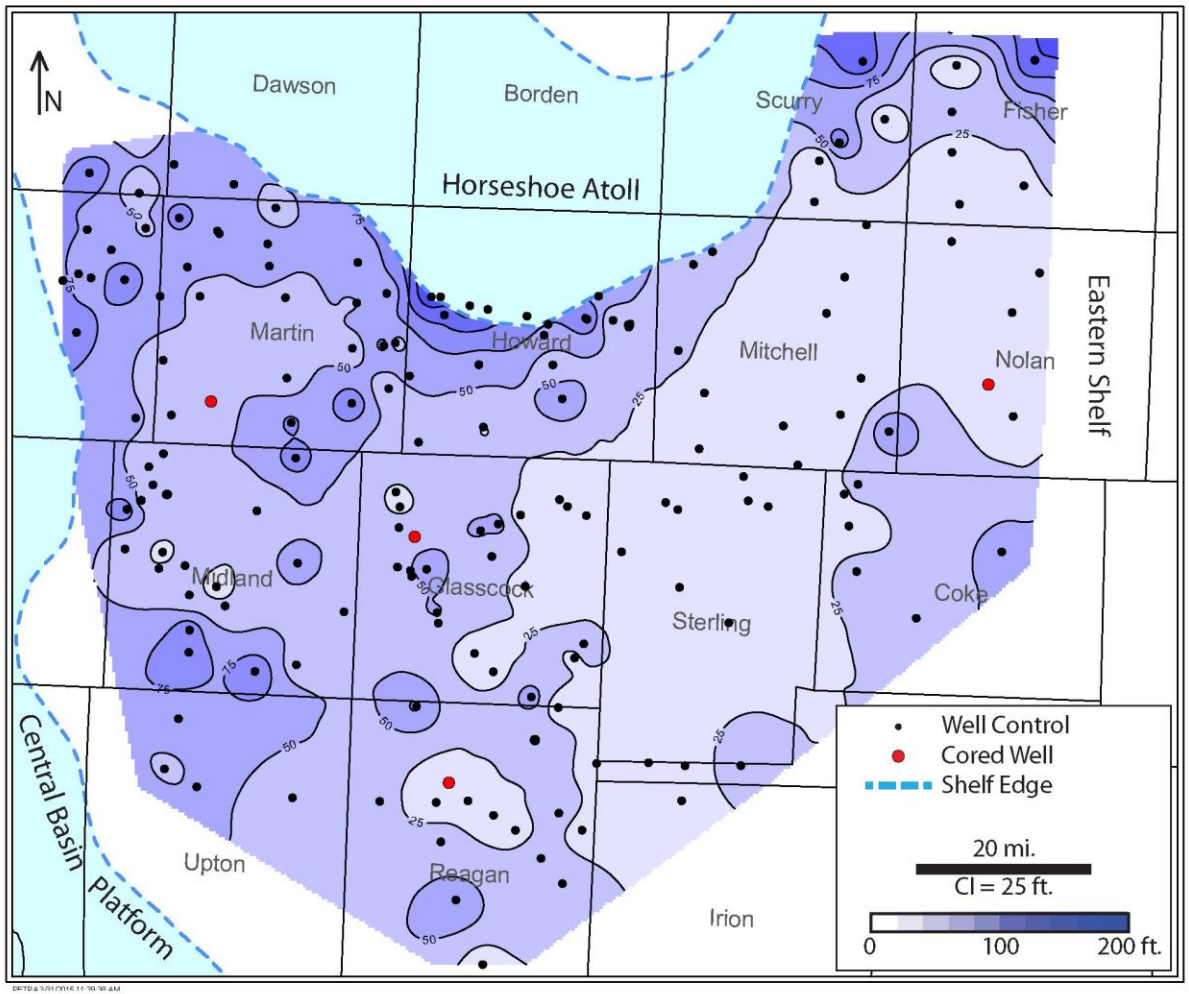

Figure 65: Middle Cline net carbonate lithofacies distribution. The thickest deposits are proximal to the Horseshoe Atoll and Central Basin Platfom.

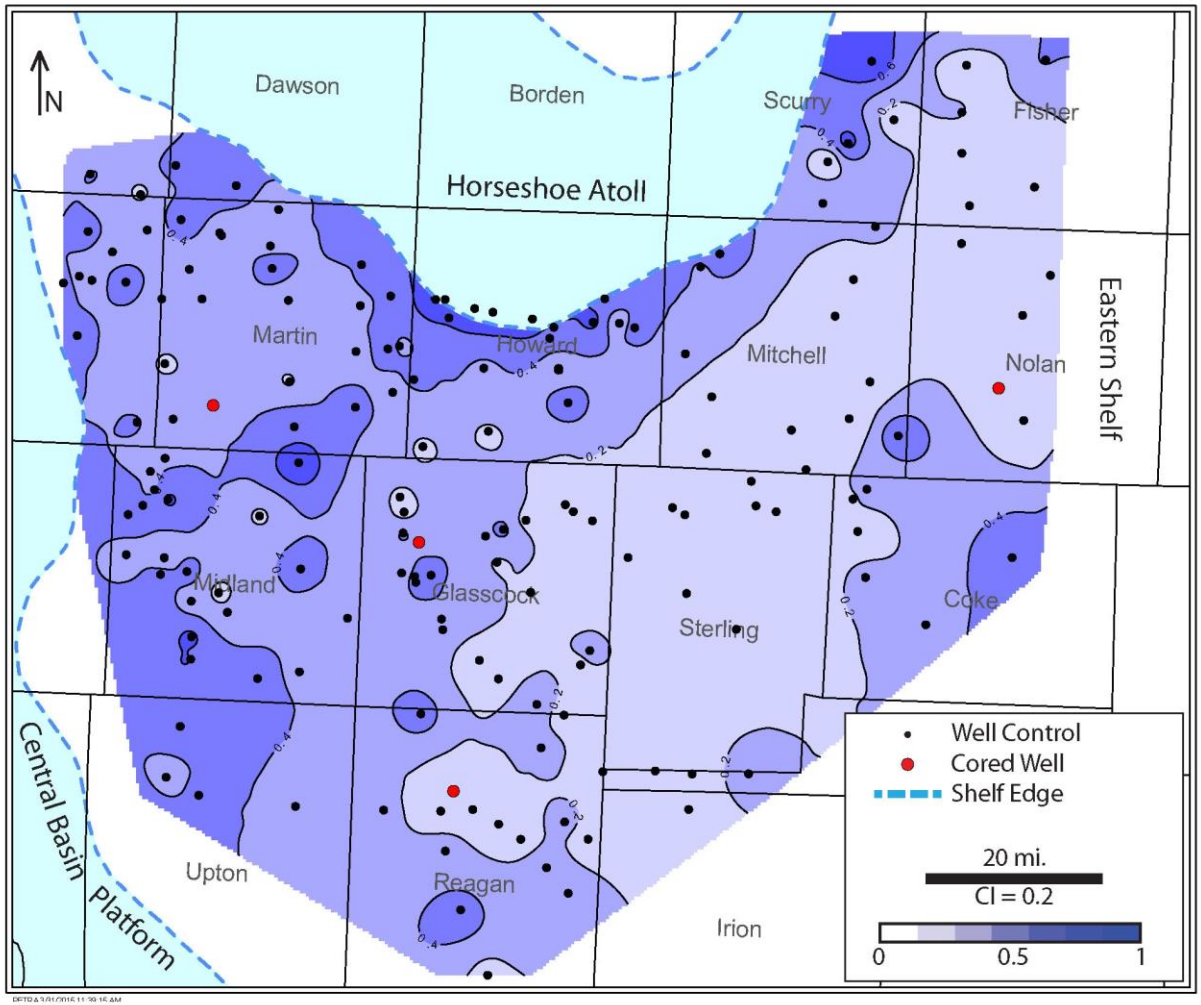

Figure 66: Middle Cline net-to-gross carbonate lithofacies distribution. The largest net-to-gross deposits are proximal to the Horseshoe Atoll and the Central Basin Platform.

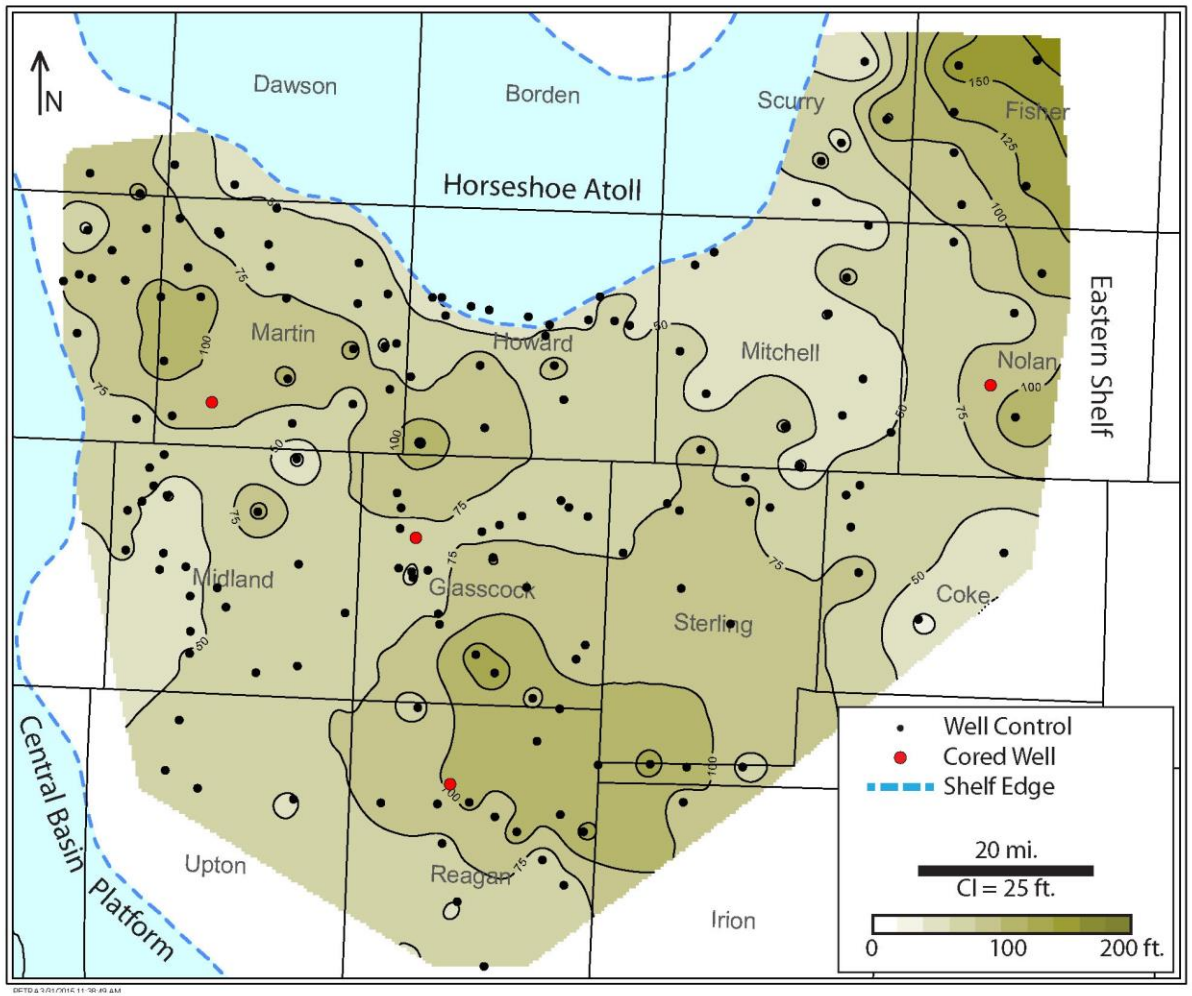

Figure 67: Middle Cline net siliciclastic OM-poor lithofacies distribution. There is a NW-SE trending thick through the basin center.

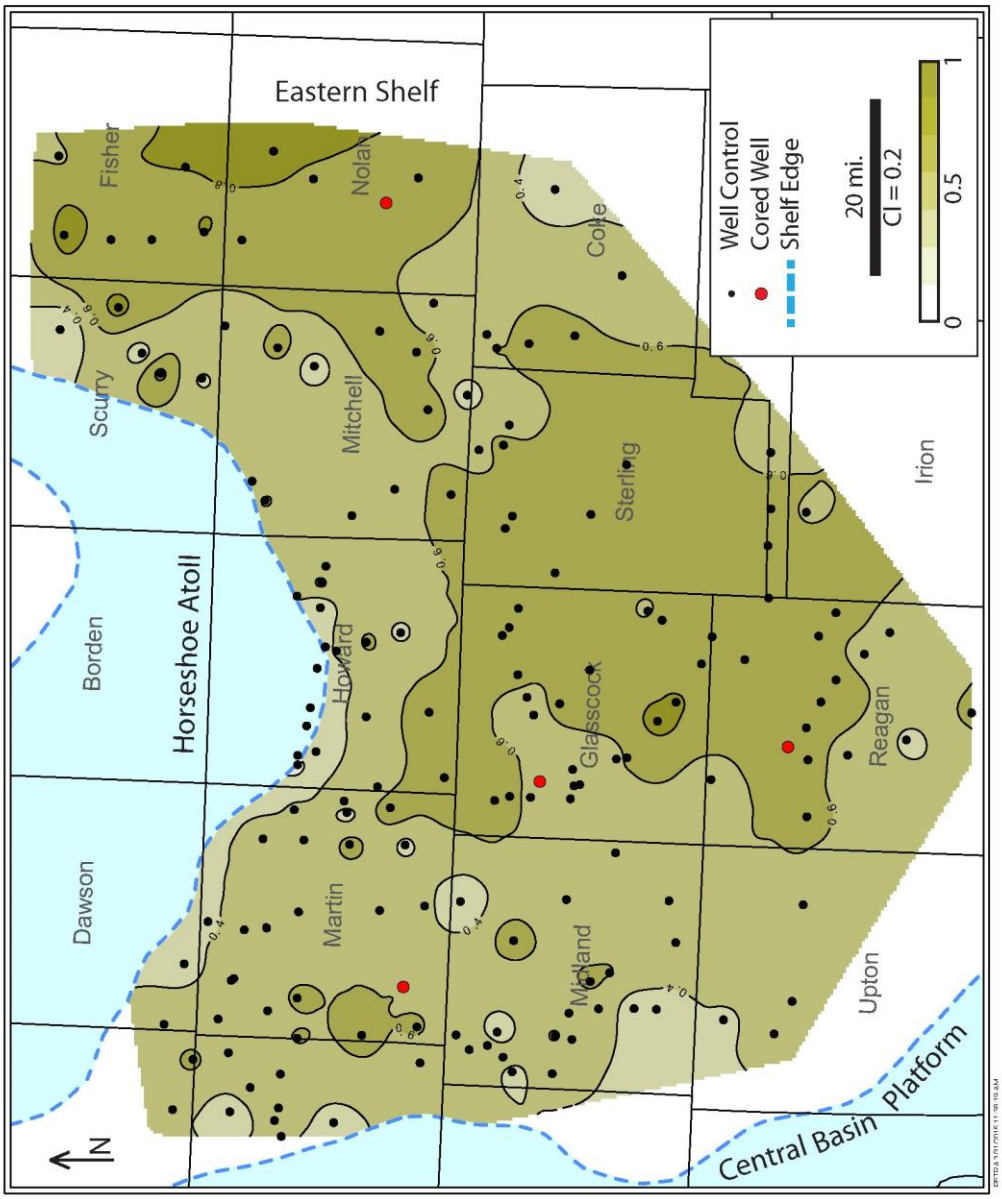

Figure 68: Middle Cline net-to-gross siliciclastic OM-poor lithofacies distribution. The largest net-to-gross values are in the southeast portion of the basin.

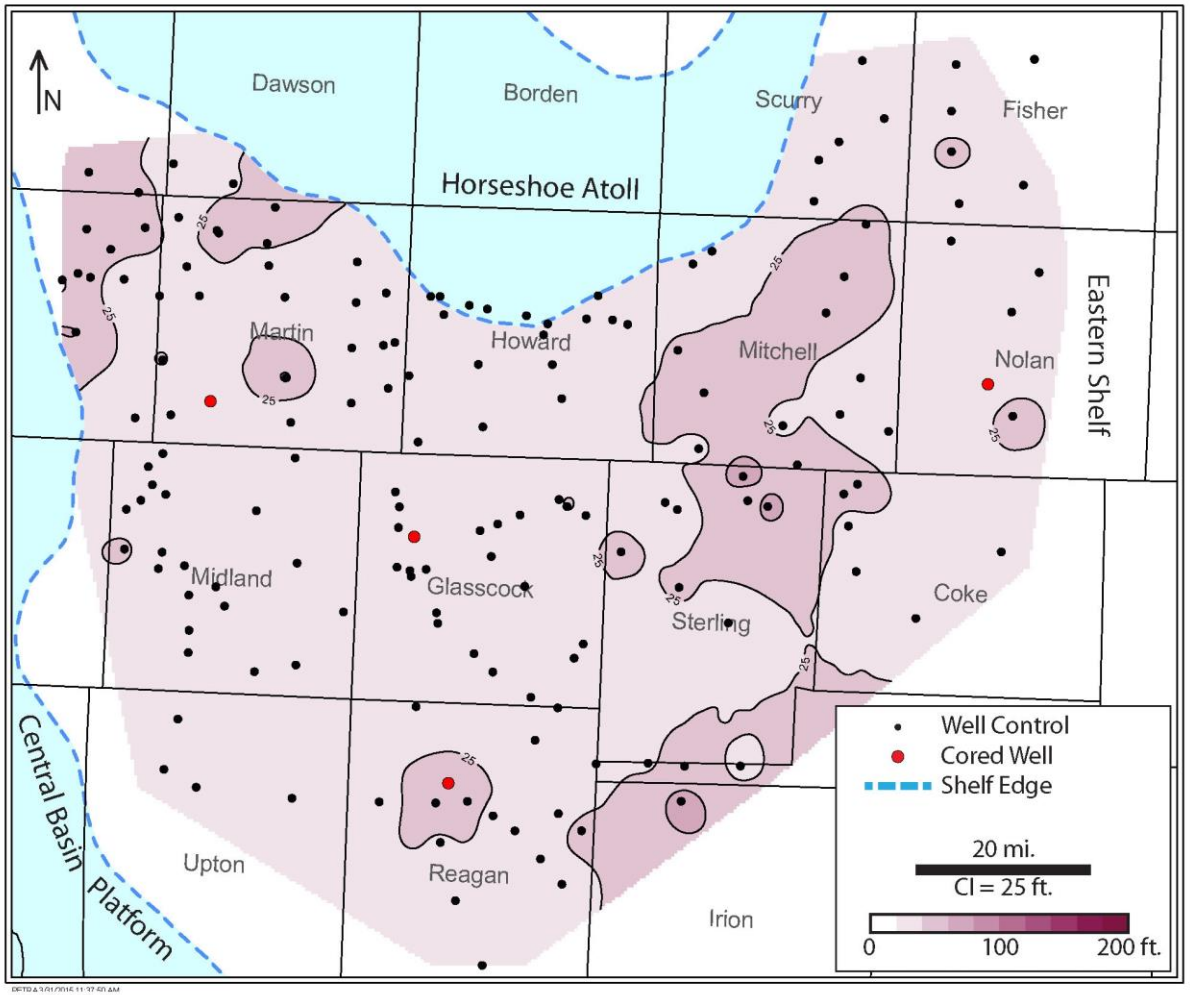

Figure 69: Middle Cline net siliciclastic OM-rich lithofacies distribution. There is a thick in Mitchell and Sterling Counties.

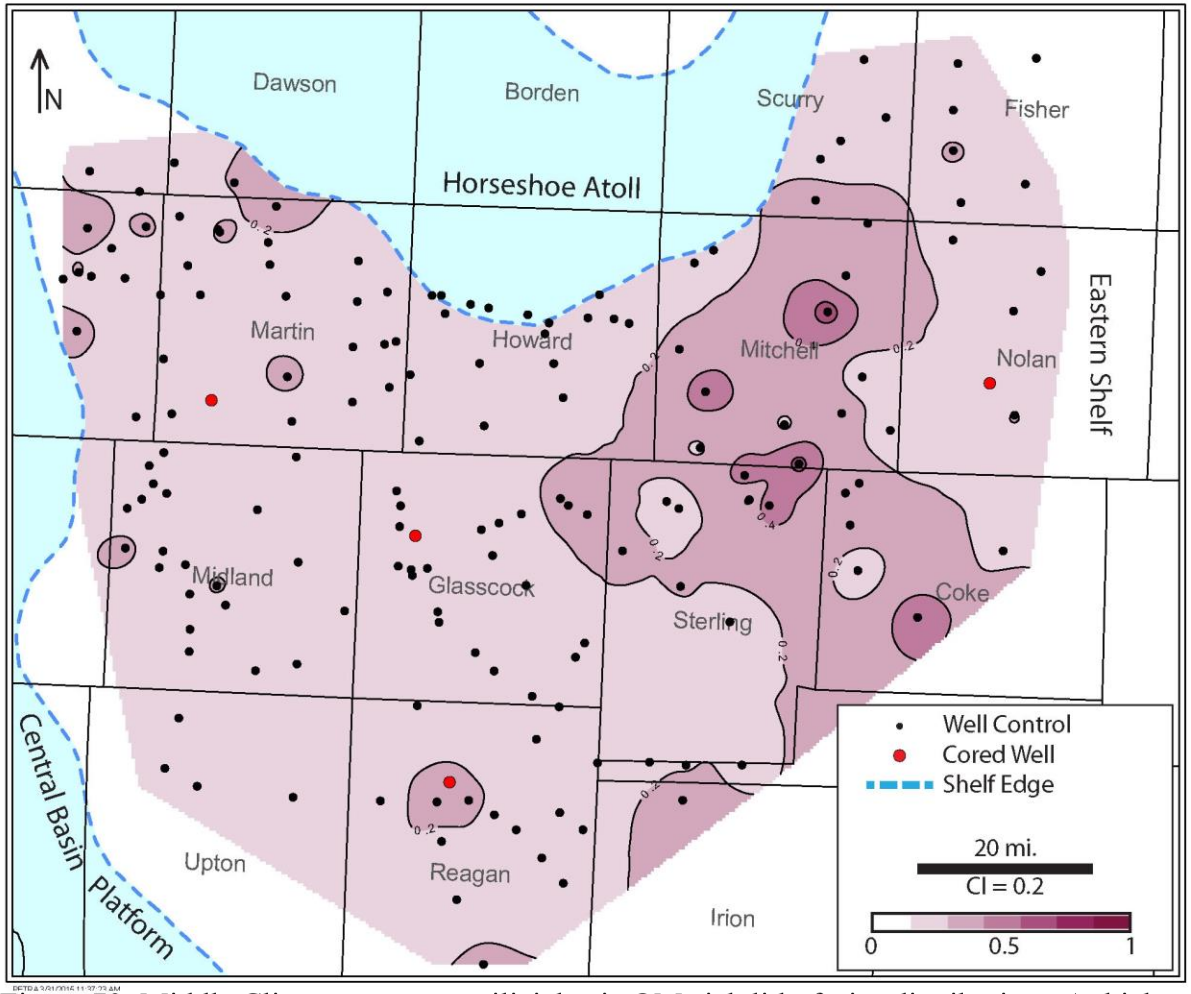

Figure 70: Middle Cline net-to-gross siliciclastic OM-rich lithofacies distribution. A thick fairway runs through Mitchell, Sterling, and Coke Counties.

Upper Cline Lithofacies Distribution Mapset

The Upper Cline was a time of siliciclastic encroachment. Though there is still a southwest-northeast trending line that separates the siliciclastic dominated area and the carbonate dominated area, the line has shifted to the northwest, and the siliciclastic lithofacies have become more dominant than in the Middle Cline.

The carbonate lithofacies is most common in the northwest portion of the study area. Although the thickest deposits occur along the edges of the basin, there was a considerable amount of carbonate deposition in the basin—especially throughout Martin County (Figure 71). Carbonate deposits exceed 50 feet throughout most of the basin during the Upper Cline. However, their relative importance diminishes to the south and east as there is a greater influence of siliciclastic sedimentation in the basin (Figure 72).

The majority of siliciclastic OM-poor lithofacies are restricted to the southern and eastern shelves and the basin floor. Thicknesses in excess of 75 feet are common throughout the basin floor, and exceed 125 feet (Figure 73). The siliciclastic OM-poor lithofacies is the dominant facies of the Upper Cline section, where the southeastern half of the study area is almost completely more that 0.6 net-to-gross siliciclastic OM-poor lithofacies (Figure 74).

The most important area of siliciclastic OM-rich deposition is the northeast portion of the study area, where there are elongate areas of more than 50 feet thick net deposits extending into the basin from the southeast and the northwest (Figure 75). The importance of the siliciclastic OM-rich deposits is reinforced with the net-to-gross map;

there is a fairway of greater than 0.2 net-to-gross siliciclastic OM-rich lithofacies, with values exceeding 0.4 in Howard, Mitchell, Sterling, and Coke Counties (Figure 76).

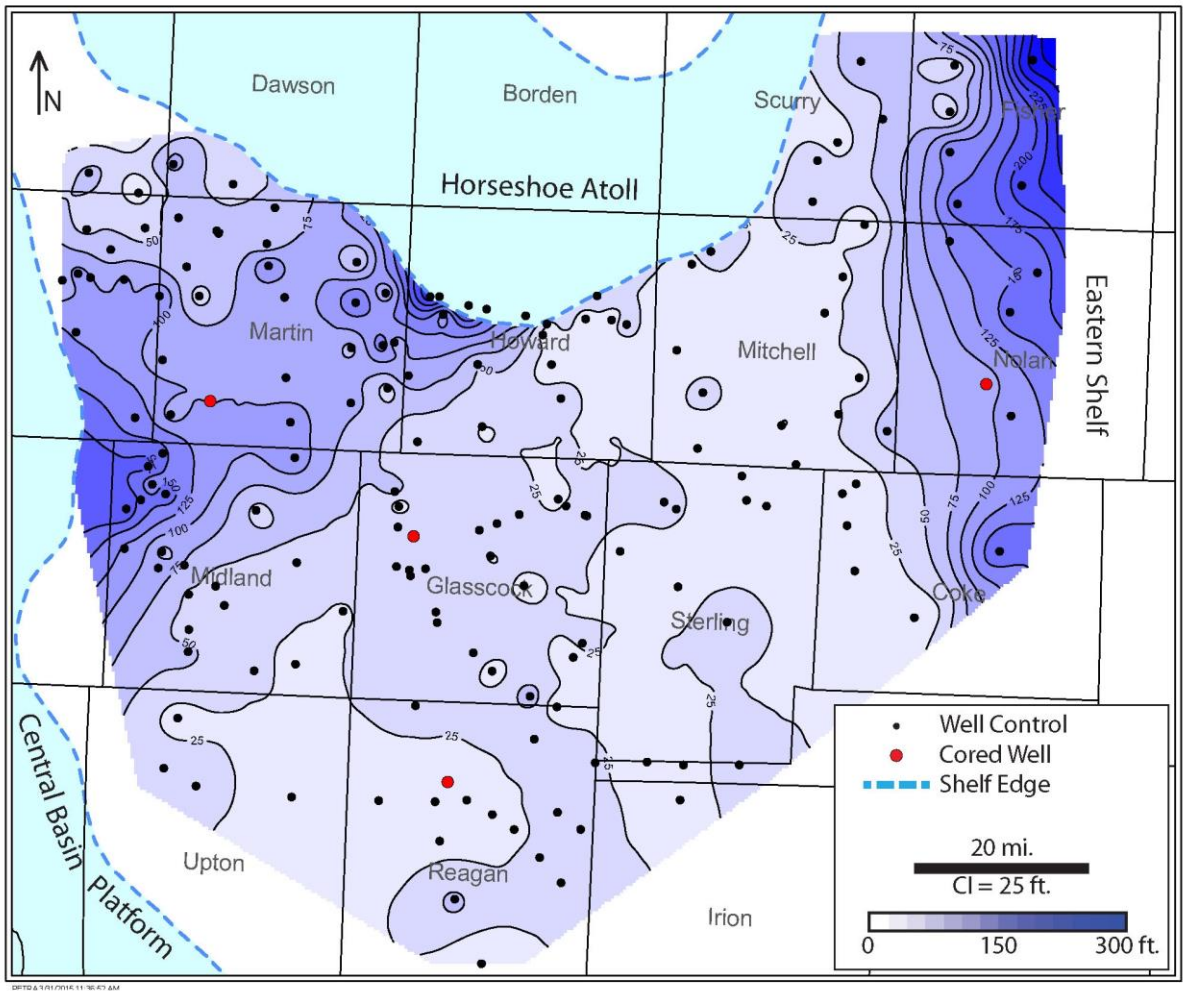

Figure 71: Upper Cline net carbonate lithofacies distribution. The thickest carbonate deposits are proximal to the Eastern Shelf, western Horseshoe Atoll, and the Central Basin Platform.

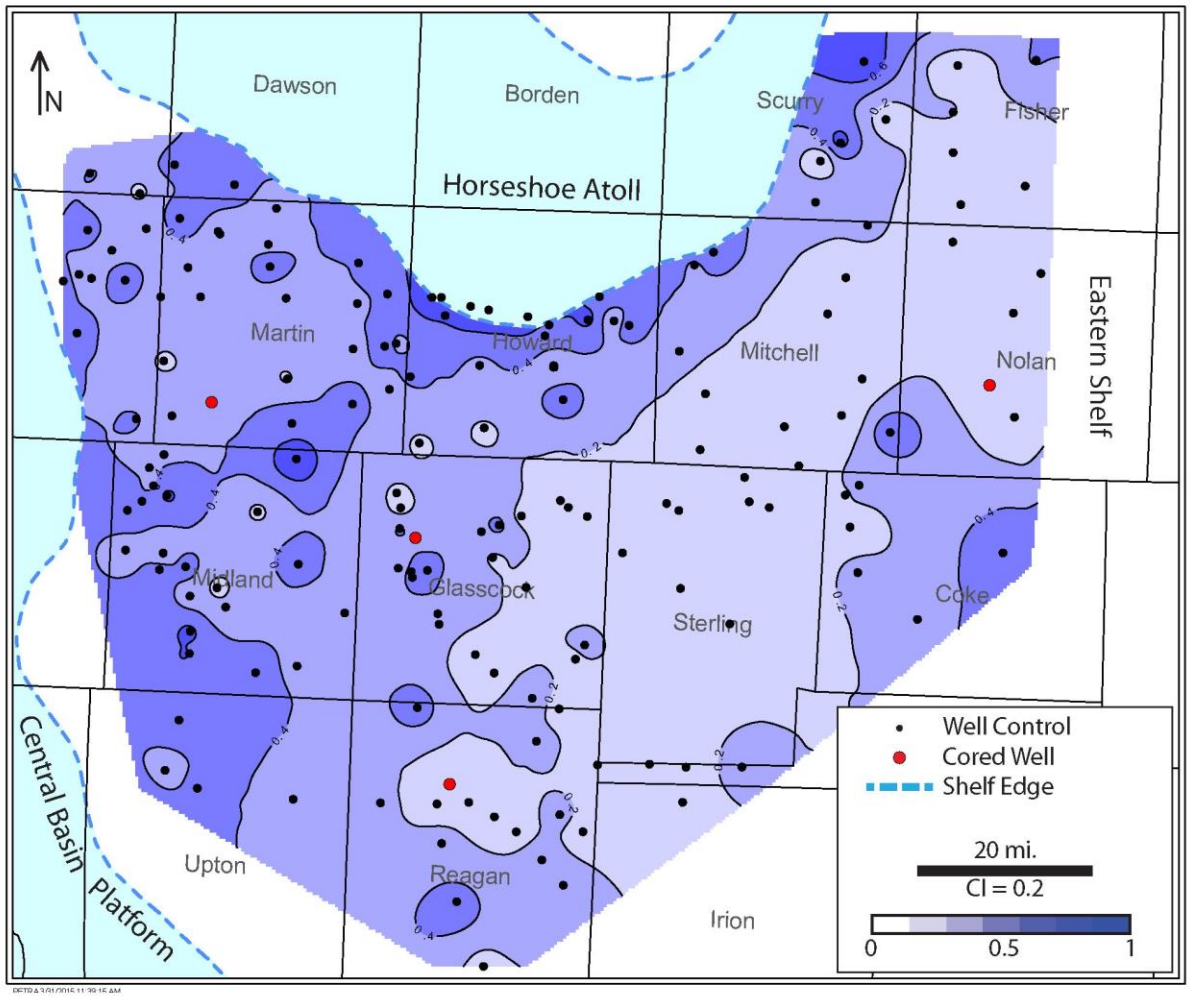

Figure 72: Upper Cline net-to-gross carbonate lithofacies distribution. The larges net-to-gross values are in the northwest portion of the basin.

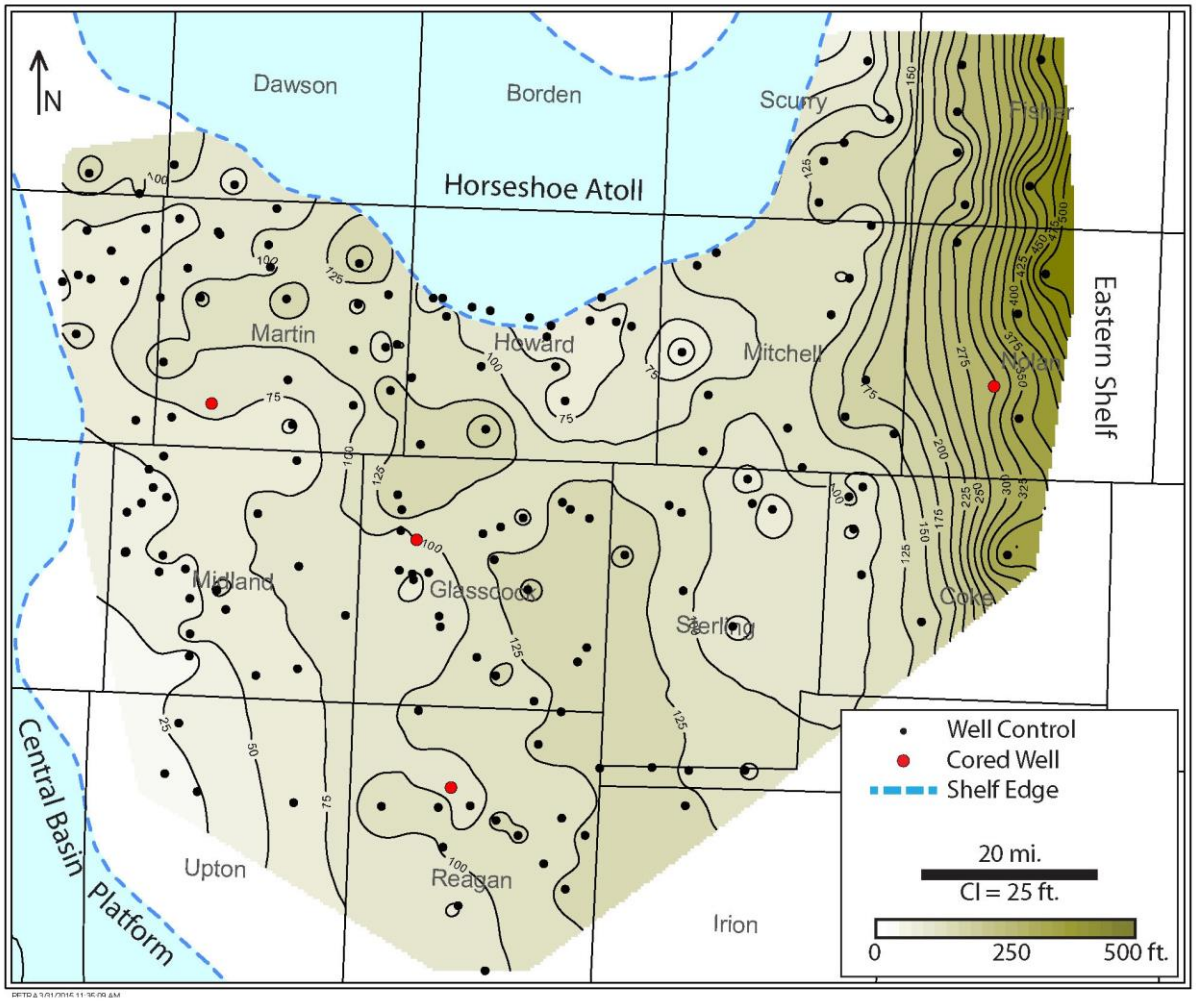

Figure 73: Upper Cline net siliciclastic OM-poor lithofacies distribution. The thickest deposits are proximal to the eastern shelf (associated with Cline-equivalent slope facies) and a NW-SE trending thick in the center of the study area.

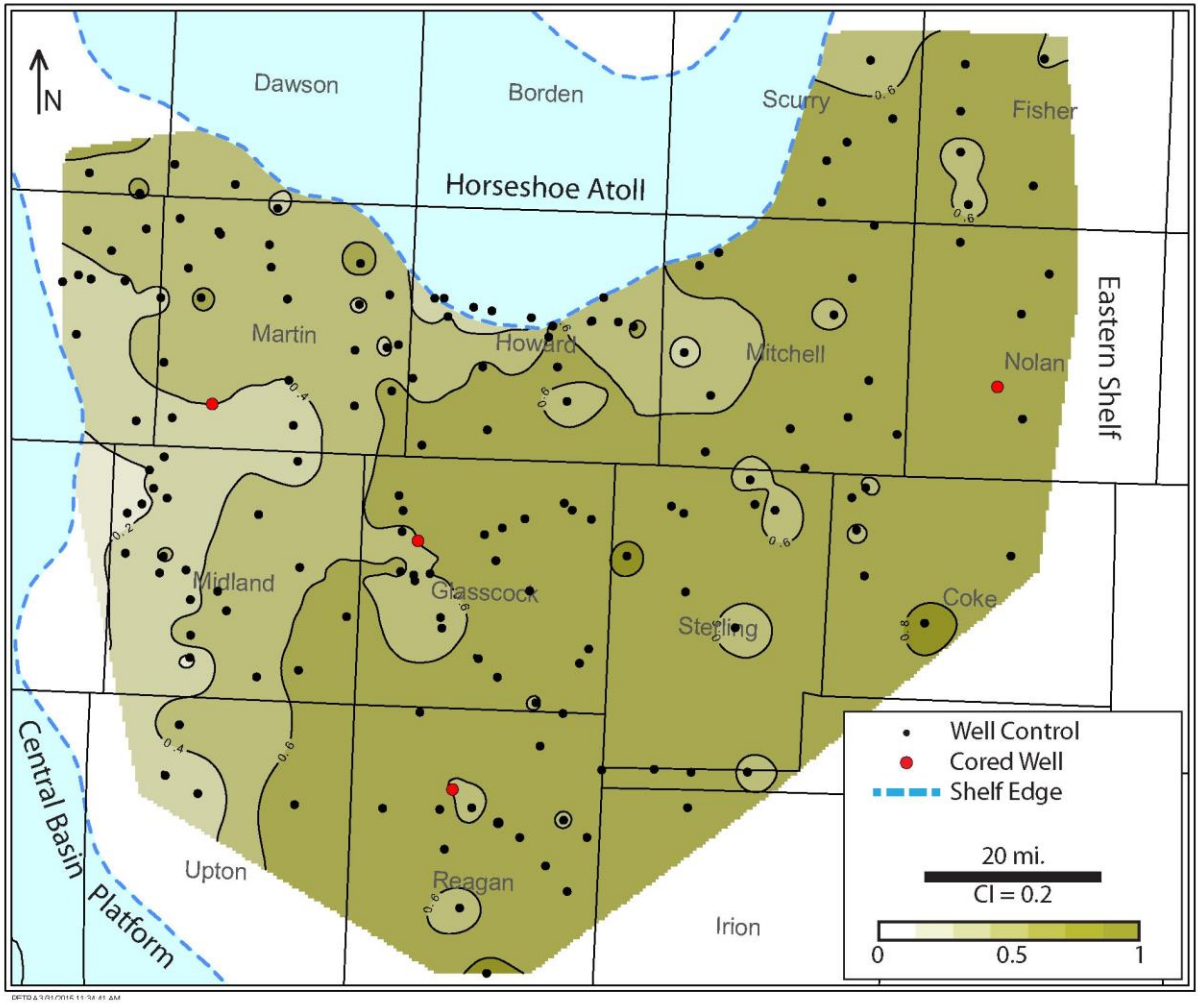

Figure 74: Upper Cline net-to-gross siliciclastic OM-poor lithofacies distribution. The largest net-to-gross values are restricted to the southeast portion of the basin.

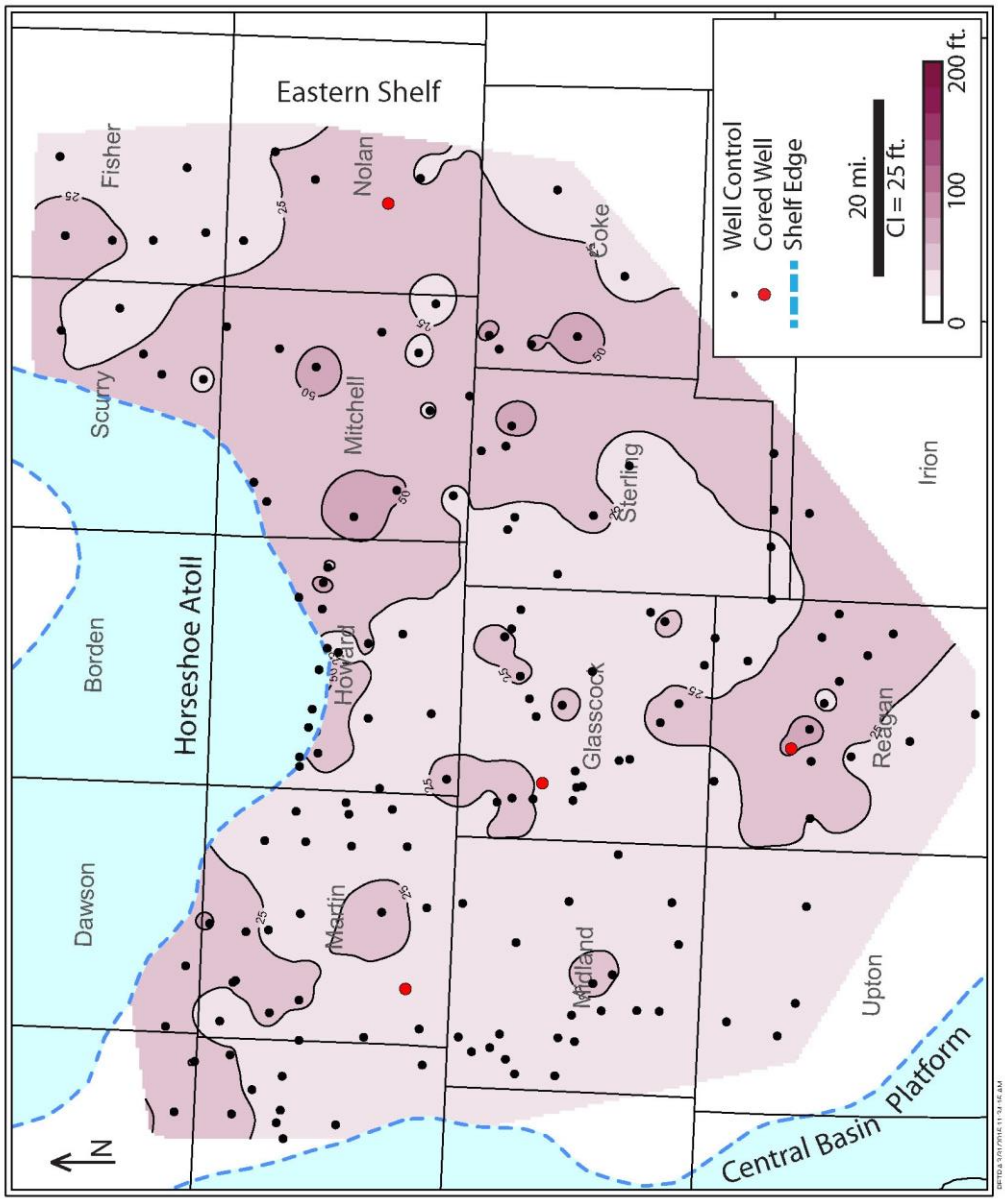

Figure 75: Upper Cline net siliciclastic OM-rich lithofacies distribution. The thickest deposits are in Mitchell, Nolan, Coke, and Reagan counties.

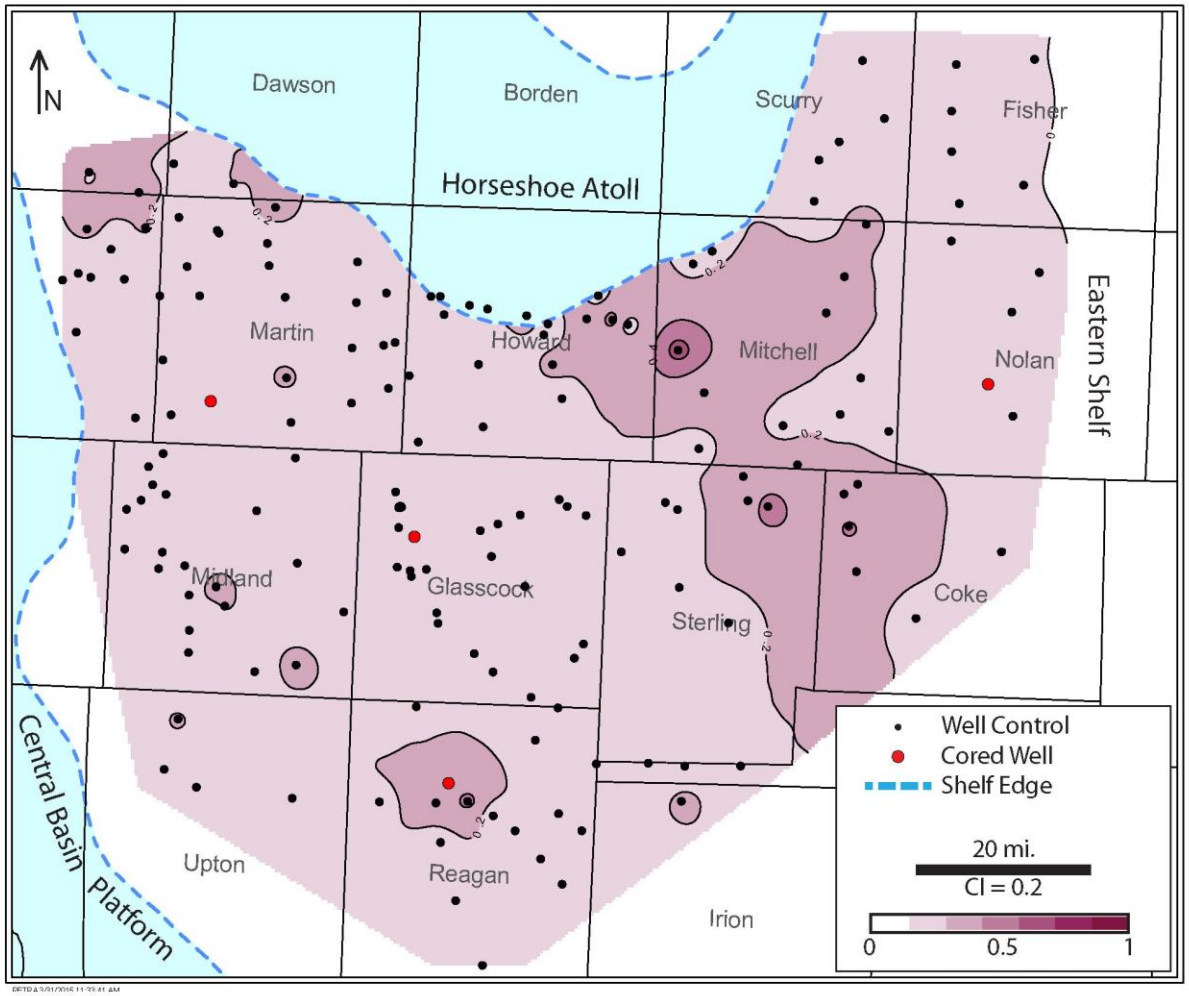

Figure 76: Upper Cline net-to-gross siliciclastic OM-rich lithofacies distribution. The largest net-to-gross values are in Mitchell, Sterling, and Coke Counties.

Regional Cross Sections

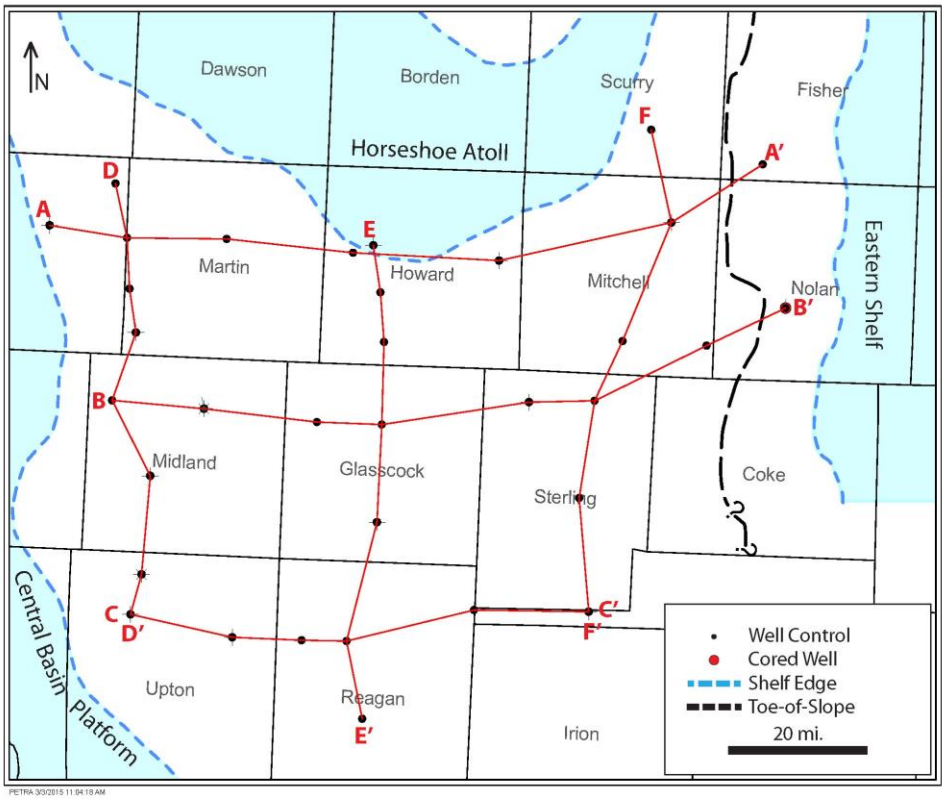

Figure 77: Basemap of six regional cross sections.

Six regional cross sections highlight the lateral and vertical heterogeneity of the Cline Shale (Figure 77). All datums for these cross is the top of the Strawn limestone, a regionally distinct marker bed. Well logs in each cross section contain the same lithofacies cutoffs as used for the lithofacies distribution maps, and the Lower, Middle, and Upper sections of the Cline are picked. The lateral and vertical heterogeneities are evident from these cross sections. Regional temporal changes in deposition become distinguishable when comparing lithofacies distributions across the Lower Cline, Middle Cline, and Upper Cline.

A to A' displays the northern portion of the basin from east to west (Figure 78). The far western section of the cross section and the well adjacent to the west side of the horseshoe atoll are carbonate rich. The remainder of the wells are dominated by siliciclastics. The incipient slope facies of the Upper Cline Eastern Shelf are visible in the easternmost well. The well in Mitchell County exhibits the largest amount of siliciclastic OM-rich lithofacies, but it is interbedded with siliciclastic OM-poor lithofacies.

B to B' transverses the central portion of the basin from west to east and contains the Harris well on the eastern margin (Figure 79). B to B' displays the increased carbonate content associated with deposition proximal to the Central Basin Platform. The blocky carbonate signatures seen in the western-most well are consistent with debris flows and other allochthonous carbonate deposits. In the far east of the cross section, the progradation of the Eastern Shelf can be seen in the Upper Cline. The Harris well contains Cline basinal facies, as well as toe-of-slope and slope facies in the uppermost portion of the Upper Cline; this change occurs at 6310'.

C to C' is the southern-most west-to-east cross section (Figure 80). C to C' displays a high degree of vertical and lateral variability. The western portion of the cross section is proximal to the Central Basin Platform. However, the western-most well in the cross section is dominated by carbonates only in the Upper Cline.

D to D' is a north-south cross section that follows closely to the platform edge of the Central Basin Platform (Figure 81). This cross section displays heterogeneities

associated with deposition of the Central Basin Platform. The Lower Cline deposition is heterogeneous, with wells containing relatively thick, blocky carbonate deposits (up to 50 feet thick) and very thin, mixed carbonate and siliciclastic deposits. The Middle Cline contains fewer carbonate deposits with the exception of the well in northern Upton County that contains over 50 feet of a single blocky carbonate deposit.

E to E' extends from the Horseshoe Atoll, through the middle of the basin and to the southern end of the study area (Figure 82). The Cross section contains a well within the Horseshoe Atoll to the north, and a well proximal to the Ozona Arch in the south. The wells from the middle of the basin display lateral heterogeneity characteristic of the Cline Shale. The wells to the far north and the far south are enriched in the carbonates lithofacies—expected because of proximity to carbonate shelves.

F to F' extends from Scurry County south to Tom Green County (Figure 83). The cross section portrays deposition occurring predominately from the Eastern Shelf. The facies heterogeneity is great, with a lack of distinguishable regional trends. There tends to be a higher siliciclastic input from the Eastern Shelf than from other source areas throughout the basin.

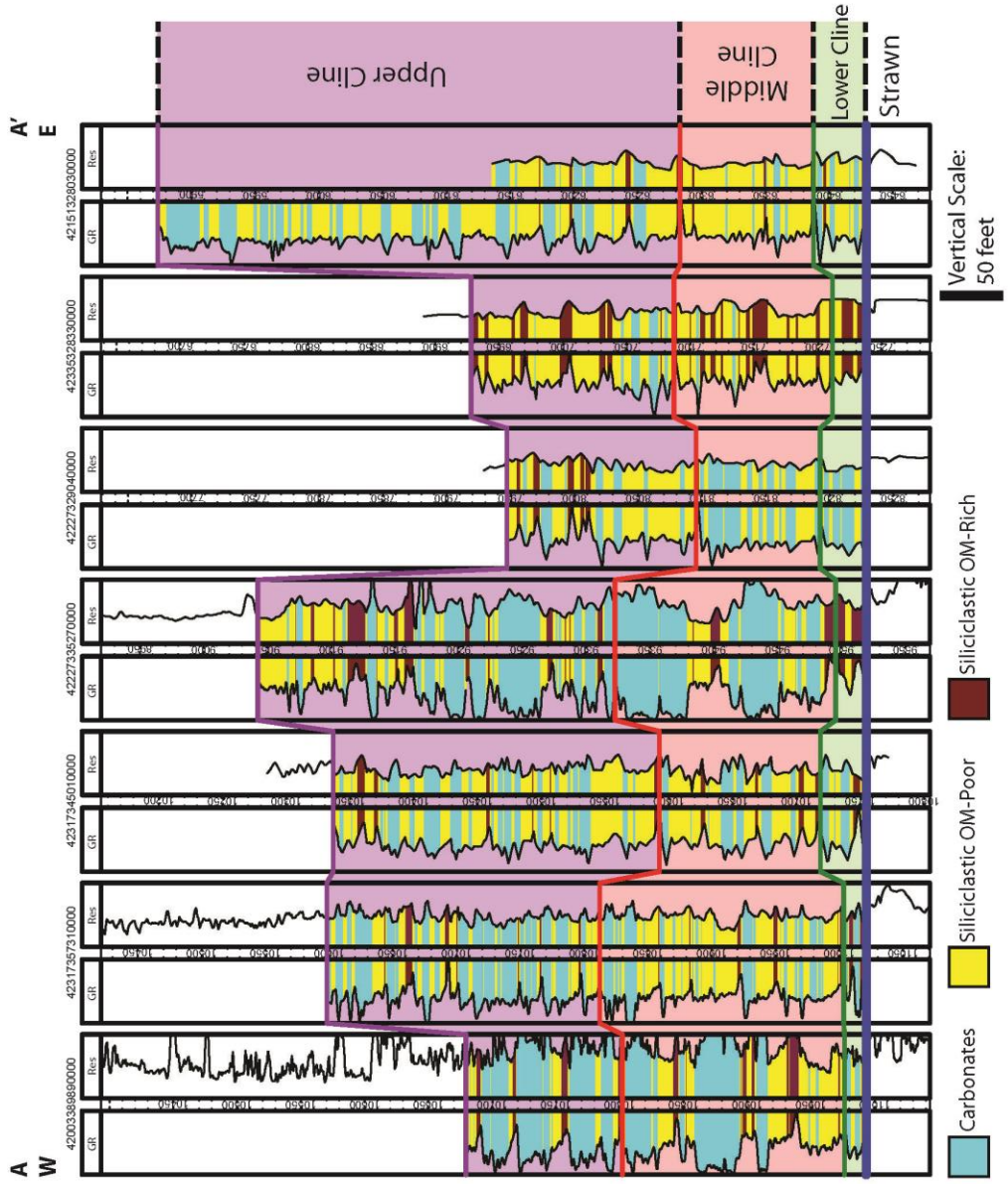

Figure 78: Stratigraphic cross section from A to A'

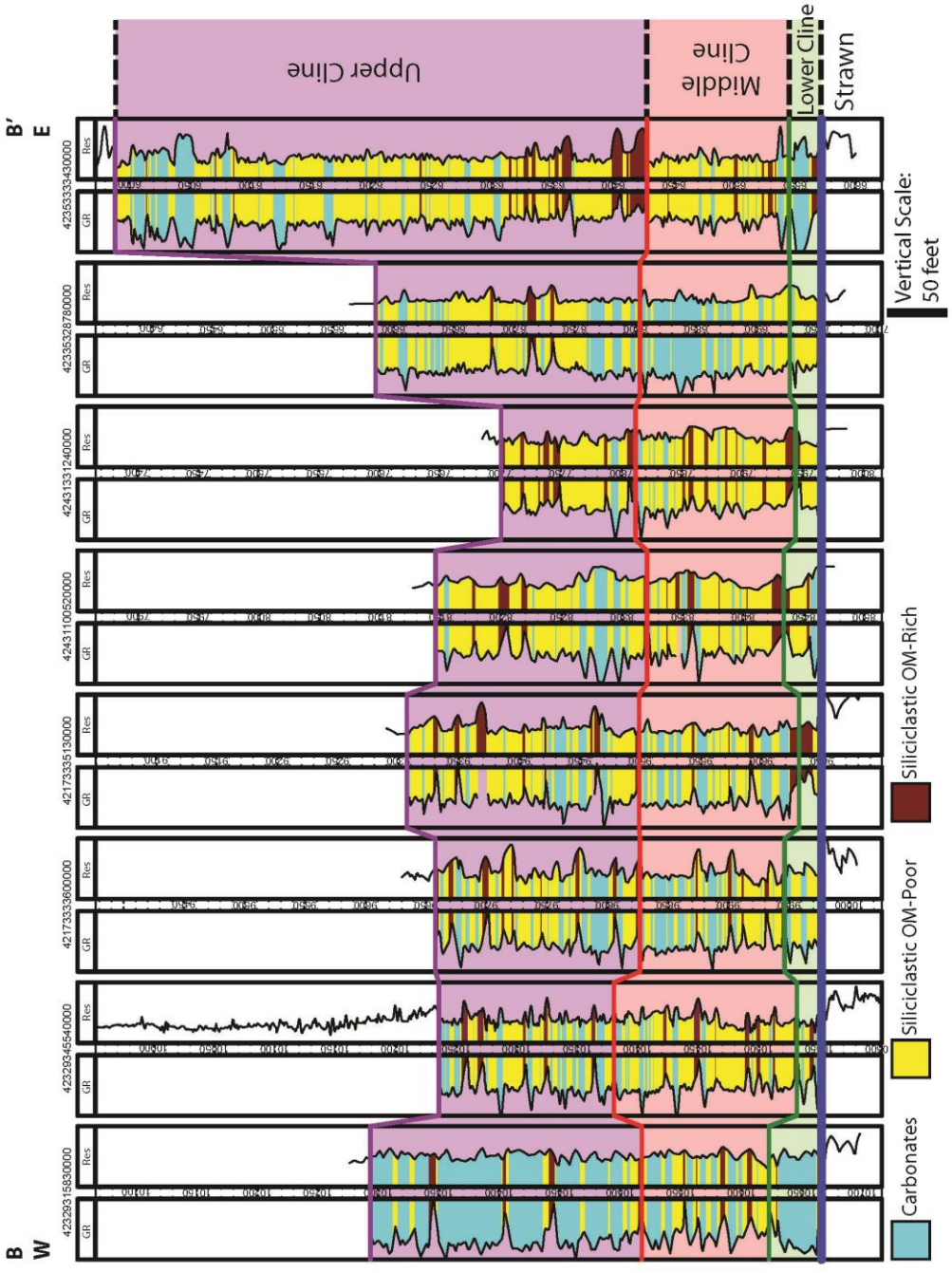

Figure 79: Stratigraphic cross section from B to B'

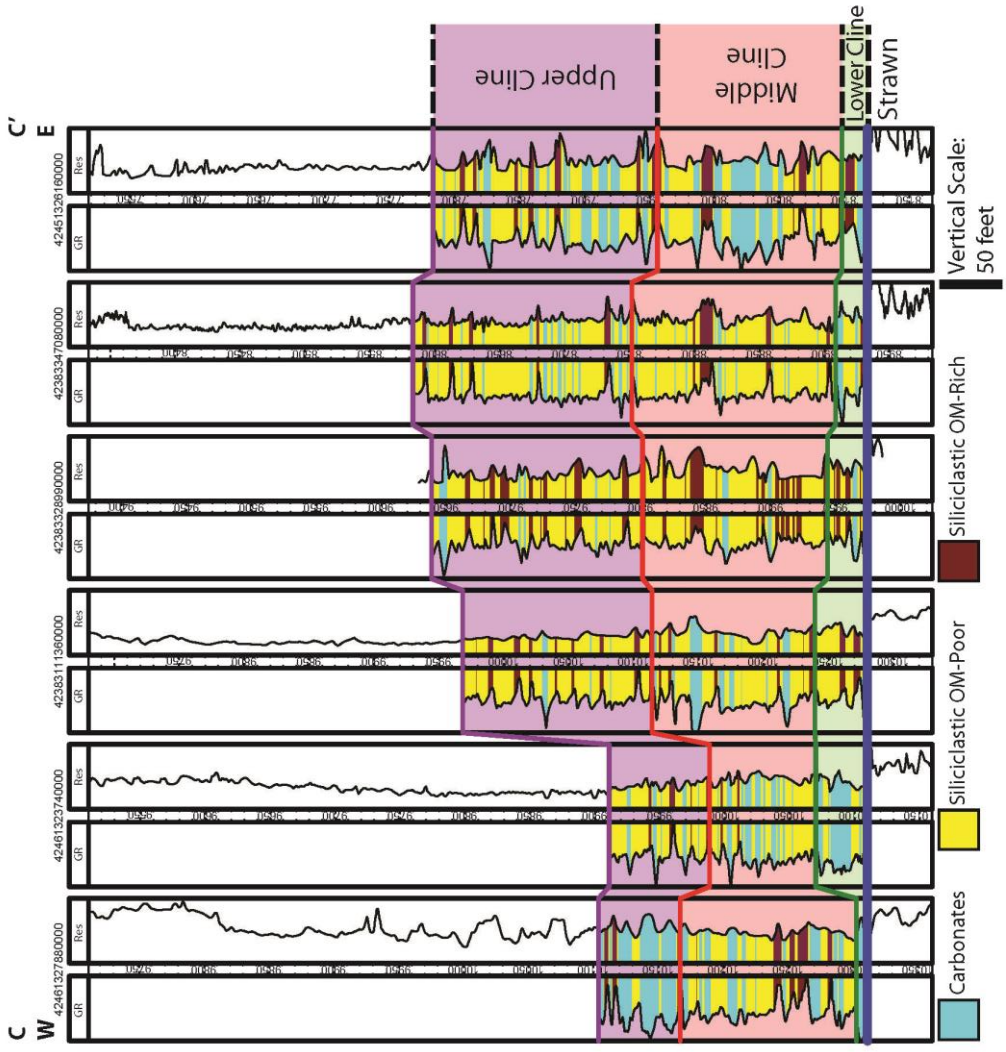

Figure 80: Stratigraphic cross section from C to C'

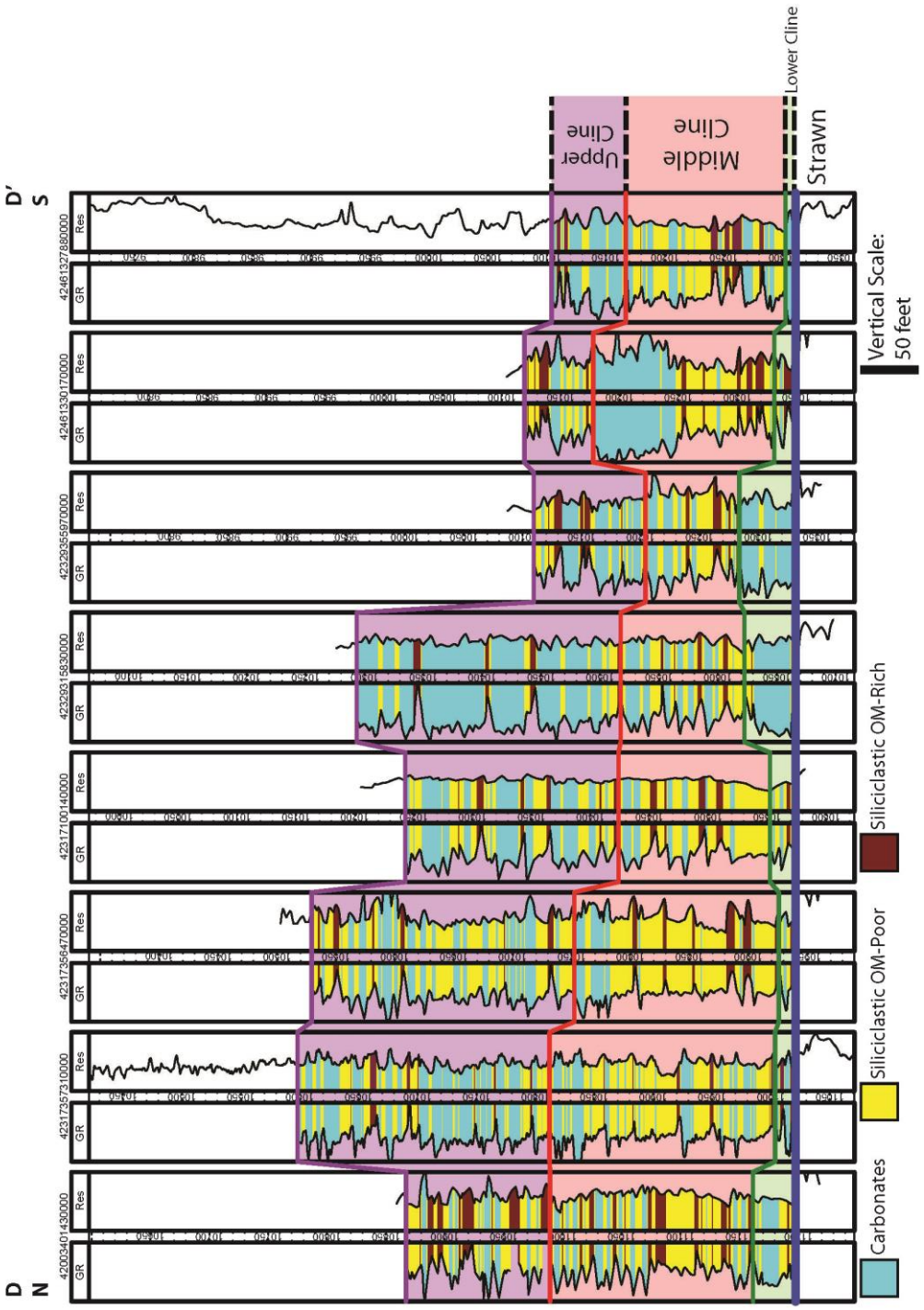

Figure 81: Stratigraphic cross section from D to D'

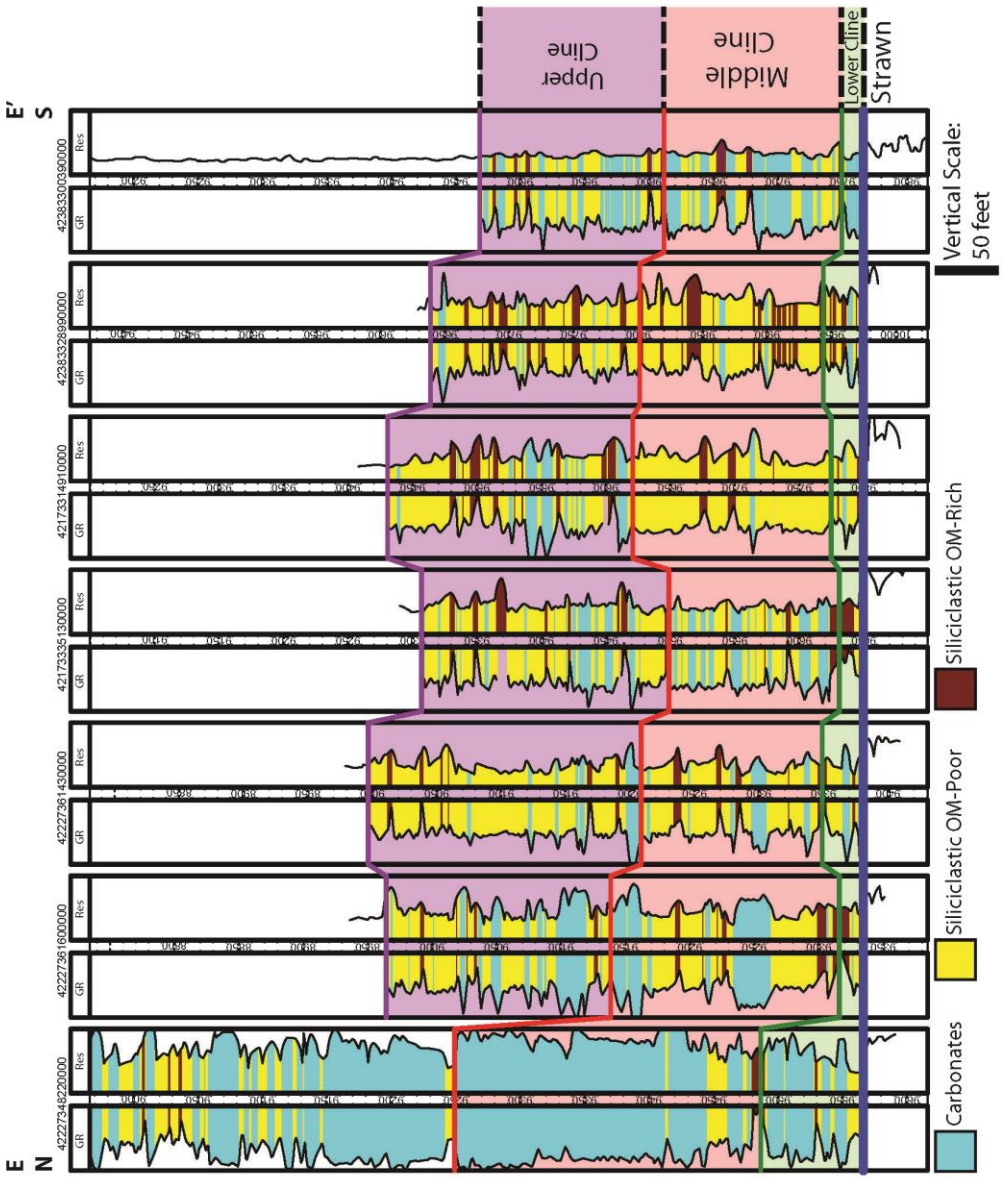

Figure 82: Stratigraphic cross section from E to E'

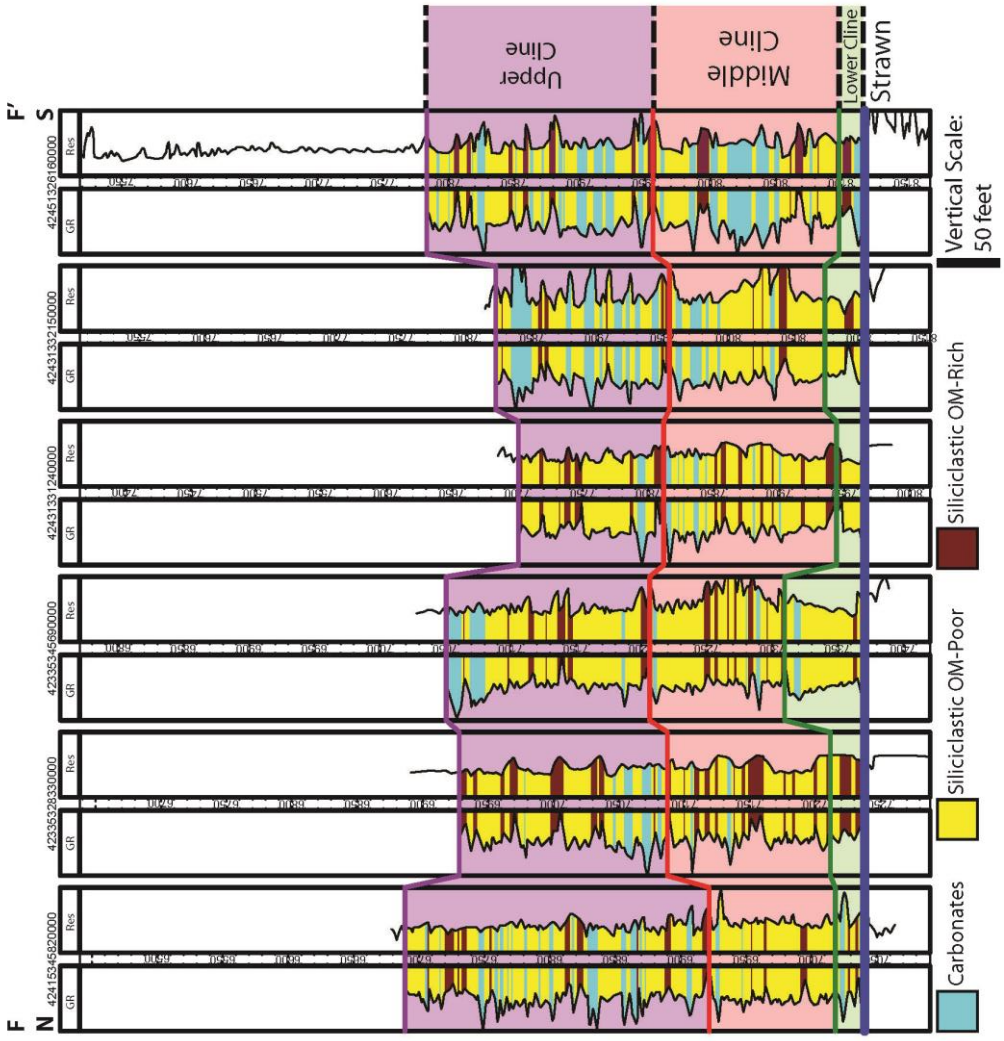

Figure 83: Stratigraphic cross section from F to F'

Summary of Regional Stratigraphy

The Cline Shale is up to 450 feet thick in the basin. Through the use of core-calibrated well logs, regional lithofacies variations were distinguished through time. Deposition of the Lower Cline was markedly thin and heterogeneous. The Lower Cline is rarely greater than 50 feet thick, and lithofacies distributions do not exhibit any regional depositional trends. The Middle Cline is up to 200 feet in thickness, and contains carbonate deposition from the Horseshoe Atoll and the Central Basin Platform, and two fairways of predominantly siliciclastic deposition from the east and from the south. The Upper Cline interval is the thickest at up to 250 feet. The Upper Cline is marked by increased siliciclastic deposition from the south and the east, and the encroachment of the Eastern Shelf as it prograded west into the Midland Basin. A fairway of OM-rich siliciclastic lithofacies is concentrated in Mitchell, Coke, and Sterling Counties throughout the deposition of the Middle and Upper Cline intervals. The concentration OM-rich siliciclastic lithofacies occurs where the total thickness of the Middle and Upper Cline thins.

Discussion

CHEMOFACIES TRENDS OF THE CLINE SHALE

Chemofacies trends can be discerned from the high-resolution XRF chemostratigraphic data in the Powell and the Harris cores. Chemofacies trends in these cores are apparent in both the mineralogy and the OM content. The chemofacies trends can exhibit a cyclic nature. However, it is difficult to link the chemofacies to depositional processes for the Cline Shale due to multiple competing source areas and a complex sequence-stratigraphic history.

The Powell well is located in the basin center, and contains the Upper Cline. The argillaceous and siliceous chemofacies exhibit reciprocal trends in the Powell well (Figure 84). There are one and a half cycles of the mineralogy decreasing in argillaceous chemofacies then increasing in argillaceous chemofacies again. The mineralogy and the OM content of the Powell well are loosely linked. Siliceous and biogenic chemofacies tend to be OM-rich, intermediate facies tend to be OM-moderate, and calcareous, calcareous siliceous, and argillaceous facies tend to be OM-poor. This linkage between mineralogy and OM produces a similar cyclicity of the OM content, but at a higher resolution. There are two and a half cycles of organic matter depletion and enrichment in the Powell core. The inverse linkage of the argillaceous and siliceous facies implies that the chemofacies are governed by competing processes for deposition. The co-variance of OM content with mineralogy is interpreted to be the product of linked processes of dilution of OM by argillaceous and calcareous chemofacie.

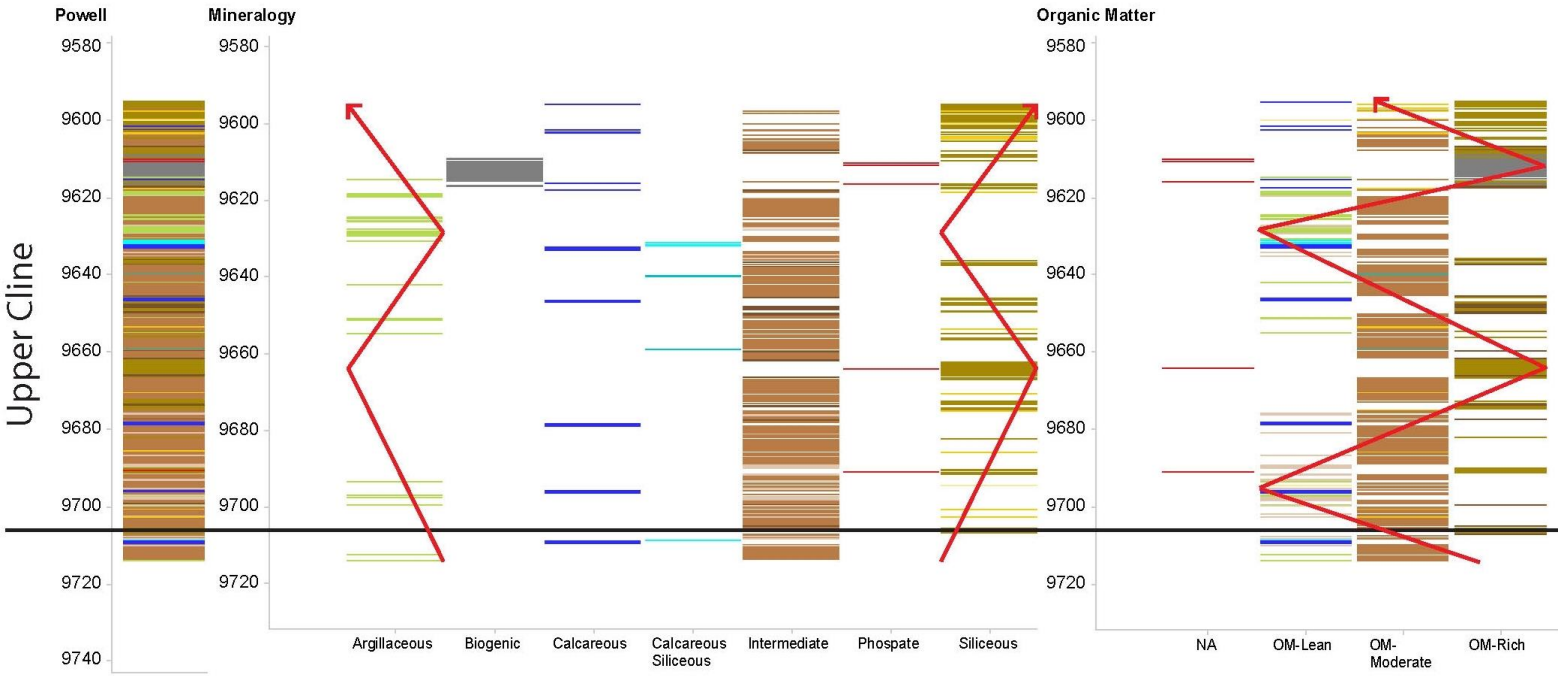

Figure 84: Chemostratigraphic plot of the Powell well with chemofacies trends. Chemoacies trends are represented with red arrows, where the chemofacies is enriched to the right and depleted to the left.

The Harris well, located on the eastern margin of the basin, contains the Lower Cline, Middle Cline, and the majority of the Upper Cline. Chemofacies trends in the Harris well are evident in the argillaceous chemofacies and the OM content (Figure 85). Three asymmetric trends of enrichment in argillaceous chemofacies occur in the Harris well; one enrichment trend encompasses the Middle Cline, and two enrichment trends of argillaceous chemofacies are present in the Upper Cline. The trends decrease in thickness vertically throughout the cored interval. The OM content of the Harris well displays six cycles of OM depletion and subsequent enrichment. The cycles are symmetric during the Lower Cline, they begin transitioning to asymmetric during the Middle Cline, and they become asymmetric during the Upper Cline. The cycles in the Upper Cline are reciprocals of the argillaceous chemofacies cycles, wherein an increase in argillaceous chemofacies content co-varies with a decrease in OM content. The mineralogy and OM content do not display a linkage in the Lower Cline and Middle Cline. However, there is a reciprocal linkage between argillaceous chemofacies and OM content in the Upper Cline. This change from unlinked to linked chemofacies trends signifies a change in the depositional processes associated with both mineralogy and OM content.

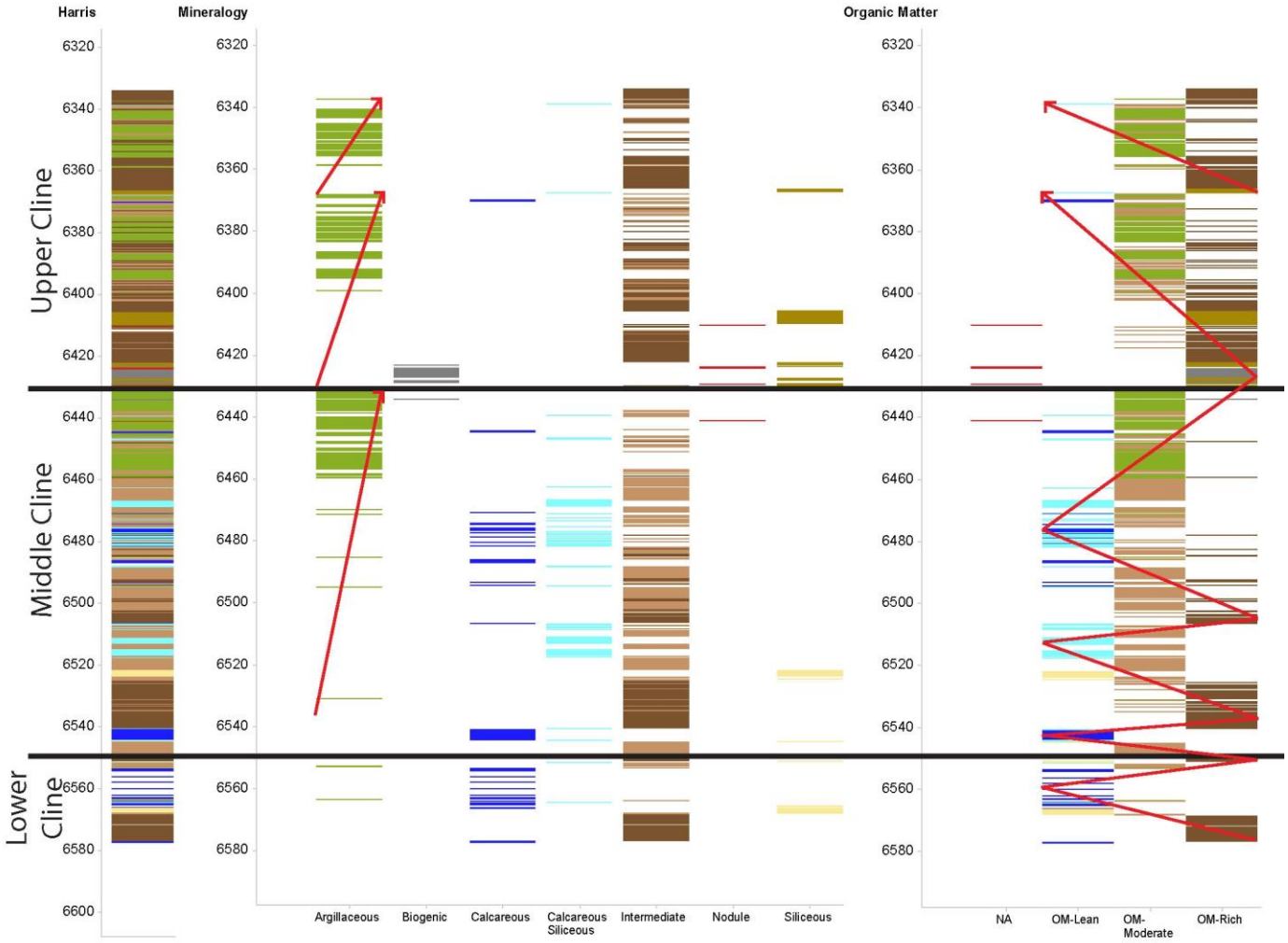

Figure 85: Chemostratigraphic plot of the Harris well with chemofacies trends. Chemoacies trends are represented with red arrows, where the chemofacies is enriched to the right and depleted to the left.

COMPOSITE LITHOACIES DISTRIBUTION OF THE CLINE SHALE

The Lower Cline is dominated by Siliciclastic Om-rich deposits (Figure 86). This was a time when the basin was sediment-starved—the majority of detrital deposits were restricted to the basin edges, allowing concentration of OM-rich deposits (Adams, 1951; Vest, 1970). The thick carbonate deposits from the Central Basin Platform were enriched in the basin (Figure 86). The Eastern Shelf contained lobate, dip-elongate channelized fan deposits shedding from the shelf (Galloway and Brown, 1973). These deposits are predominantly siliceous. However, there is a lobe of carbonates in southern Nolan County; this may be an insitu carbonate bank common during lower Canyon (figure 86) (Galloway and Brown, 1973; Vest, 1970). Though the Lower Cline interval is pervasively organic rich, it is quite thin, with thickness values rarely greater than 50 feet.

The Middle Cline exhibits increased basinal deposition of carbonates and siliciclastic OM-poor deposits (Figure 87). There are four distinct source areas that shed detrital sediment during the Middle Cline. The Horseshoe Atoll and the Central Basin Platform were both responsible for shedding allochthonous carbonate debris. These carbonate-rich deposits are limited to the edge of the basin (Figure 87). The Eastern Shelf and a southern source area both were shedding siliciclastic OM-poor lithofacies into the basin. The lithofacies are not restricted to the shelf edge, and they are extensive along the basin floor. Between OM-poor deposition form the two source areas, there is a fairway of OM-rich deposits (Figure 87). This fairway exists because the deposits were

not being diluted by OM-poor detrital sediments of siliciclastic or carbonate origin. The Middle Cline is relatively thin over the OM-rich fairway.

Upper Cline deposition is marked by progradation of the eastern and southern source areas relative to the Middle Cline, and increased basinal sedimentation of detrital deposits (Figure 88). The progradation of the eastern shelf is evident from the thickening of the Upper Cline in the eastern portion of the regional cross sections (Figure 79). The southern source area, though out of the study area, is very similar to the Eastern Shelf because of the morphology and lithology of associated basinal deposits. The Central Basin Platform was also shedding more carbonates at this time, and they extend further into the basin than during deposition of the Middle Cline in the northern portion of the study area. There was a fairway of OM-rich deposits in Howard, Mitchell, Sterling, and Coke Counties, again associated with a relatively thin depositional region. However, it had shrunk in size from the Middle Cline, probably because the deposits were diluted by the OM-poor deposits from the encroaching Eastern Shelf. The Horseshoe Atoll was a major source of carbonates only on the southwestern side of the carbonate platform. The wind was predominantly from the northeast at the time; aiding in shedding to the southwest (Waite, 1993). The allochthonous deposits on the eastern side of the Horseshoe atoll were most likely also diluted by the siliciclastic deposits of the Eastern Shelf. The Cline Shale is a heterogeneous mudrock; the stacking vertical facies stacking patterns and the composite lithofacies distributions display this heterogeneity (Figure 89).

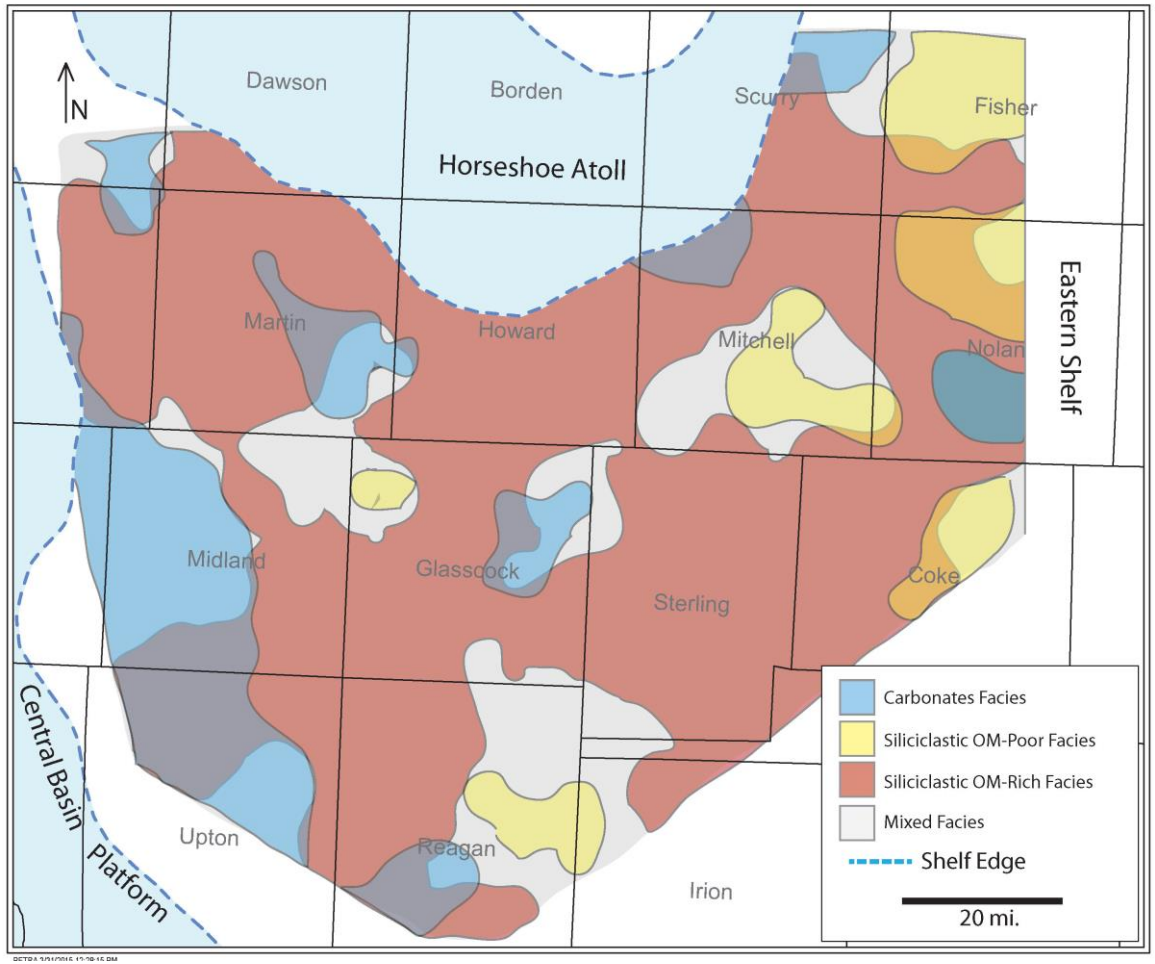

Figure 86: Composite facies distribution of the Lower Cline. The unit is pervasively enriched in OM-rich lithofacies.

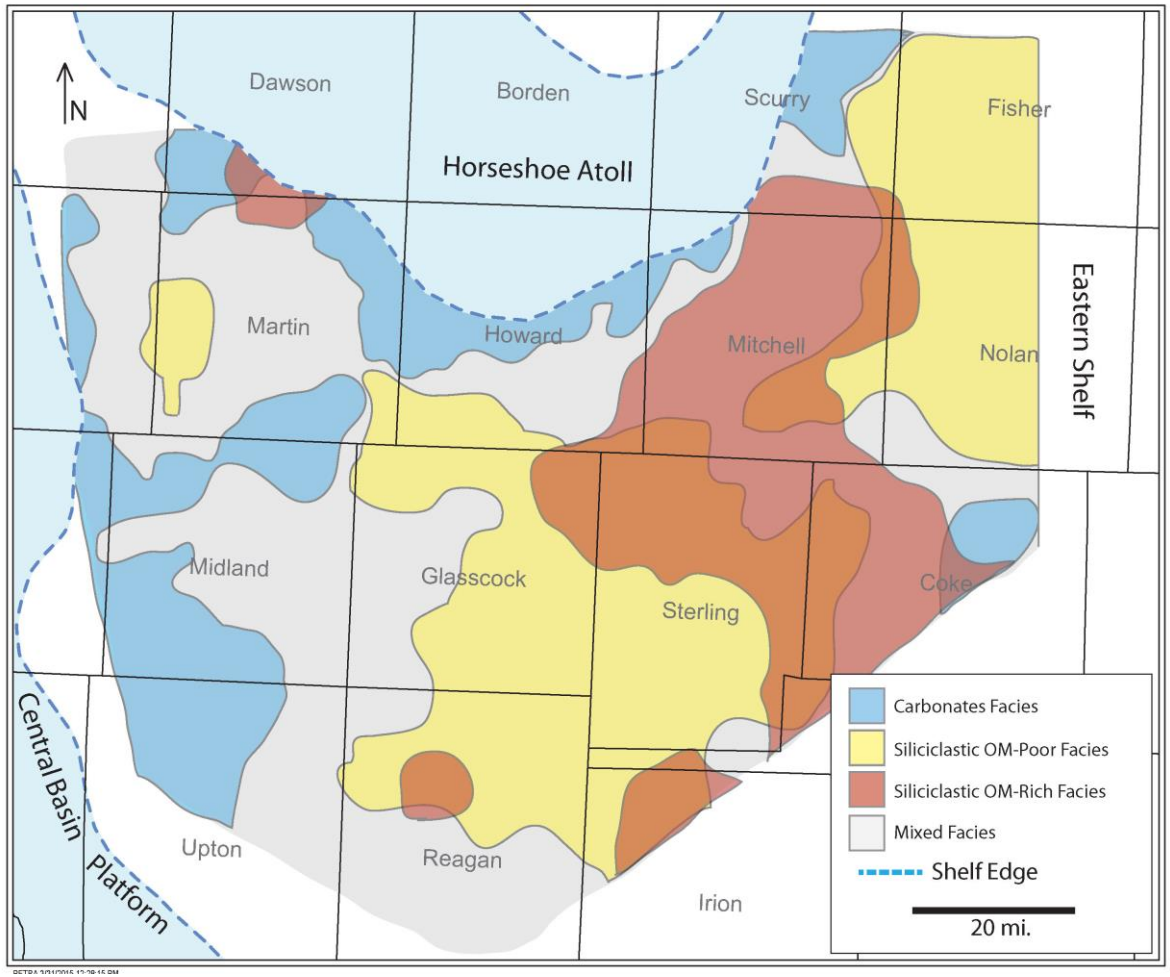

Figure 87: Composite facies distribution of the Middle Cline. The unit is enriched in carbonates proximal to the Horseshoe Atoll and the Central Basin Platform. Siliciclastic OM-poor facies occur proximal to the Eastern Shelf and in the southeast portion of the study area.

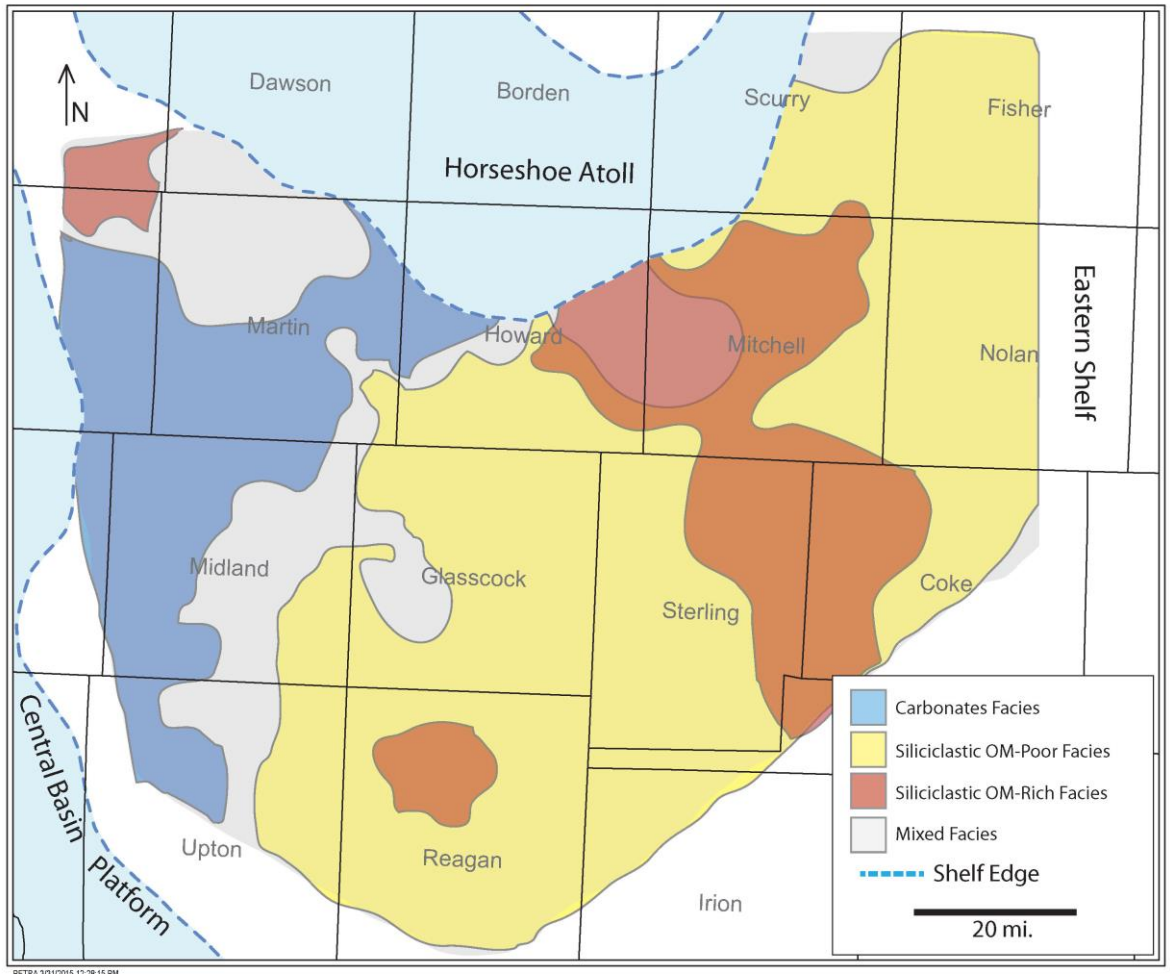

Figure 88: Composite facies distribution of the Upper Cline. Carbonates are enriched in the Northwest, and siliciclastics are enriched in the southeast and the basin center. There is a fairway of OM-rich deposits in Mitchell, Sterling, and Coke Counties.

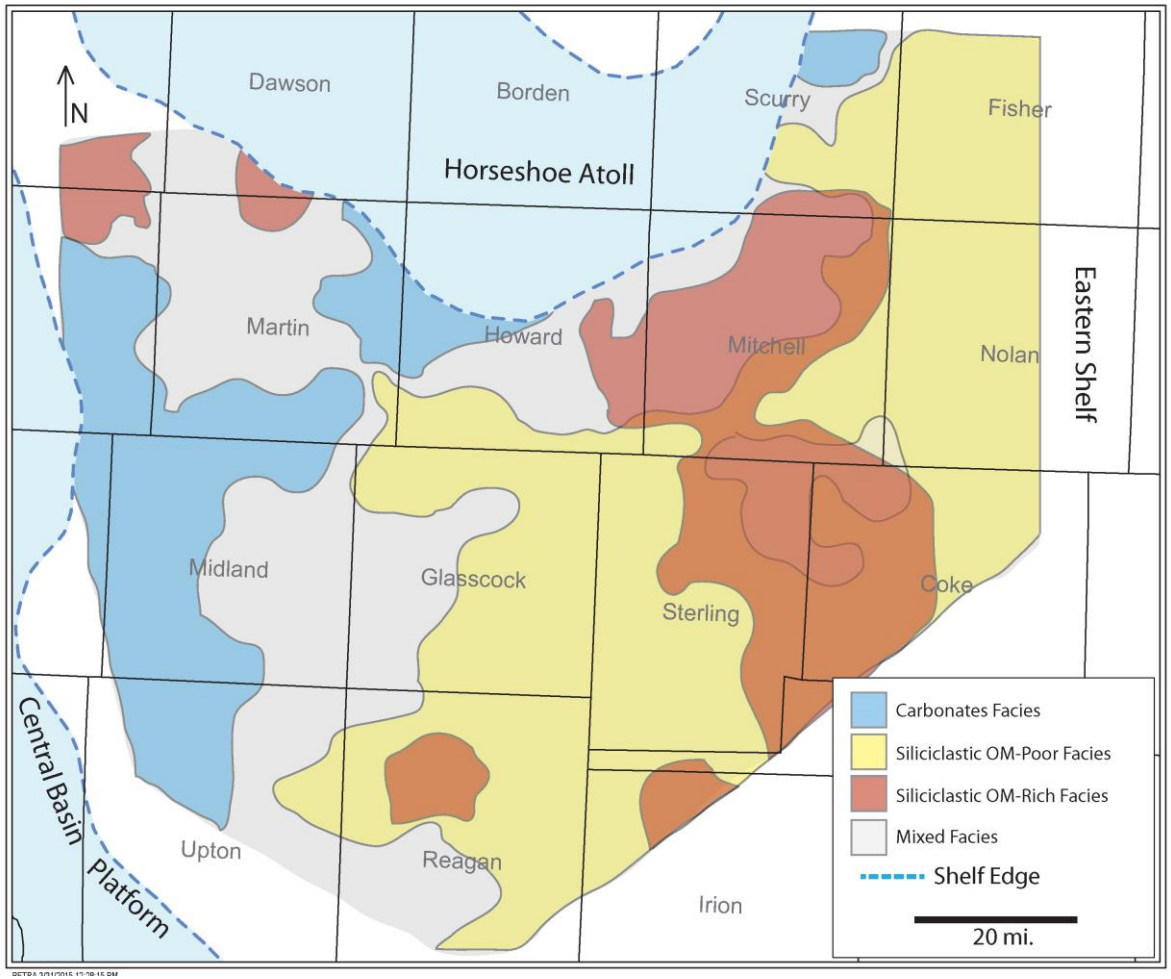

Figure 89: Composite facies distribution of the gross Cline Shale. OM-rich deposits are concentrated in Mitchell, Sterling, and Coke Counties. Siliciclastic lithofacies dominate the southest portion of the study area, and carbonate lithofacies are restricted to the northwest.

Conclusions

The Cline Shale is a basinal mudrock deposited in the Southern Midland Basin during the Uppermost Pennsylvanian (Canyon and Cisco Series) (Wahlman et al., in preparation). The Cline was deposited under complex sequence-stratigraphic conditions. The Cline Shale was divided into distinct units of the Lower Cline, the Middle Cline, and the Upper Cline. The Lower Cline-Middle Cline contact was delineated from the top of the Home Creek Limestone on the Eastern Shelf, equivalent to the top of the Canyon (Brown et al., 1990). The Middle and Upper Cline were divided based on chemostratigraphic facies differences and an increase in TOC content. The Horseshoe Atoll, Eastern Shelf, Ozona Arch, and Central Basin Platform bound the Southern Midland Basin. Paleobathymetric changes associated with slope and shelf environments controlled facies changes to non-Cline facies. Cline Shale facies exhibit great vertical and lateral heterogeneity associated with deposition during icehouse conditions. The Cline Shale is a mudrock with a dominantly ternary mineralogy; clays, quartz, and carbonates compose the majority of mineral types, and can be used to distinguish mineralogical facies.

Thin deposits of OM-rich (greater than 2% TOC) mudrocks exist throughout Cline deposition, and are most common during the Lower Cline and Upper Cline. OM-rich deposits were distinguished through the use of empirical relationships of TOC and XRF in core that were then used to calibrate gamma ray well logs. The organic matter in the Cline is predominantly Type I and II throughout the Lower and Upper Cline, and

Type III in the Middle Cline. There is an empirical correlation between TOC and Porosity; exhibiting the importance of organic matter hosted porosity in the total porosity network of the Cline Shale. The thermal maturity of the Cline Shale is the oil window to early condensate window in the basin-centered wells. The OM-rich deposits are interbedded with carbonates and siliciclastic OM-poor rocks. Commonly carbonates and clays serve as diluents to the OM in the Cline Shale system—increasing the rate of deposition and diluting the OM accumulation.

The Lower Cline was markedly thin and OM-rich; carbonate and siliciclastic OM-poor deposits were restricted to basin edges. In core, the Lower Cline was dominated by allochthonous OM-poor carbonate deposits and OM-rich intermediate deposits. This was a time of basin restriction and organic matter concentration. Throughout the deposition of the Middle Cline, the southeastern half of the basin was dominated by siliciclastic OM-poor deposits that were sourced from the Eastern Shelf. The northwestern half of the basin was dominated by carbonate deposits sourced from the Horseshoe Atoll and the Central Basin Platform. The Upper Cline deposits showed siliciclastic OM-poor encroachment. The siliciclastic OM-poor deposits, sourced from the Eastern Shelf, extended farther in the basin, and dominated the deposition of the basin. The only exception is carbonate-dominated deposition near the basin edges associated with the western Horseshoe Atoll and the Central Basin Platform. These characteristics of the Cline Shale will contribute to developing the mudrock as an unconventional resource play.

Appendices

Please refer to the attached DVD in the back of the Volume for the Appendices.

APPENDIX A: HIGH-RESOLUTION XRF DATASET

APPENDIX B: ROCK PROPERTIES DATASET

APPENDIX C: WELLS USED IN REGIONAL STRATIGRAPHIC ANALYSIS

References

Adams, J. E., Frenzel, H. N., Rhodes, M. L., Johnson, D. P., 1951, Starved Pennsylvanian Midland basin: AAPG Bulletin, v. 35, p. 2600-2607.

Atchley, S.C., Kozar, M.G., Yost, L., 1999, A predictive model for reservoir distribution in the Permian (Leonardian) ClearFork and Glorieta formations, Robertson field area, west Texas: AAPG Bulletin, v. 83, p. 1031– 1056.

Aldis, D. S., Grossman, E. L., Yancey, T. E., McLerran, R. D., 1988, Isotope stratigraphy and paleodepth changes of Pennsylvanian sedimentary deposits: PALAIOS, v. 3, p. 487-506.

Binnion, M., 2012. How the technical differences between shale gas and conventional gas projects lead to a new business model being required to be successful: Marine and Petroleum Geology, v. 31, p. 3-7.

Blakey, R., 2013, http://cpgeosystems.com/namP290.jpg accessed November, 2013

Boyer, C., Kieschnick, J., Suarez-Rivera, R., Lewis, R. E., Waters, G., 2006, Producing gas from its source: Oilfield Review, 18(3), p. 36-49.

Breyer, J. A., 2012, Shale reservoirs-giant resources for the 21st century: AAPG Memoir 97, 68 pp.

Brown, L. F., Jr., Solis-Iriarte, R. F., Johns, D. A., 1990, Regional depositional systems tracts, paleogeography, and sequence stratigraphy, Upper Pennsylvanian and Lower Permian strata, north- and west-central Texas: University of Texas at Austin, Bureau of Economic Geology Report of Investigations No. 197, 116 p.

Brown, L. F., Jr., Cleaves, A. W., II, Erxleben, A. W., 1973, Pennsylvanian depositional systems in north-central Texas a guide for interpreting terrigenous clastic facies in a cratonic basin: Bureau of Economic Geology, Guidebook Number 14, 121 pp.

Brumsack, H.J., 1989, Geochemistry of recent TOC-rich sediments from the Gulf of California and the Black Sea: Geologische Rundschau, 78/3, p. 851-882.

Calvert, S. E., and Pedersen, T. F., 2007, Chapter Fourteen Elemental Proxies for Palaeoclimatic and Palaeoceanographic Variability in Marine Sediments: Interpretation and Application, *in*: Claude Hillaire–Marcel and Anne De Vernal, Editor(s), Developments in Marine Geology, Elsevier, v. 1, p. 567-644.

Cheney, M.G., Dott, R. H., Hake, B. F., Moore, R. C., Newell, N. D., Thomas, H. D., Tomlinson, C. W., 1945, Classification of Mississippian and Pennsylvanian rocks of North America: American Association of Petroleum Geologists Bulletin, v. 29, no. 2, p. 125-169.

Chermak, J. A., and Schreiber, M. E., 2014, Mineralogy and trace element geochemistry of gas shales in the United States; environmental implications: International Journal of Coal Geology, v. 126, p. 32-44.

Cys, J. M., and Gibson, W. R., 1988, Pennsylvanian and Permian geology of the Permian Basin region, *in* Sloss, L. L., ed., Sedimentary Cover— North American Craton: U. S., The geology of North America, v. D-2, p. 277–289.

Davis, H. E., 1953, North-south cross-section through Permian Basin of west Texas: West Texas Geol. Soc. Pub, 1 sheet.

Davydov, V. I., Glenister, B. F., Spinosa, C., Ritter, S. M., Chernykh, V. V., Wardlaw, B. R., Snyder, W. S., 1998, Propsal of Aidaralash Creek as global stratotype section and point base for Permian system: Episodes, 21, p. 11-18.

Dominguez, G. C., and Samaniego V. F., 1992, Carbonate reservoir characterization: a geologic engineering analysis, part I: Elselvier, 992 pp.

Eros, J. M., Montañez, I. P., Osleger, D. A., Davydov, V. I., Nemyrovska, T.,2012, Sequence stratigraphy and onlap history of the Donets Basin, Ukraine: insight into Carboniferous icehouse dynamics: Palaeogeography Palaeoclimatology Palaeoecology, v. 313–314, p. 1–25.

Folk, R. L., 1980, Petrology of sedimentary rocks: Hemphill Publishing Co., Austin, Texas, 182 pp.

Fertl, W. H., G. V. Chilingar, 1988, Total Organic Carbon Content Determined From Well Logs: Society of Petroleum Engineers Formation Evaluation, v. 3, p. 407-419.

Galley, J. E., 1958, Oil and gas geology of the Permian Basin of West Texas, in Habit of oil—a symposium: American Association of Petroleum Geologists, Special Publication, p. 395–446.

Galloway, W. E., and Brown, L. F., 1973, Depositional systems and shelf-slope relations on cratonic basin margin, uppermost Pennsylvanian of north central Texas: American Association of Petroleum Geologists Bulletin, v. 57, p. 1185-1218.

Hamlin, H. S. and Baumgardner, R. W., 2012, Wolfberry (Wolfcampian-Leonardian) Deep-water Depositional Systems in the Midland Basin: Stratigraphy, Lithofacies, Reservoirs, and Source Rocks: University of Texas at Austin, Bureau of Economic Geology Report of Investigations No 277, 61 p.

Hastie, T., Tibshirani, R., Friedman, J., 2009. The elements of statistical learning: Springer Science+Business Media, LLC, 745 pp.

Hayes, J. D., Imbrie, J., Shackleton, N. J., 1976, Variations in the Earth's orbit: Pacemaker of the ice ages: Science, v. 194, p. 1121–1132.

Heckel, P. H., 1986, Sea-level for Pennsylvanian eustatic marine transgressive-regressive depositional cycles along midcontinent outcrop belt. North America: Geology, v. 14, p. 330-334.

Hoak, T., Sundberg, K., Ortoleva, P., 1991, Overview of the Structural Geology and Tectonics of the Central Basin Platform, Delaware Basin, and Midland Basin, West Texas and New Mexico: Department of Energy Publication, 49 pp.

Ibach, L. J., 1980, The relationship between sedimentation rate and total organic carbon content in ancient marine sediments: American Association of Petroleum Geologists Bulletin, v. 66, no. 2, p. 170-188.

Jacobs, T., 2013, Cracking the Cline: A new shale play develops in the Permian Basin: Journal of Petroleum Technology, November 2013, p. 70-77.

Jones, J. W., 1980, Depositional environment & reservoir morphology of canyon sandstones, central Midland Basin, Texas: American Association of Petroleum Geologists Bulletin, v. 66, no. 2, p. 244-245.

Kerans, C., and Anonymous, 2001, Stratigraphic and diagenetic controls on reservoir architecture of a non-reefal icehouse isolated platform: Sacroc Unit, Horseshoe Atoll, Texas, *in* American Association of Petroleum Geologists Southwest Section meeting abstracts, v. 85, no. 2, p. 386–387.

Langford, F. F., and Blanc-Valleron, M. M., 1990, Interpreting rock-eval pyrolysis data using graphs of pyrolizable hydrocarbons vs. total organic carbon: American Association of Petroleum Geologists Bulletin, v. 74, no. 6, p. 799-804.

Legendre, P. and Legendre, L., 1998, Numerical ecology: 2nd. ed., Elsevier, 989 pp.

Loucks, R. G., R. M. Reed, S. C. Ruppel, and D. M. Jarvie, 2009, Morphology, genesis, and distribution of nanometer- scale pores in mudstones of the Mississippian Barnett Shale: Journal of Sedimentary Research, v. 79, p. 848– 861.

Loucks, R. G., R. M. Reed, S. C. Ruppel, and U. Hammes, 2012, Spectrum of pore types and networks in mudrocks and a descriptive classification for matrix-related mud-rock pores: AAPG Bulletin, v. 96, p. 1071–1098.

Lucia, F. J., 1999, Carbonate reservoir characterization: Springer, 233 pp.

Lüning, S. and Kolonic, S., 2003, Uranium spectral gamma-ray response as a proxy for organic richness in black shales: applications and limitations: Journal of Petroleum Geology, v. 26 (2), p. 153-174.

Matchus, E.J. and Jones, T. S., 1984, East-west cross section through Permian Basin of West Texas: prepared by Stratigraphic Problems Committee of the West Texas Geological Society, 1 sheet.

Mazzullo, S. J., and Reid, A. M., 1988, Stratigraphic architecture of Pennsylvanian and Lower Permian facies, northern Midland Basin, Texas: *in* Cunningham, B. K., (ed.), Permian and Pennsylvanian stratigraphy, Midland Basin, West Texas; studies to aid hydrocarbon exploration: Society of Economic Paleontologists and Mineralogists Publication, Permian Basin Chapter, v. 88-28, p. 1-6.

Mazzullo, S. J., and Reid, A. M., 1989, Lower Permian platform and basin depositional systems, northern Midland Basin, Texas, *in* Crevello, P. D., Wilson, J. J., Sarg, J. F., and Read, J. F., eds., Controls on carbonate platform and basin development: Society of Economic Paleontologists and Mineralogists Special Publication No. 44, p. 305-320.

Milliken, K. L., Esch, W. L., Reed, R. M., and Zhang, T., 2012, Grain assemblages and strong diagenetic over-printing in siliceous mudrocks, Barnett Shale (Mississippian), Fort Worth Basin, Texas, U.S.A.: American Association of Petroleum Geologists Bulletin, v. 96, p. 1553–1578.

Milliken, K. L., Rudnicki, M., Awwiller, D. N., Zhang, T., 2013, Organic matter–hosted pore system, Marcellus Formation (Devonian), Pennsylvania: American Association of Petroleum Geologists Bulletin, v. 97, p. 177- 200.

Montañez, I. P. and Poulsen, C. J., 2013, The late Paleozoic ice age: an evolving paradigm: Annual Review of Earth Planetary Science 2013, p. 629-656.

Nance, H. S. and Rowe, H., 2014, Eustatic controls on stratigraphy, chemostratigraphy, and water mass evolution preserved in a Lower Permian mudrock succession, Delaware Basin, west Texas, USA: Interpretation, vol. 3, no. 1, 25 pp.

Neal, J., and Abreu, V., 2009, Sequence stratigraphy hierarchy and the accommodation succession method: Geology, v. 37, no. 9, p. 779-782.

Passey, Q. R., Bohacs, K. M., Esch, W. L., Kimentidis, R., Sinha, S., 2010, From oil-prone source rock to gas-producing shale reservoir: Geologic and petrophysical characterization in unconventional shale-gas reservoirs: Chinese Petroleum Society/Society of Petroleum Engineers International Oil & Gas Conference and Exhibition, Beijing, China, June 8–10, 2010, SPE Paper 121250, 29 p.

Peters, K. E., 1986, Guidelines for evaluating petroleum source rock using programmed pyrolysis: AAPG Bulletin, v. 70, no. 3, p. 318-329.

Piper, D.Z. ,1994, Seawater as the source of minor elements in black shales, phosphorites and other sedimentary rocks: Chemical Geology, v. 114, p. 95-114.

Piper, D.Z, Calvert, S.E., 2009, A marine biogeochemical perspective on black shale deposition: Earth-Science Reviews, v. 95, p. 63-96.

Piper, D.Z., Perkins, R.B., 2004, A modern vs. Permian black shale – the hydrography, primary productivity, and water-column chemistry of deposition: Chemical Geology, v. 206, p. 177-197.

Pioneer Natural Resources Company, 2013, Pioneer Natural Resources Continues to Deliver Record Horizontal Spraberry/Wolfcamp Drilling Results in the Midland Basin: http://investors.pxd.com/phoenix.zhtml?c=90959&p=irol-newsArticle&ID=1875863, accessed April 2015.

Phillips, Nestor Donovan, 1991, Refined Subsidence Analyses as a Means to Constrain Late Cenozoic Fault Movement, Ventura Basin, California. Thesis, The University of Texas at Austin, 121 pp.

Prochnow, S. J. and Hinterlong, G. D., 2014, Pennsylvanian and Wolfcampian Sequence Stratigraphy Using FMI and Log Analysis on the Western Edge of the Midland Basin: A Tool for Guiding Well Completions: AAPG 2014 Southwest Section Annual Convention, May, 2014.

Romesburg, H. C., 1989, Cluster analysis for researchers: Lulu Press, 333 pp.

Ross, C. A., 1986, Paleozoic evolution of southern margin of Permian basin: Geological Society of America Bulletin, v. 97, p. 536-554.

Rowe, H. D., Dunbar, R. B., Mucciarone, D. A., Seltzer, G. O., Baker, P. A., Fritz, S., 2002, Isolation, moisture balance and climate change on the South American Altipano since the last glacial maximum: Climate Change, v. 52, p. 175-199.

Rowe, H. D., Hughes, N., and Robinson, K., 2012, The quantification and application of handheld energy-dispersive x-ray fluorescence (ED-XRF) in mudrock chemostratigraphy and geochemistry: Chemical Geology, v. 324-325, p. 122-131.

Saller, A. H., Dickson, J. A. D., Boyd, S. A., 1994, Cycle Stratigraphy and Porosity in Pennsylvanian and Lower Permian Shelf Limestones, Eastern Central Basin Platform, Texas: American Association of Petroleum Geologists Bulletin, v. 78, no. 12, p. 1820-1842.

Seifoddini, H., 1989, Single linkage versus average linkage clustering in machine cells formation applications: Computers and Industrial Engineering, v. 16, p. 419-426.

Skaar, K. M., 2012, The Cline of West Texas – Past, Present, Future: Oil and Gas Reporter, Oct. 2012.

Sutton, L., 2015, Permian Basin production – Midland vs Delaware Basins: http://info.drillinginfo.com/permian-basin-production/ accessed February 2015

Templ, M., Filzmoser, P., Reimann, C., 2008, Cluster analysis applied to regional geochemical data – problems and possibilities: Applied Geochemistry, v. 23, p. 2198–2213.

Van Siclen, D. C., 1958, Depositional Topography—Examples and Theory: American Association of Petroleum Geologists Bulletin, v. 42, no. 8, p. 1897-1913.

Veevers, J.J.and Powell, C.M., 1987, Late Paleozoic glacial episodes in Gondwanaland reflected in transgressive-regressive depositional sequences in Euramerica: Geological Society of America Bulletin, v. 98, p. 475–487.

Vest, E. L., Jr., 1970, Oil fields of Pennsylvanian-Permian Horseshoe Atoll, West Texas, *in* Halbouty, M. T., ed., Geology of giant petroleum fields: a symposium of papers on giant fields of the world including those presented at the 53rd Annual Meeting of the Association in Oklahoma City, Oklahoma, April 23-25, 1968: American Association of Petroleum Geologists Memoir 14, p. 185-203.

Wahlman, G.P., J.E. Barrick, and R. Baumgardner, (in preparation), Upper Pennsylvanian fusulinid and conodont biostratigraphy from cores through the lower "Wolfcamp Shale" in the Midland Basin, West Texas.

Wahlman, G. P., 2013, Pennsylvanian to Lower Permian (Desmoinesian-Wolfcampian) fusulinid biostratigraphy of midcontinent North America: Stratigraphy, v. 10, no. 1-2, p. 73-104.

Waite, L. E., 1993, Upper Pennsylvanian seismic sequences and facies of the eastern and southern Horseshoe Atoll, Midland Basin, West Texas, *in* Loucks, R. G., and Sarg, J. F., eds., Carbonate sequence stratigraphy: recent developments and applications: American Association of Petroleum Geologists, v. 57, p. 213–240.

Walker, D. A., Golonka, J., Reid, A., and Reid, S., 1995, The effects of paleolatitude and paleogeography on carbonate sedimentation in the late Paleozoic, *in* A. Y. Huc, ed., Paleogeography, paleoclimate, and source rocks: AAPG Studies in Geology 40, p. 133–155.

Wedepohl, K.H., 1971. Environmental influences on the chemical composition of shales and clays. *in* Ahrens, L.H., Press, F., Runcorn, S.K., Urey, H.C. (Eds.), Physics and Chemistry of the Earth. Pergamon, Oxford; 305–333.

Yancey, T. E., and McLerran, R. D., 1988, Cyclic stratigraphy of the Late Pennsylvanian of north-central Texas; *in*, Permian and Pennsylvanian Stratigraphy, Midland Basin, West Texas-Studies to Aid Hydrocarbon Exploration, B. K. Cunningham, ed.: Society of Economic Paleontologists and Mineralogists, Permian Basin Section, Research Seminar 1, p. 65-77.

Yang, K. and Dorobek, S. L., 1995, The Permian Basin of west Texas and New Mexico: tectonic history of a “composite” foreland basin and its effects on stratigraphic development, in Dorobek, S. L. and Ross, G. M., eds., Stratigraphic evolution of foreland basins: SEPM (Society for Sedimentary Geology) Special Publication no. 52, p. 149–174.

Vita

Reed Smart Roush was born in Atlanta, Georgia, and grew up in Oklahoma City, Oklahoma. He completed his high school education at Casady School in Oklahoma City in 2007. The following fall, Reed matriculated to The University of Texas at Austin where he received a Bachelor of Science in geologic sciences. During the summer of 2013, Reed entered the Jackson School of Geosciences at The University of Texas at Austin for a second time; pursing a Masters of Science in geologic sciences and a Business Foundations Certificate.

Permanent e-mail: reedroush@gmail.com

This thesis was typed by Reed Smart Roush